Durham E-Theses

An optically guided atomic fountain

Hilary Jane Davies

AN OPTICALLY GUIDED ATOMIC FOUNTAIN

Hilary Jane Davies

A thesis submitted in partial fulfilment of the requirements
for the degree of Doctor of Philosophy at the
University of Durham

Department of Physics
University of Durham
December 1999

ABSTRACT

An Optically Guided Atomic Fountain

Hilary Jane Davies, University of Durham, Dec. 1999
Ph.D. thesis

This thesis describes the development of a laser-cooling experiment aimed at efficient transfer of cold atoms over a short distance, for loading into a conservative atom trap. We detail the construction of a 3D magneto-optical trap (MOT) and perform characterisation measurements to optimise the number and temperature of the cold atoms. The atoms are launched vertically in a fountain from the MOT using a 'moving molasses' technique and a red-detuned far-off-resonant laser beam is used to guide them into an UHV chamber. Loading into the guiding beam is optimised with respect to the beam and MOT parameters. We demonstrate a maximum loading of 20% and guiding over a distance of more than 10 cm without loss of atoms. The atoms are delivered to the UHV chamber in a cloud with a transverse dimension of order 200 μm.

We discuss the extension to continuous operation of the guided atomic fountain. The 3D MOT is replaced by a funnel with 2D trapping and 3D cooling which continuously extracts the cold atoms using moving molasses. A comparison between the flux of guided atoms obtained in a pulsed fashion from the 3D MOT and continuously from the funnel indicate that the pulsed case is a factor of ten more efficient. The difference is due to inferior loading from the funnel.

The optically guided fountain is used to load an optical dipole trap in the UHV chamber, using an 'optical trap door'. No additional cooling is required. The dynamics of the atoms in the optical dipole trap are studied. We discuss multiple loading of a conservative trap with the view of accumulating more atoms than can be obtained in a MOT.

ACKNOWLEDGEMENTS

Contents

List of Figures

Statement of copyright:

The copyright of this thesis rests with the author. No quotation from it should be published without their prior written consent and information derived from it should be acknowledged.

H.J.Davies

Chapter 1

Introduction

Laser cooling, first demonstrated in 1985, has provided sources of dense, cold atomic vapours that have found application in many and diverse areas. Ultracold atoms are now used, for example, in precision measurements of gravity [1] and $\hbar/m$ [2], in the new generation of atomic clocks [3] and in atom lithography [4, 5] and spectroscopy [6, 7]. Perhaps the most prominent advance was the observation of the quantum degenerate phenomenon of Bose-Einstein condensation (BEC) in a weakly interacting system in 1995 [8, 9]. Weakly interacting condensates promise to provide insight into related, but more complicated systems, such as superfluid liquid helium. In addition, the coherence properties of atoms coupled out of the condensate are in many ways analogous to properties of photons in a laser beam. Thus, BECs can also be used to create the 'atom laser' [10, 11, 12, 13].

For most cold atom experiments the initial cooling and collection is performed in a magneto-optical trap (MOT). The MOT combines the dissipative nature of near-resonant light with position dependent Zeeman shifts, leading to a confining force. An important quantity defining a trapped atomic distribution is the phase space density, $\rho_{ps} = n\lambda_{dB}^3$, where n is the number density and λ_{dB} is the de Broglie wavelength of the atoms. Whilst the MOT is a good source of cold atoms it has a limited phase space density of $\sim 10^{-5}$. The minimum temperature and the maximum density are set by processes involving near-resonant light. In addition, these high phase space densities can only be obtained for a limited number of atoms ($\sim 10^{10}$). Therefore, the high phase space densities characteristic of quantum degenerate phenomena are beyond the capabilities of the MOT. Current BEC experiments load atoms from the MOT, *in situ* into a magnetic trap, where they can be further cooled by evaporation. Precision measurements are also prohibited in the MOT due to the strong magnetic and optical forces present. Cold atoms are often dropped or launched away from the MOT region to a perturbation free environment.

For many experiments it would be desirable to have a much larger number of atoms or a continuous supply. Overcoming the number and density limits of the MOT requires the absence of near-resonant light. This condition is met in conservative traps (e.g. magnetic or far-off-resonant optical traps). However, these have limited depth and can only be loaded with precooled atoms. One method, then, to accumulate a large number of atoms is to load laser-cooled atoms into a conservative trap spatially separated from the MOT. This motivates the development of techniques to transfer cold atoms efficiently from one region to another with a minimum loss of phase space density, and techniques to load a conservative trap without the aid of near-resonant light. Continuous loading of a conservative trap could lead to steady state BEC and a continuous atom laser.

As mentioned above, two main classes of conservative traps are based on magnetic forces and the dipole force of far off-resonant light. Magnetic forces are generally stronger, but dependent on the internal state of the atom. The dipole force is weak and does not depend on the internal state of the atom. Light potentials are also flexible, providing good spatial and temporal control. In this work we have chosen to concentrate on the use of far-off-resonant light for the manipulation of atoms.

This thesis considers the efficient transfer of cold atoms over a short distance using an optical guiding potential and the subsequent loading of an optical trap without the aid of near-resonant light. Guiding atoms prevents ballistic expansion in two dimensions, reducing the loss of phase space density in the transfer process. We use a focused red-detuned far-off-resonant beam, the simplest optical guide. The atoms are transferred in a vertical, 'fountain', geometry since at the apex of the fountain the atoms are nearly at rest and this facilitates the loading of an atom trap.

The outline of this thesis is as follows: Chapter 2 gives some background to laser cooling and an overview of some related techniques, looking particularly at methods of extracting atoms from the MOT and methods of guiding cold atoms. In chapter 3, we discuss the optically guided atomic fountain for loading a conservative trap. Chapters 4 and 5 are dedicated to describing the experimental details and the process of characterisation and optimisation of the MOT. Since the experiment was set up from scratch, building the MOT represents a major part of our work. Chapter 6 goes on to look at the guided atomic fountain, operating in a pulsed fashion and the

extension to continuous operation. In chapter 7 we investigate a method of loading an optical dipole trap at the apex of the guided fountain. Finally some conclusions and future directions for the experiment are outlined in chapter 8.

During the course of this thesis, the following work has been published:

1. K. Szymaniec, H. J. Davies and C. S. Adams, '*An atomic fountain guided by a far-off resonance laser beam*', Europhys. Lett. **45**, 4, pp. 450 - 455 (1999).

2. L. Nilse, H. J. Davies and C. S. Adams, '*Synchronous tuning of extended cavity diode lasers : the case for an optimum pivot point*', Appl. Opt. **38**, 3, pp.548 - 553 (1999).

3. H. J. Davies and C. S. Adams, '*Mean-field model of a weakly interacting Bose condensate in a harmonic potential*', Phys. Rev. A **55**, 4, R2527 - R2540 (1997).

4. H. J. Davies, K. Szymaniec and C. S. Adams, '*Cold atom accumulation using an optical trap door*', to be submitted.

Items 1 and 4 are discussed in some detail in chapters 6 and 7.

Chapter 2

Laser Cooling and Atomic Beams

2.1 Introduction

The mechanisms of laser cooling have now been extensively studied and much is understood about the behaviour of atoms in a MOT. Magneto-optical traps are now found in many laboratories around the world and form the basis of most experiments with cold atoms. In this chapter the principles of laser cooling are discussed and the mechanisms which limit the phase space density in the MOT are explained. We review some of the existing methods of extracting cold atoms from the MOT and look at how the flux of atoms produced by these methods could be improved by guiding.

2.2 Laser Cooling and the Magneto-Optical Trap

Reviews of the theory of laser cooling can be found in references [14, 15, 16]. The following sections do not aim to reproduce the theory in detail, but instead provide an outline of the main concepts which will be necessary for understanding later chapters.

2.2.1 Doppler Cooling

The first basic tenet of laser cooling is that photons carry momentum which is transferred to any atom absorbing that photon. Atoms absorb uni-directional photons from a laser beam. The subsequent spontaneous emission is a random process, where photons are emitted with a symmetric distribution. Averaging over many emitted photons there is no net change of momentum. The intrinsic asymmetry in the absorption and emission process leads to a radiation force which can be exploited to slow the atom using a laser beam tuned to resonance, counter-propagating with the atom. The idea can be adapted to perform cooling by using two counter-propagating

laser beams and red-detuning the beams such that the atom is Doppler shifted into resonance with the laser beam which is moving towards it. It is thus more likely to absorb a photon from that beam and be slowed. This simple process is known as Doppler cooling. In contrast, diffusive heating, corresponding to a random walk in velocity space of the atoms, arises due to the different direction of the absorbed and spontaneously emitted photons. A balance between cooling and diffusive heating leads to a 'Doppler limit' in temperature, which for one dimensional Doppler cooling is given by:

$$T_{min} \sim \frac{\hbar \Gamma}{2 k_B} \tag{2.1}$$

where Γ is the natural linewidth of the transition. The idea is easily extended to three dimensions producing a system known as *optical molasses* because of the frictional nature of the force. The 1-D case was first proposed in 1975 by Hänsch and Schawlow [17] and by Wineland and Dehmelt [18]. Ten years later, the 3-D case was demonstrated experimentally by Chu *et al.* [19].

Doppler cooling theory assumes a two level atom such that the atom is returned back to the same initial state after one absorption and emission cycle. Alkali metal atoms approximate a two level system, having only a single electron in the outer shell of energy levels. The laser is tuned to an excited state where the dominant decay is back to the ground state and this is referred to as a 'closed transition'. The level structure of ^{85}Rb, the element used in this work, is shown in figure 2.1. For rubidium, T_{min} is 141 μK. The cooling transition is $5S_{1/2}, F = 3$ to $5P_{3/2}, F = 4$. Occasionally an off-resonant excitation to $5P_{3/2}, F = 3$ and subsequent decay to $5S_{1/2}, F = 2$ will remove an atom from the cooling cycle. For this reason an additional laser is needed, tuned to the $5S_{1/2}, F = 2$ to $5P_{3/2}, F = 3$ transition. This laser is commonly known as the *repumping laser*.

2.2.2 Multi-Level Atoms

Doppler cooling as described above is not the whole story. The multi-level nature of real atoms and polarisation gradients of the light field add a further degree of complexity which fortuitously turns out to aid the cooling process [21, 22, 23, 24, 25, 26]. Polarisation gradients lead to wells in the light potential and atoms are cooled into these potential wells, a process known as 'orientational', or 'polarisation gradient cooling'. The optical molasses temperature is proportional to the well depth, which is determined by the light shift, discussed in section 2.4.1:
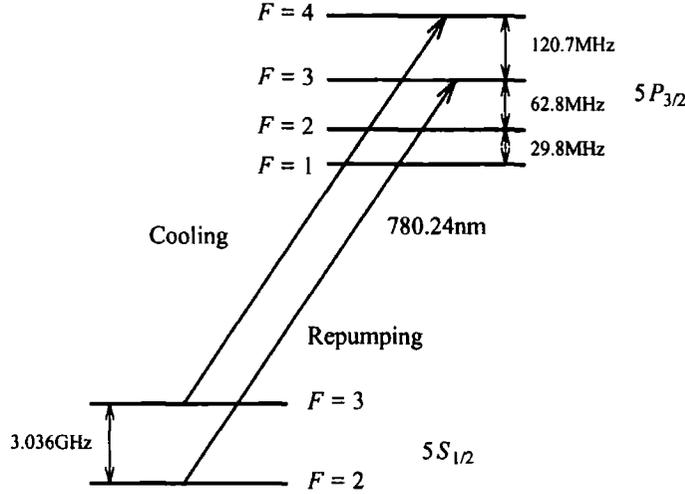
Figure 2.1: The $5S_{1/2}$ and the $5P_{3/2}$ energy levels of [85]Rb [20] . The cooling and repumping transitions are marked.

$$k_B T \propto \frac{\hbar \omega_R^2}{\Delta} \tag{2.2}$$

where ω_R is the Rabi frequency, $(\omega_R = \Gamma \sqrt{I/2I_{sat}}$ and I_{sat} is the saturation intensity) and Δ is the detuning from resonance. In practice this means that the best cooling is achieved by increasing the detuning and lowering the Rabi frequency i.e. lowering the intensity of the cooling light.

Unfortunately there is a limit and this equation does not apply down to absolute zero! Polarisation gradient cooling will not work when the de Broglie wavelength of the atom becomes comparable with the size of the potential wells and thus the semi-classical description above no longer applies. This corresponds to $k_B T \sim \hbar^2 k^2 / 2m$, where k is the wavevector of the light and m is the mass of the atom. This limit is known as the *recoil limit*.

Two sub-recoil cooling mechanisms are known: Raman cooling; and velocity selective coherent population trapping. Both have been demonstrated in the laboratory [27, 28], but neither method was implemented in our work, because of the complexity of the experimental techniques.

2.2.3 The Magneto-Optical Trap

Atoms cooled in optical molasses are not trapped and are free to diffuse out of the cooling region, defined by the overlap of the laser beams. The magneto-optical

trap (MOT) was developed by Raab *et al.* [29] in order to localise the atoms and therefore obtain a higher density. A MOT can be formed using three pairs of counter-propagating beams with $\sigma^+\sigma^-$ polarisations and a magnetic field gradient, where the zero of the magnetic field coincides with the intersection of the laser beams. The magnetic field Zeeman shifts the magnetic hyperfine levels. As the atom moves away from the centre of the MOT it is Zeeman shifted closer to resonance with the relevant counter- propagating beam and is therefore pushed back towards the centre.

Only atoms moving slower than a critical velocity, v_c, can be slowed sufficiently as they pass through the laser beams to remain trapped. A typical value for v_c is 40 ms^{-1} (calculated from the parameters used in our experiment). The MOT can therefore be loaded either from a slow atomic beam or directly from a vapour, where only atoms in the slow tail of the Boltzmann distribution are trapped. The vapour cell MOT [30] is particularly attractive because of its simplicity.

Magnetic fields in the MOT degrade the polarisation gradient cooling, but sub-Doppler temperatures can still be obtained in a MOT. However, the lowest temperatures are achieved by turning off the magnetic field, ramping down the intensity and increasing the detuning for a couple of milliseconds in a final 'molasses' phase.

2.2.4 Density and Number Limiting Processes in the MOT

Initially as atoms are loaded into the MOT, both the number and density increase. The size of the cloud is determined by the temperature of the atoms and thus this phase is known as the '*temperature limited regime*'. However, the maximum density is limited by processes involving near-resonant light. Once the density reaches $\sim 10^{11}$ cm^{-3} it remains constant and adding more atoms simply increases the size of the cloud. In the '*density limited regime*' the temperature of the atoms also starts to increase. The excess temperature goes as $N^{1/3}$ [31], where N is the number of trapped atoms. Thus the highest phase space density will be obtained when the number of atoms is just sufficient to reach the maximum density.

The number of atoms is limited by collisions between ground and excited state atoms in the presence of near-resonant light which can release sufficient energy to eject an atom from the MOT during fine structure changing collisions or radiative redistribution. Collisions between excited state and ground state ultracold atoms take place on a time scale comparable to the radiative lifetime of the excited state. Therefore, emission of a photon during the collision can have a large effect. Ra-

diative redistribution is the process in which a ground state and excited state pair emit a photon during a collision. As a consequence of the attractive potential of the ground-excited state bound pair, the emitted photon has significantly less energy than the photon initially absorbed to create the excited state atom. The energy difference provides sufficient kinetic energy to eject them from the MOT. In a fine structure changing collision the excited state atom changes its fine state. Some of the excess energy, equal to the fine structure splitting, is converted into kinetic energy of the ground and excited state pair.

The density limit, on the other hand, is determined mainly by a process known as *'radiation trapping'*. Reabsorption of scattered photons produces a repulsive force between atoms. This force is balanced by a radiation pressure arising from the optical thickness of the atomic cloud - the outer atoms absorb photons and attenuate the cooling light. The resulting intensity gradient produces a force which compresses the cloud. These two opposing effects do not cancel out, since the frequency spectrum of the re-emitted light is slightly different to that of the cooling light, with the re-emitted light containing a component closer to resonance. The resulting repulsive force sets a limit to the density.

If no effort is made to reduce these effects, the density limit is around 10^{11} cm^{-3} [32, 33, 34, 35]. Ketterle *et al.* improved on this limit by almost a factor of ten by keeping sodium atoms predominantly in the lower hyperfine state (uncoupled to the cooling light) once captured [36]. This was achieved by lowering the intensity of the repumping laser in the central region of the MOT, a so-called *dark spot*. Attempts to reproduce this phase space density increase for heavier alkali metal atoms have been less successful [37]. The larger hyperfine splittings mean that off-resonant excitation into the dark state is lower and it is more difficult to accumulate atoms in the dark hyperfine state by simply lowering the repumping intensity. Alternatively, a 'depumping laser' can be used to pump atoms into the dark state [38].

Overcoming this density limit seems to require the absence of any resonant light and for this reason atoms are often transferred to an alternative trap e.g. a magnetic trap or an optical dipole trap. The conservative trap can be simply overlapped with the MOT and atoms loaded by turning off the MOT. For other applications, e.g. precision measurements, where a perturbation free environment is more important than high density, atoms are extracted from the MOT to form an atomic beam.

2.3 Atomic Beams

Atomic beams have been used in many significant experiments in the past, for example Stern and Gerlach's experiment which showed 'space quantisation' of angular momentum [39] and Rabi's measurement of the magnetic moment of the atom [40]. A great deal of information on atomic structure has been gathered by numerous spectroscopic and scattering experiments on atomic beams. Traditionally beams are produced by effusion from an oven or by supersonic expansion [41], methods that both give a high flux of atoms. A series of slits and shutters leads to a reasonably monochromatic velocity distribution, but at the expense of atomic flux. Typical beam velocities of a few hundred metres per second result in short transit times through the apparatus. In addition, thermal atoms have short de Broglie wavelengths, making the observation of the wave properties of atoms very difficult.

Work with atomic beams has a new dimension due to the development of laser cooling techniques. Initially laser cooling was used to slow a beam in one dimension. For many applications it is now preferred to cool atoms in the magneto-optical trap and extract them to form cold beams or fountains.

Cold atomic beams with their longer de Broglie wavelengths have accelerated the development of atom optics which exploits the wave properties of atoms. Many precision measurements, in particular the atomic clock [3], have also benefited from cold atomic beams because of longer interaction times and greatly reduced Doppler shifts. Collisional shifts then become important. These factors combine to simplify spectroscopic measurements of the internal structure of the atom. Recently, atom lasers have been realised by extracting a coherent beam of atoms from an atomic Bose Einstein condensate [10, 11, 12, 13]. It is possible that in the future the 'atom laser' will replace the MOT as a source of cold atoms for precision measurements.

2.3.1 Slow atomic beams : Review of existing techniques

The first slow atomic beams were produced using the radiation force of a counter-propagating laser beam to slow the atoms in one dimension only. Since the frequency of the light seen by the atoms is velocity dependent through the Doppler shift, the atoms move out of resonance with the beam as they are slowed. Therefore, the frequency of either the laser beam or the atomic transition must be changed accordingly. Two suitable methods are frequency chirping the laser [42, 43, 44] or using a varying magnetic field in a Zeeman slower [45, 46, 47] to arrange for the Zeeman

shift to exactly cancel the Doppler shift at any point along the beam. These schemes produce atomic beams with a velocity of a few tens of metres per second. However, the beams suffer severely from transverse diffusion effects (the atoms are very hot in the directions transverse to propagation). The method was extended to three dimensions using isotropic light in a 'light tunnel', to help alleviate this problem [48].

With the development of the MOT a new source of cold atoms is available and only an extraction technique is necessary in order to produce a beam. The simplest extraction technique is to switch off the MOT and allow the atoms to fall. With a more advanced method a continuous beam can be created.

The 'atomic funnel', first realised by Riis *et al.* [49], is essentially a 2D MOT with trapping in two dimensions, but cooling in three. The MOT is loaded from a Zeeman slower. Atoms are extracted along the axis of zero trapping by shifting the frequency of two counter-propagating beams to cool the atoms in a moving frame with a drift velocity of a few metres per second, a technique known as 'moving molasses'. The funnel produced an integrated flux of sodium atoms of 10^9 s^{-1} with a temperature of 200 μK in a beam moving between 1 and 5 ms^{-1}. A similar funnel was made for rubidium by Swanson *et al.* [50]. In this case a 45° laser beam geometry was used such that the cold beam did not propagate along the axis of a laser beam, with obvious advantages for application of the beam downstream. Swanson *et al.* achieved a flux of 10^{10} s^{-1}, with a temperature of 500 μK, and a beam velocity of 3 - 10 ms^{-1}. The new generation of atomic clocks use similar technology but in a pulsed fashion.

The above schemes could be considered to be methods of *brightening*, rather than *generating* an atomic beam, since the MOT in each case is loaded from a slow beam from a Zeeman slower. The first group to demonstrate the generation of a cold atomic beam from thermal atoms was in Neuchatel (Berthoud *et al.* [51]). The Neuchatel experiment was a vapour cell 2D MOT with atoms extracted using a dc magnetic field rather than moving molasses, which also imposes a drift velocity due to the Zeeman shift of the m = ± 1 magnetic sub-levels. The beam produced had a flux of 1.3 x 10^8 s^{-1} (similar to the loading rate of the MOT), a temperature of 200 μK and a low velocity, between 0.7 and 3 ms^{-1}.

Another scheme known as the LVIS (low velocity intense source), envisaged by

Lu *et al.* [52], uses unbalanced light pressure to extract the atoms. A standard vapour cell 3D MOT was made using three retro-reflected beams. A small hole was drilled in one of the retro mirrors, generating a beam with a narrow, dark central region. Atoms moving into this dark region are accelerated along it by the counter-propagating beam. The atomic beam produced has a flux of 5 x 10^9 Rb atoms/s in continuous operation and 5 x 10^{10} s^{-1} in pulsed operation. The beam velocity was 14 ms^{-1} with a temperature of 25 mK, three orders of magnitude higher than that obtainable in a MOT. Dieckmann *et al* [53] have compared the performance of an LVIS and a 2D MOT with no trapping along one dimension but Doppler cooling in all three dimensions. Atoms are extracted from the 2D MOT using unbalanced light pressure. They found the 2D MOT to be significantly more efficient than the LVIS. They achieved a beam flux of 9×10^9 s^{-1} at a velocity of 8 ms^{-1} and a temperature of 37 mK. Williamson *et al.* have combined the ideas of the LVIS and the pyramidal atom trap of Lee *et al.* [54] to produce a pyramidal funnel where atoms leave in a beam through the apex of the pyramid and enter an UHV vacuum chamber. This funnel was used to load a magneto-optical trap in the UHV chamber ([55]). A similar pyramidal magneto-optical trap was built by Arlt *et al.* [56] in Oxford. Both Dieckmann *et al.* and Arlt *et al.* have used the atomic beams for loading a second magneto-optical trap in an UHV and subsequently obtained BEC.

2.4 Guiding

In all the above schemes the beam expands because of its finite temperature so the density downstream decreases. This is undesirable for applications such as lithography and studies of cold collisions. In addition, in schemes involving transfer from a MOT to another atom trap, the transfer would ideally take place without loss of phase space density.

One method to reduce the loss of density is to guide the atomic beam using a conservative potential, for example, magnetic fields or far-off resonant light. Magnetic forces arise from the Zeeman shift of magnetic sub-levels in a magnetic field and are thus dependent on the internal state. They offer confining potentials of up to 100 mK and are truly conservative. For strong fields permanent magnets are used which prevents switching of the potential.

Far-off resonant light, on the other hand, is very flexible. The light can be quickly switched and the guides are state-independent. The disadvantages include shallow

confining potentials of up to only a few mK and the presence of spontaneous emission, meaning that optical guides are not truly conservative. Almost conservative potentials can be created using very large detunings.

The first atom guide using magnetic fields was made by Friedburg and Paul [57], using six current carrying bars to create a hexapole magnetic field. For a thermal beam only atoms entering the guide with an angle of less than 10 mrad from the axis could be guided. Magnetic guides for laser cooled atoms are very efficient. Examples include work by Kaenders *et al.* [58] using rare earth hexapole magnets and Myatt *et al.* [59] who used permanent magnets fixed along the sides of a tube to guide atoms from a vapour cell MOT to a UHV chamber. Schmiedmayer [60] has demonstrated guiding of atoms orbiting around a current carrying wire. Manipulation of atoms using magnetic fields is discussed in detail in a review by Hinds and Hughes [64]. An interesting extension of guiding is the waveguide, where the de Broglie wavelength of the guided atom is comparable to the transverse dimensions of the guide, implying single mode coherent propagation. A number of schemes have been proposed ([61, 62, 63]).

In this thesis we have concentrated on constructing a guide using the optical dipole force, which is discussed below.

2.4.1 The Optical Dipole Force

There are various ways to understand the origin of the optical dipole force. In a classical picture the force arises from the interaction between an induced atomic dipole moment and the electric field. The atom is viewed as a simple oscillator and the in-phase component of the oscillation gives rise to the conservative potential and the out-of-phase component corresponds to the dissipative part. In an intensity gradient the atom experiences a force known as the optical dipole force.

Alternatively, in a quantum mechanical picture, the optical dipole force can be thought of as a result of the AC stark shift or coupling of the atomic energy levels in an electric field. Perhaps the most convenient description is in terms of *dressed states*.

Dressed states consider the atom and light field jointly. Initially we shall neglect the atom-light coupling. Consider a two level system with a ground state $|g\rangle$ separated from an excited state $|e\rangle$ by an energy of $\hbar\omega_0$, in a light field with a variable

number of photons, N, of energy $\hbar\omega_L$. There will be a ladder of energy levels, where each 'rung' or manifold contains two states $|g, N+1\rangle$ and $|e, N\rangle$ (the next rung down contains $|g, N\rangle$ and $|e, N-1\rangle$). The two states in each manifold are separated by $\hbar\Delta = \hbar(\omega_L - \omega_0)$ and the manifolds are separated by $\hbar\omega_L$. Now, introducing a coupling between the atom and field, the dressed states $|1(N)\rangle$ and $|2(N)\rangle$ are a linear combination of the uncoupled energy levels:

$$|1(N)\rangle = \sin\theta|g, N+1\rangle + \cos\theta|e, N\rangle, \qquad (2.3)$$

$$|2(N)\rangle = \cos\theta|g, N+1\rangle + \sin\theta|e, N\rangle. \qquad (2.4)$$

where $\tan 2\theta = -\omega_R/\Delta$ and ω_R is the Rabi frequency. The Rabi frequency characterises the strength of the interaction,

$$\omega_R = \frac{1}{\tau}\sqrt{\frac{I}{2I_{sat}}}, \qquad (2.5)$$

where $I_{sat} = (\pi hc)/(3\tau\lambda^3)$ is the intensity at which the atom spends one quarter of its time in the excited state and τ is the lifetime of the excited state.

The dressed states differ in energy by $\hbar\Omega_R$ where Ω_R is known as the *generalised Rabi frequency*:

$$\hbar\Omega_R = \hbar\sqrt{\omega_R^2 + \Delta^2}. \qquad (2.6)$$

Neglecting spontaneous emission, atoms propagate in a single dressed state. The optical dipole force arises if there is a gradient in the Rabi frequency, caused by a gradient in the intensity of the electric field (for example across a laser beam). The dressed states then appear as in figure 2.2. Outside the laser beam the states are $|g, N+1\rangle$ and $|e, N\rangle$. Inside the laser beam there is a coupling between the atom and the light, giving the dressed states. Note that if $\Delta > 0$ (blue detuning) an atom in the dressed state $|2(N)\rangle$ sees a repulsive potential and an atom in $|1(N)\rangle$ sees an attractive potential and vice versa for $\Delta < 0$ (red detuning).

Spontaneous emission, however, couples the dressed states giving rise to heating and fluctuations in the sign of the optical dipole force. The heating is a consequence
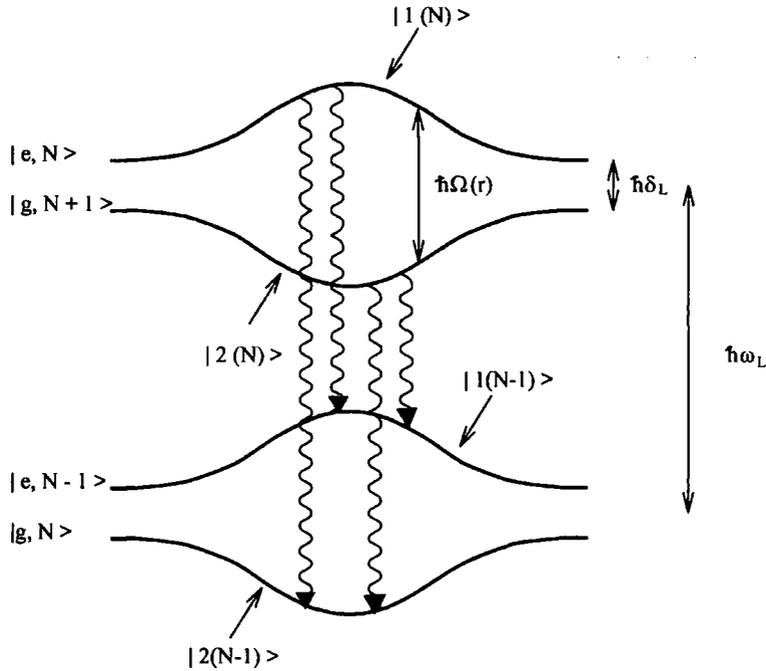
Figure 2.2: Dressed state energy levels as a function of position, across a region of varying light intensity (e.g. across a laser beam). The arrows show allowed transitions for spontaneous emission between dressed states.

of the fact that atoms absorb uni-directional photons from the laser beam and emit the photons in a symmetric distribution. This results in a heating of order E_{rec} for every photon emitted. Fluctuations in the optical dipole force occur because atoms in different dressed states see the opposite sign of the force. The net force felt by the atom will depend on the proportion of time which the atom spends in each state. For resonant light the atoms spend an equal amount of time in each state so that the dipole force averages to zero. For off-resonant light the population of the dressed states can be calculated from the transition rates between the states. According to Fermi's Golden Rule the transition rates between the dressed states will be proportional to the square of the matrix elements. The relevant matrix elements between the states are given by:

$$\langle 1(N)|e\rangle\langle g|1(N-1)\rangle = (\langle e|g\rangle)_{11} = \sin\theta\cos\theta,$$
$$\langle 2(N)|e\rangle\langle g|2(N-1)\rangle = (\langle e|g\rangle)_{22} = -\sin\theta\cos\theta,$$
$$\langle 1(N)|e\rangle\langle g|2(N-1)\rangle = (\langle e|g\rangle)_{12} = \cos^2\theta,$$
$$\langle 2(N)|e\rangle\langle g|1(N-1)\rangle = (\langle e|g\rangle)_{21} = -\sin^2\theta. \tag{2.7}$$

Using equations 2.3, 2.4 and 2.7, we can calculate two important quantities for laser

beam guides and traps, namely the trap depth and the spontaneous scattering rate.

The trap depth at some point in the light field is given by the light shift:

$$U = \frac{\hbar}{2}[\Delta - \sqrt{\omega_R^2 + \Delta^2}].$$ (2.8)

In the limit where $\Delta \gg \omega_R$ the light shift becomes:

$$U = -\frac{\hbar \omega_R^2}{4\Delta}.$$ (2.9)

The limit $\Delta \gg \omega_R$ is known as the *secular approximation* and essentially means that during spontaneous emission, the photons of the laser field are spectators. The spontaneous emission occurs on a much shorter timescale than the atom/light coupling so there is no coherence between the dressed states.

The spontaneous scattering rate can be calculated from equations 2.7 where the transition rates between the states are $\Gamma(\text{matrix element})^2$. In the secular approximation the atom will spend most of its time in the state $|2(N)\rangle$ and will most often fall into the equivalent state one rung down the ladder on emitting a photon. For $\Delta \gg \omega_R$ then:

$$|2(N)\rangle \simeq |g, N+1\rangle + \frac{\omega_R}{2\Delta}|e, N\rangle$$ (2.10)

which leads to a scattering rate for the $|2(N)\rangle$ to $|2(N-1)\rangle$ transition of:

$$\gamma_s = \Gamma \frac{\omega_R^2}{4\Delta^2}.$$ (2.11)

For a more complete description of the dressed state picture see [65].

2.4.2   Guides Using the Optical Dipole Force

The first work using the optical dipole force to manipulate atoms was that of Bjorkholm in 1978 [66] who demonstrated focusing of an atomic beam co-propagating with a laser beam red-detuned from resonance. More recently optical guiding experiments have concentrated on guiding atoms inside hollow fibres [67, 68, 70, 71, 72]. Either red-detuned or blue-detuned light can be used to guide the atoms along the fibre. The red-detuned case was the first to be demonstrated due to its simplicity.

Renn *et al.* loaded atoms into a TEM_{00} mode red-detuned laser beam, which propagates inside the fibre at grazing incidence [67]. The attractive potential prevents the atoms from being absorbed on the fibre walls. However, this method suffers from loss due to spontaneous emission. The laser cannot be sufficiently far detuned to eliminate this effect since the corresponding intensity necessary to guide the atoms would damage the fibre. In addition grazing incidence propagation is very lossy. In Renn's experiment the attenuation length of the laser beam was 6.2 cm, limiting the possible guiding distance. Alternatively a blue detuned TE_{01} mode laser beam can be coupled into the walls of the fibre and the evanescent field in the core provides a repulsive force preventing absorption of the atoms by the fibre walls [72]. The laser beam in this case propagates without significant attenuation. Efficient coupling of the atoms and light to the fibre has proved difficult since fringing modes repel atoms entering the first few millimetres. An additional red-detuned escort laser solved the problem by coupling the atoms into the first few millimetres of the fibre after which the fringing modes have decayed away.

A guide can also be constructed using a free-propagating laser beam. A doughnut-mode blue-detuned laser or a far-red-detuned laser both provide conservative guiding potentials. The doughnut-mode beam can be generated using an axicon [73] or using the LP_{01} mode selectively excited in a micrometer-sized hollow optical fibre by a gaussian laser beam [74]. Schiffer *et al.* have guided atoms loaded into a doughnut mode beam from a Zeeman slower, reducing the waist of the atomic beam from 750 μm to 17 μm [75]. The peak intensity was increased by a factor of two but only 10% of the initial atoms were guided.

The simplicity of the red-detuned focused laser beam as a guide makes it a very attractive option. The downside is that since atoms are guided in the high intensity region of the beam a very high power and large detuning are necessary in order to reduce spontaneous emission.

2.5 Summary

In this chapter we have outlined the main concepts of laser cooling and reviewed some of the existing techniques for manipulating atoms, including the creation of cold atomic beams and atom guides. The processes that lead to a phase space density limit in the MOT were discussed.

Chapter 3

Loading a Conservative Trap

3.1 Introduction

A scheme for loading a conservative trap without the limitations of near resonant light could provide a way to exceed the number limit of the MOT. The shallow depth of atom traps means that atoms must be precooled before loading. The MOT could be used as the source of cold atoms to load a conservative trap which is spatially separated from the MOT. By multiple loading it would be possible to accumulate more atoms than can be obtained from a single load of the MOT. Ideally the transfer to the conservative trap should take place without loss of phase space density.

A number of existing BEC experiments already involve transfer between two atom traps. A double MOT scheme is used to combine efficient collection of atoms in a vapour cell MOT with long lifetimes in an UHV chamber [76]. After multiple loading of the second MOT the atoms are transferred to a magnetic trap for further cooling by evaporation. The second MOT is necessary to regain the phase space density which is lost during the transfer process, despite magnetic guiding. Improved transfer would remove the need for a second MOT. One technique already demonstrated involves magnetic focusing [77] of atoms launched vertically from a MOT to load into an ac magnetic trap. However, fringing fields from the magnetic trap complicate the focusing process. An optical guiding potential is simpler and a good alternative. The most appropriate choice of geometry is the fountain since atoms are nearly at rest at the apex, facilitating loading of a conservative trap. The experimental realisation of an optically guided fountain is discussed below in section 6.3.

The remainder of the chapter discusses techniques for loading conservative traps, including optical pumping, time dependent potentials and buffer gas loading. All

three methods could be used to improve on the number limit of the MOT.

3.2 The Optically Guided Atomic Fountain

In the previous chapter we discussed techniques for creating cold atomic beams and introduced the optical dipole force for guiding atoms. We now look at the specific case of the combination of an atom beam projected vertically and an optical guiding potential to give an optically guided atomic fountain. In any geometry, a continuous beam can provide a high flux of atoms. In a continuously operating guided atomic fountain one could expect to form a column of cold atoms, confined within the guiding beam. The Monte Carlo simulations presented in the following section show that the fountain geometry leads to a density enhancement at the apex.

3.2.1 Density of a Column of Guided Atoms

As previously mentioned, the main motivation for using a guiding potential is to prevent the ballistic expansion of an atom cloud that occurs due to finite temperature. Consider a continuous beam of cold atoms. If they are unguided the density decreases as $1/t^2$, where t is the time of flight, since the cloud can spread out in two dimensions. There is no density decrease along the direction of propagation because the beam is continuous. Adding a 2D tubular guiding potential, with parallel walls, the beam is confined and the density remains constant.

Now consider projecting the beam of atoms vertically, rather than horizontally. Typical trajectories of guided and unguided atoms are shown in figure 3.1, illustrating how the guiding beam confines the atoms.

In this case there is a density enhancement at the point where the atoms turn around under gravity. Such an enhancement could be useful for studying atomic collisions or for loading an atom trap using collisions. It is easy to see how the increase in density arises by simply plotting the parabolic trajectory of the atom's flight. The height, s and the inverse velocity, dt/ds, are plotted as a function of time in figures 3.2a and b, respectively.

Obviously at the top of the trajectory the atom is moving more slowly and hence spends more time. Since $\rho \propto dt/ds$, if we project a continuous beam of atoms vertically with a velocity v and assume a zero velocity spread, the density in the fountain is given by:
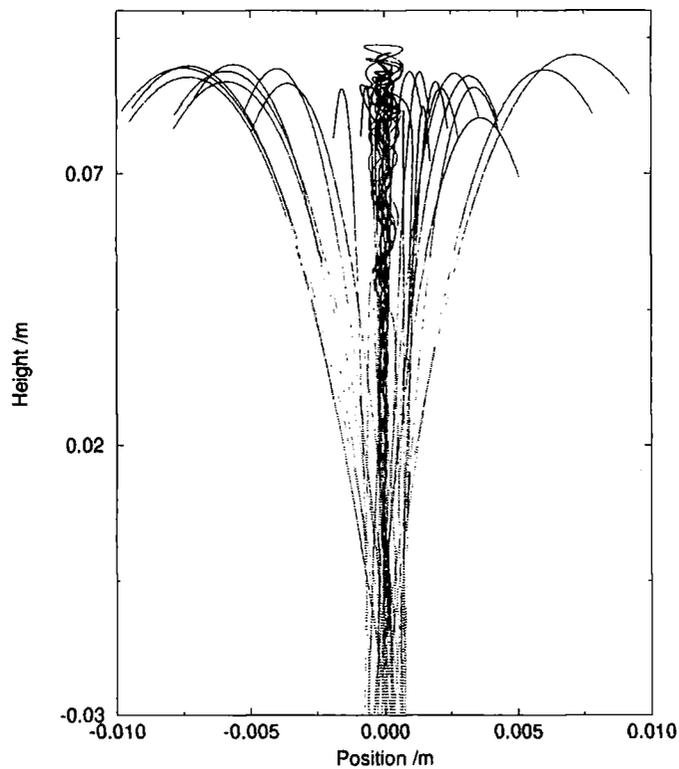
Figure 3.1: Showing typical trajectories of atoms on leaving the optical funnel region. Some are loaded into the optical dipole guide beam and guided in a near vertical trajectory. The others follow parabolic trajectories.
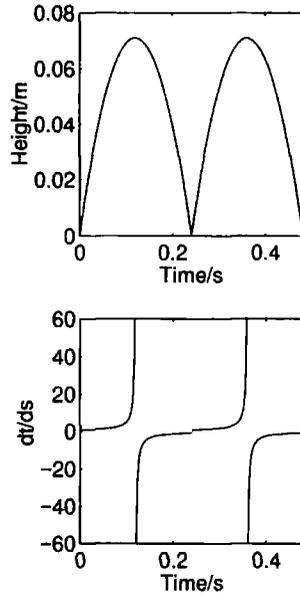
Figure 3.2: a) Height, s, as a function of time, t, for an atom projected vertically with an initial velocity $v = 1.18$ ms^{-1} and subsequently bouncing on a hard potential. b) $\mathrm{d}t/\mathrm{d}s$.

$$\rho \propto \frac{1}{(v^2 + 2gs)^{1/2}}, \tag{3.1}$$

where s is the height in the fountain and g is the acceleration due to gravity.

Assuming a zero velocity spread is unphysical. Figure 3.3 shows the results of a simulation where the atoms loaded into the guiding beam have a temperature of 20 μK.

In our case the guiding potential is not a tube with parallel walls, but a focused gaussian laser beam, with the intensity distribution:

$$I = \frac{w_0^2 I_0}{w^2(z)} \exp\left[\frac{-2(x^2 + y^2)}{w^2(z)} \right], \tag{3.2}$$

and

$$w^2(z) = w_0^2 \left(1 + \frac{z^2}{z_R^2} \right), \tag{3.3}$$

where w_0 is the beam waist at the focus and z_R is the Rayleigh range ($z_R = \pi w_0^2/\lambda$). We performed a Monte Carlo simulation to calculate the density of atoms in an
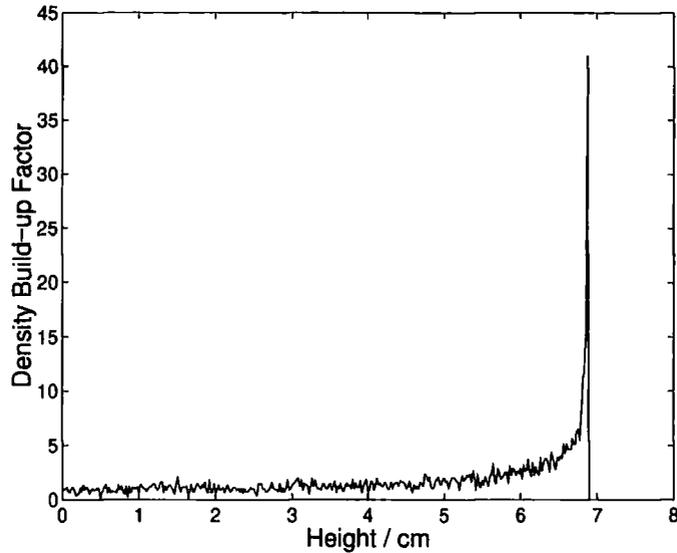
Figure 3.3: Density on axis of an atomic fountain, guided in a potential with hard parallel walls. The temperature of the atomic distribution loaded into the guide is 20 μK.

atomic fountain guided by a focused laser beam. Atoms were chosen at random from a distribution having a gaussian velocity spread of 14 $\hbar k/m$ in all three dimensions and a gaussian position distribution with a diameter of 1 mm in each of the two horizontal directions. The atom is selected if it is trapped in the guiding beam. The atom is then projected vertically with a velocity of 1.18 ms^{-1} starting from a height of -7 cm relative to the position of the focus of the guide. The trajectory is calculated according to:

$$m\ddot{\mathbf{x}} = -\nabla U, \tag{3.4}$$

where U includes the guiding potential and the gravitational potential. The position of the atom is recorded after a random time t, uniformly distributed between zero and T, where T is the time taken for the atom to travel to the apex of the fountain and return to the initial height again. From the final position distribution the distribution of atoms in a continuously operating fountain is deduced. The photon scattering rate in the guide is very low (about 1 s^{-1}), so the effects of spontaneous emission are neglected. Collisions between an atom and another trapped atom or with a background gas are also neglected.

Figure 3.4 shows the results of a simulation for a laser beam of power 10 W, detuning 300 nm and focused to 100 μm.
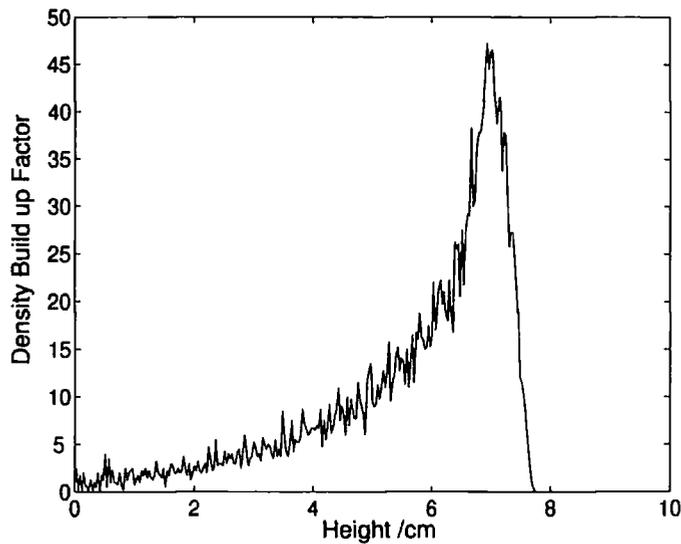
Figure 3.4: Result of a simulation showing the density as a function of height, along the axis of an optically guided atomic fountain. The atoms are launched with a vertical velocity of 1.18 ms^{-1} and have a temperature of 36 μK. The guide laser (power 10 W, detuning 300 nm) is focused to a 100 μm waist at the apex $z =$ 0.07 m. The bin size in the transverse direction was 10 μm.
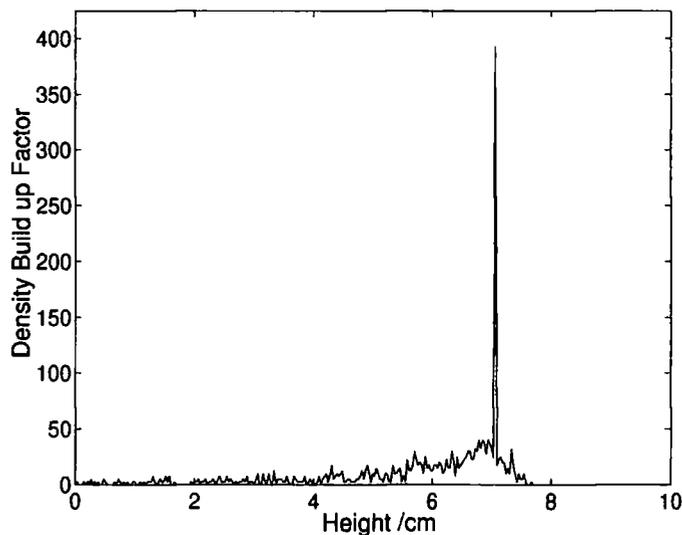
Figure 3.5: Density on axis of a guided atomic fountain with the addition of a crossed dipole beam, focused to 20 μm and aligned horizontally at the apex of the fountain. The bin size in the transverse direction is 10 μm.
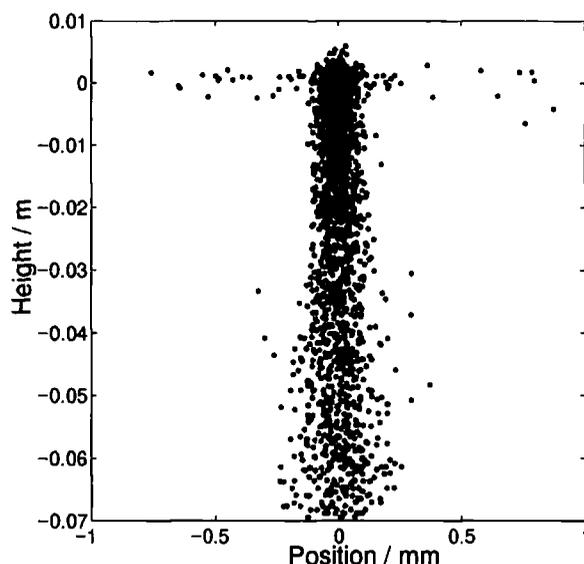
Figure 3.6: Positions of atoms at a random time in an optically guided atomic fountain with a cross-dipole beam at the apex. The guide beam is focused to 100 μm at $z = 0$ and the crossed-dipole beam is focused to 20 μm at x = 0.

There are two effects of the focused beam guiding potential. The first is that as the atoms approach the focus they fall into a potential well. The second is that the focus more tightly confines the atoms in the horizontal directions. This changes the shape of the density distribution. The density at the apex of the fountain is a factor of 45 higher than the initial density. The exact shape of the curve depends on the temperature of the initial distribution.

Finally, a simulation was performed to calculate the density in a guided atomic fountain with an additional red-detuned far-off resonant beam focused to a 20 μm waist and aligned horizontally at the apex of the fountain to form a cross-dipole trap. Figure 3.5 shows the density on axis of the fountain. There is a large density enhancement in the region where the dipole beams cross. Atoms are not actually trapped in this region, since there is no dissipative mechanism, but tend to be compressed into the point where the beams cross, giving rise to the density build up. Such a density enhancement could be useful for collisional loading of an atom trap. The cross dipole beam also couples some of the atoms out along the horizontal direction and these are lost. This loss is visible in figure 3.6, which shows the position distribution at the end of a simulation.

3.2.2 Liouville's Theorem

The well known Liouville's theorem of classical mechanics states that:

'In any isolated system a group of representative points occupying a small hyper-volume in phase space will continue to occupy a constant hypervolume as it moves through phase space' [78]

In an equilibrium system the density of points in any small hypervolume in phase space must stay constant. This implies that there must be no gradient of phase space density, ρ_{ps}, along any trajectory. Otherwise ρ at any given point along the trajectory would change with time. Therefore, *'for an isolated system in equilibrium the phase space density is constant for all mutually accessible localities'*.

The guided atomic fountain is a quasi-equilibrium distribution since atoms enter and exit the fountain at the same rate and with the same velocity distribution. However, the same atomic distribution could be obtained by replacing the input with a hard wall potential and allowing the atoms to bounce. Therefore, whilst there is a density enhancement at the apex of the fountain, Liouville's theorem suggests that the phase space density is constant so the temperature of the atoms has also increased. This was confirmed by comparison of the velocity distribution of the atoms at different points in the fountain.[1]

3.2.3 Summary

A focused red-detuned laser beam can be used to guide laser cooled atoms over a distance of a few centimetres. By using a high power, far-detuned beam the heating due to spontaneous scattering ($\propto I/\Delta^2$, where I is intensity and Δ is detuning from resonance), can be reduced whilst maintaining sufficient trap depth ($\propto I/\Delta$).

In continuous operation, in a fountain geometry, there is a density enhancement at the apex where the atoms are nearly at rest. This can be increased with the addition of a crossed-dipole beam and has potential application in collisional loading of an atom trap.

---

[1] A falling cloud of atoms, in contrast, is not an equilibrium distribution. Consequently the phase space density is conserved locally but not globally.

3.3   Loading Conservative Traps

The optically guided fountain is a good solution to the problem of delivering cold atoms to a conservative trap at a phase space density similar to that obtained in a MOT. Below we shall discuss three techniques for loading the trap: (i) optical pumping; (ii) time-dependent potentials; and (iii) buffer gas loading.

3.3.1   Optical Pumping

Magnetic traps can be loaded by optical pumping from an untrapped state to a trapped state. Obviously resonant photons can disturb trapped atoms. This can be avoided by pumping to a dark state. One such scheme is used in Cornell's scheme for multiply loading strong-field seekers into an ac magnetic trap [77]. Caesium atoms are launched towards the trap in $F = 4$, $m_F = 4$, a weak-field seeking state, which is repelled by the trap. As they come to rest they are optically pumped using light tuned to $F = 4 \rightarrow F' = 4$, linearly polarised along the magnetic field, with the corresponding selection rule $\Delta m = 0$. Atoms are transferred to $F' = 4$, $m'_F = 4$ and can then decay to the $F = 3$, $m_F = 3$ ground state. The optical pumping removes energy from the atoms and also transfers them to a trapped state, which is transparent to the optical pumping light. A similar scheme could be used to transfer atoms into a conventional magnetic trap for weak-field seeking atoms. An appropriate scheme for ^{85}Rb would involve transfer to the trap in $F = 3$, $m_F = -3$, which is pumped to $F' = 3$, $m'_F = -3$ using light linearly polarised along the magnetic field. The atoms could then decay to $F = 2$, $m_F = -2$, a low-field seeking state.

Optical pumping could be an excellent method for accumulating atoms in a magnetic trap and increasing the phase space density. Williams *et al.* have presented calculations suggesting that it should be possible to obtain steady state BEC by this method [79]. However, the presence of the few resonant photons scattered by atoms added to the trap would probably destroy the condensate. Steady state BEC may require a loading technique that does not involve any near-resonant light.

3.3.2   Time-Dependent Potential

Most conservative traps are loaded by overlapping the trap with the MOT and then switching the MOT off. This is essentially a time-dependent scheme, where atoms are initially nearly at rest and the trapping potential is introduced around them. A similar scheme could be used at the apex of the guided fountain where the atoms are nearly at rest.
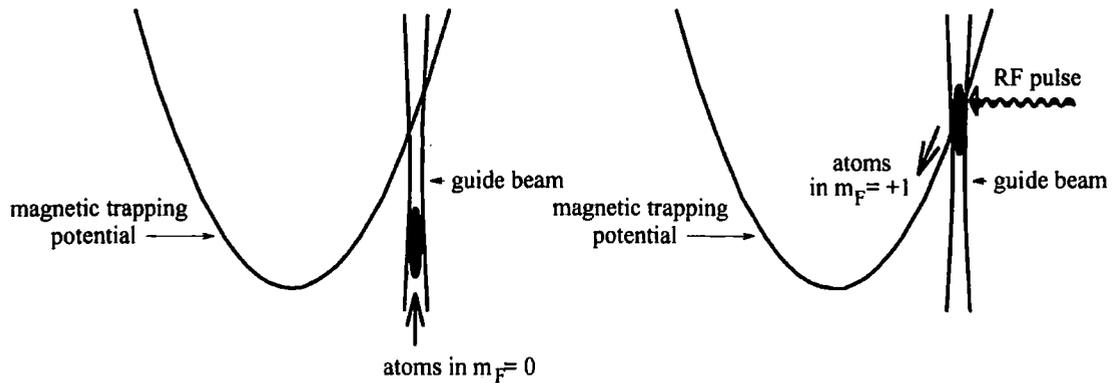
Figure 3.7: Schematic for loading into a magnetic trap using a time dependent potential. Atoms are delivered to the trapping region in a magnetically insensitive state and are coupled into the trap using an rf transition to a trapped state.

A great number of trapping geometries using far-detuned light or magnetic fields can be envisaged. Figure 3.7 illustrates just one possible geometry for a trap with a time-dependent input. In the case illustrated, the trap is a magnetic trap and the input is a pulse of rf radiation which couples atoms from an untrapped to a trapped state. The frequency of the transition is position dependent so the atoms can be coupled into the side of the trap. Atoms can therefore only leave the trap at this position. Atoms coupled in fall into the potential and oscillate in the trap. By switching the input, multiple bunches could be loaded. Obviously, in order to see any accumulation the number added to the trap on each load must be greater than the loss in between loads (trap loss) and the loss occuring when the trap is opened to allow a new bunch of atoms to enter (trap leakage).

If the trap leakage can be neglected and the lifetime for each load of atoms is the lifetime of the trap (limited, for example, by collisions with a background gas), the steady state number of atoms is equal to the product of the lifetime and loading rate. A typical loading rate curve might look like the solid line of figure 3.8 (10^{10} atoms added every second to a trap with a lifetime of 10 seconds). Traps with lifetimes greater than 200 s have been demonstrated using magnetic fields or very far-detuned, high power light, in UHV [80]. With a loading rate of 10^{10} s^{-1} one could expect to accumulate more than 10^{12} atoms, two orders of magnitude higher than has been obtained in a MOT.

However, as the density in the trap builds up the trap leakage increases. The
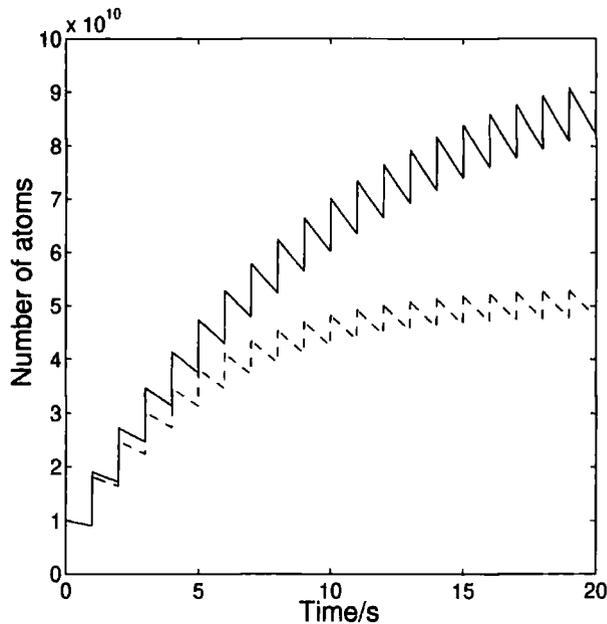
Figure 3.8: Theoretical loading curves for multiple loading of a trap with a time-dependent input. For both curves 10^{10} atoms are added every second and the lifetime of the trap is 10 seconds. For the solid curve, trap leakage on adding each new bunch of atoms has been neglected. For the dotted line there is a loss of 10% of the trapped atoms each time the trap is opened to allow a new load in.

steady state occurs when the density of trapped atoms at the input is equal to the density of the incoming atoms. In this case the maximum number in the trap is limited by the trapping volume and the filling curve resembles the dashed line in figure 3.8. An experimental realisation of loading in a time dependent conservative potential is described in section 7.4.

3.3.3 Buffer Gas Loading

A group at Harvard have demonstrated magnetic trapping of atoms and molecules without using any near-resonant light [81, 82, 83, 84]. The method relies on thermalising a paramagnetic species by collisions with a cold buffer gas, for example ^{3}He or ^{4}He. The paramagnetic species can be cooled from room temperature to a few hundred milliKelvin, cold enough to load a trap. To date, buffer gas loading and magnetic trapping of atomic europium [82], atomic chromium [83] and calcium monohydride [84] has been demonstrated. Since no near-resonant light is used, the number and density limits of the MOT do not apply. In fact, 10^{12} europium atoms were trapped (two orders of magnitude higher than has been obtained in a MOT), at a peak density of 5×10^{12} cm^{-3} and a temperature of 800 mK. The method re-
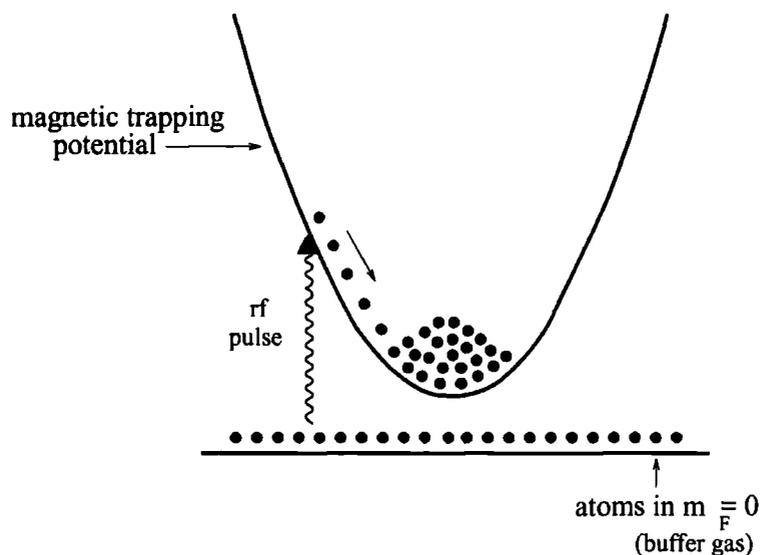
Figure 3.9: Schematic for buffer gas loading into a magnetic trap. Atoms are delivered to the trap in an untrapped state. A proportion are coupled into the trap. Collisions with untrapped atoms, which are continually replaced, thermalises the trapped distribution.

quires a very large number of buffer gas atoms. Further cooling by evaporation from the magnetic trap could be used to increase the phase space density of the trapped sample [85].

A very attractive feature of the buffer gas loading scheme is its general applicability - *any* paramagnetic species can be trapped. However, adapting the scheme to temperatures characteristic of laser cooled atoms would lead to a high initial phase space density [86]. The optically guided fountain in combination with a magnetic trap could be used for this purpose.

A schematic is depicted in figure 3.9. Cold atoms are delivered to the trapping region in an untrapped state. A proportion are coupled into the trap using an rf transition. The radiation is then switched off so that there is essentially no evaporation from the trap. Instead, excess energy is removed by collisions with cold, untrapped atoms. One possible method of providing the buffer gas is to use atoms of the same species in an untrapped state that are continually delivered to the trapping region, can collide with the trapped atoms, but then leave the region, carrying away the excess kinetic energy. An alternative is to use a MOT of a different species. The trapped atoms would be transparent to the cooling light.

In this scheme the ratio of buffer gas atoms to trapped atoms is much smaller than in the helium scheme. We present simulations of the ratio of buffer gas to trapped atoms that is necessary to efficiently remove energy.

Simulations

We have performed simple Monte Carlo simulations to model the loading process. Simulations of collisional processes in a harmonic trap leading to evaporation are discussed in [87]. Here, we aim solely to gain insight into the necessary conditions for buffer gas loading.

In the simulations, the trap is represented by a box potential, of depth ξ_t. A distribution of atoms are initially trapped, with temperature T and a uniform position distribution. The simulation proceeds in time steps dt where $dt \ll \tau_i$, the initial mean collision time. Typically dt is $0.01\ \tau$. At each time step, atoms which may collide are selected randomly from the distribution. An acceptance/rejection method [88] is used to determine whether a collision does occur. The probability of a collision, $p(coll)$ is equal to dt/τ_{atom}, where τ_{atom} is the mean collision time, weighted by the relative velocity of the two atoms selected. The rejection method involves selecting a random number I_{ran} from a Poisson distribution with a mean given by dt/τ_{atom} and comparing the random number to $p(coll)$. If $p(coll) > I_{ran}$ then a collision occurs. The collision is calculated in the centre of mass frame of the two particles and after transforming back to the laboratory frame, the velocities of the particles are updated. If τ is a function of time, a new mean collision rate is calculated from the new velocity and number of trapped atoms after each time step.

First consider the rate of thermalisation in a homogeneous trap. Consider a distribution, where the initial mean square velocity along the x and y axes is v_i^2 and the initial along the z axis is $2v_i^2$ (figure 3.10) or $3v_i^2$ (figure 3.11) in an infinitely deep trap (i.e. no evaporation). The time constants for thermalisation are both $0.9\ \tau_i$.

The buffer gas is modelled by a distribution of atoms that have equal probability of colliding with the trapped atoms, but whose velocity is not changed in a collision, since the colliding buffer gas atoms are replaced by new 'cold' atoms. Let the number atoms already in the trap be N_t, the number of atoms added in be N_a and the number of buffer gas atoms be N_b.

Figure 3.12 shows the evolution of the mean energy of trapped atoms after adding
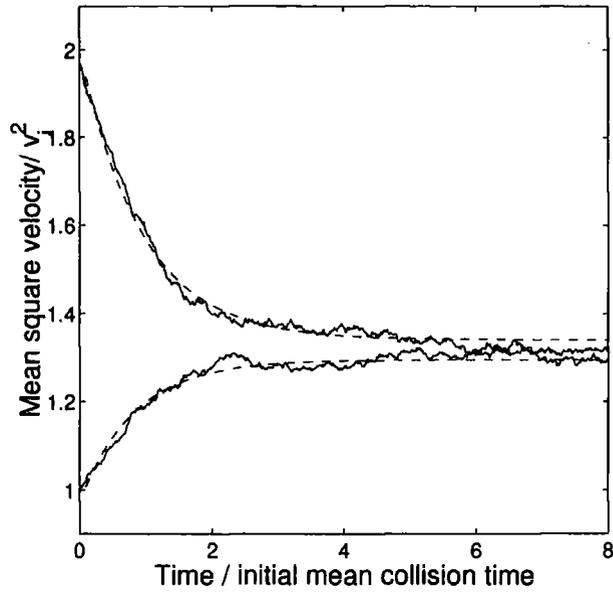
Figure 3.10: Rate of thermalisation of a gas in a homogeneous potential, where the initial mean square velocity along the x and y axes is v_i^2 and along the z axis is $2v_i^2$. The upper curve shows the evolution of the mean square velocity along the z axis and the lower curve shows the evolution of the mean square velocity along the x axis. The curves have been fitted with exponentials (dashed lines).
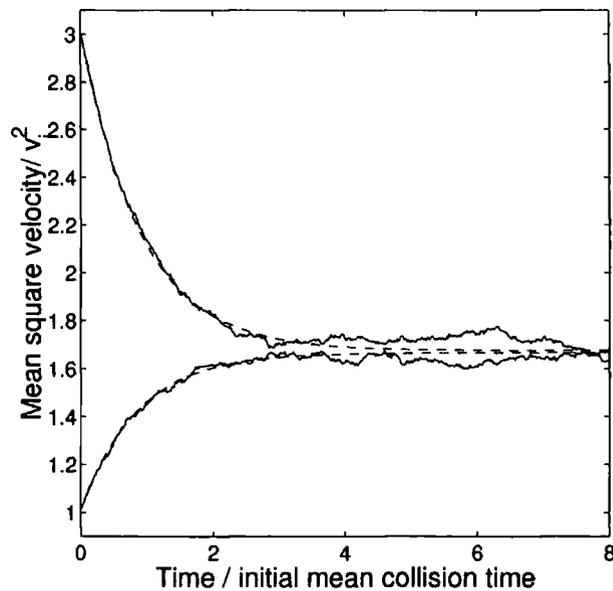
Figure 3.11: Rate of thermalisation of a gas in a homogeneous potential, where initially the mean square velocity along the x and y axes is v_i^2 and along the z axis is $3v_i^2$. The upper curve shows the evolution of the mean square velocity along the z axis and the lower curve shows the evolution of the mean square velocity along the x axis. The curves have been fitted with exponentials (dashed lines).
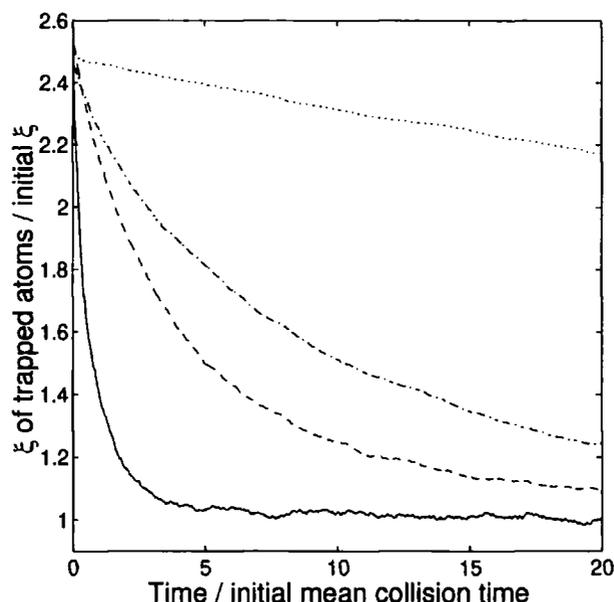
Figure 3.12: Mean energy per particle as a function of time for a distribution of trapped atoms, after adding some hot atoms, in the presence of a buffer gas. The ratio of $N_t : N_a$ is 5 : 1. The ratio $N_b : N_a$ is: solid 5 : 1, dashed 1 : 1, dot-dashed 1 : 2, dotted 1 : 20.

some hotter atoms, for different ratios $N_b : N_a$. The ratio $N_t : N_a$ is 5 : 1. The atoms are coupled in at a trap depth of 10 kT. The temperature of the buffer gas and of the initial trapped distribution is kT. For a ratio of $N_b : N_a$ of 5 : 1 the atoms thermalise after less than 2 collisions; for a ratio of 1 : 1, approximately 10 collision times are required; for a ratio of 1 : 2, more than 20 collision times are needed. The thermalisation for different ratios of $N_t : N_a$, for constant $N_a : N_b$ is shown in figure 3.13. Figure 3.14 shows the rate of thermalisation for different energies of the atoms added in, for constant ratio of $N_t : N_b : N_a$ of 5 : 1 : 1. Complete thermalisation occurs after approximately 15 τ_i regardless of the energy of the atoms added in.

We should note here that in a homogeneous potential the collision rate increases with temperature since the density remains constant. The opposite is true for a parabolic trap.

Summary

To relate these results to a real situation, consider a magnetic trap containing 4 $\times$ 10^6 atoms at a density of 2 $\times$ 10^{10} cm^{-3} and a temperature of 90 μK (these are
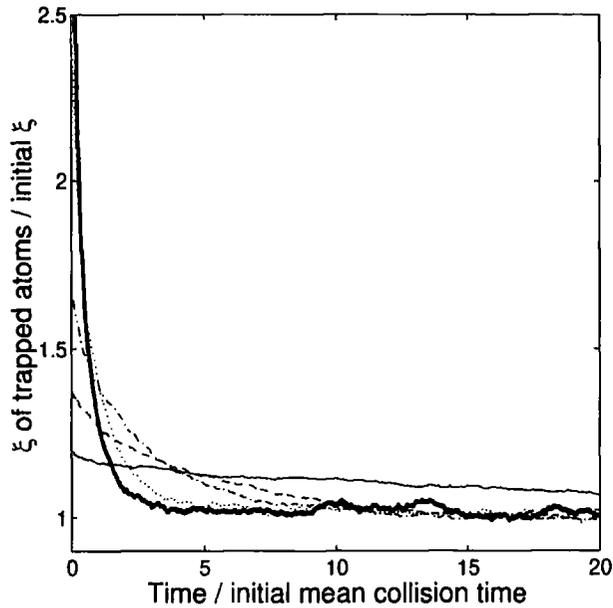
Figure 3.13: Mean energy per particle as a function of time for different ratios of $N_t : N_b : N_a$. Solid line: $N_t : N_b : N_a = 50 : 1 : 5$, dashed: $50 : 2 : 10$, dotdashed: $50 : 4 : 20$, dotted: $50 : 10 : 50$, thick solid: $50 : 20 : 100$
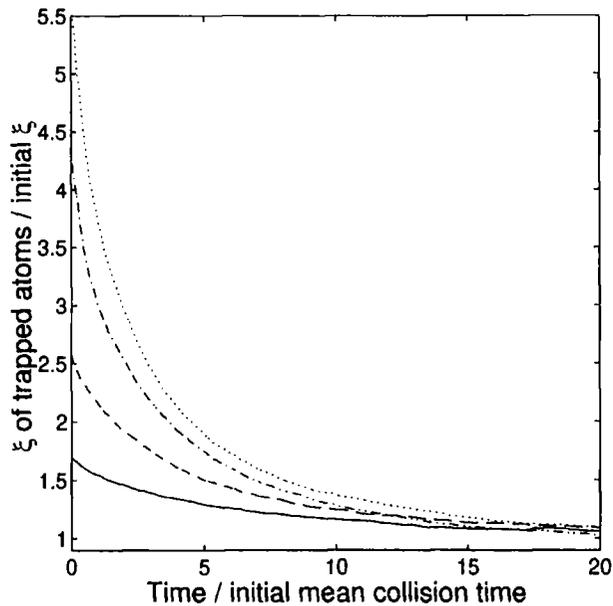
Figure 3.14: Mean energy per particle as a function of time for a constant ratio $N_t : N_b : N_a$ of $5 : 1 : 1$ for different energies of the added particles. The temperature of the buffer gas and of the initial trapped distribution is T. For the solid line $T_{add} = 5\ T$, dashed $T_{add} = 10\ T$, dotdashed $T_{add} = 20\ T$, dotted $T_{add} = 30\ T$.

the parameters for the starting conditions for the magnetic trap in the first BEC experiment [8]). This corresponds to an initial mean collision rate of 3 s^{-1}. For a ratio of $N_t : N_a : N_b$ of 5 : 1 : 1, 8×10^5 atoms must be coupled in and there must be a background of 8×10^5 buffer gas atoms that are continually replaced on a timescale much shorter than the timescale for thermalisation. Approximately 15 initial mean collision times or 5 seconds is needed for complete thermalisation. These conditions might be met at the apex of a guided fountain with a flux of 10^8 s^{-1}, operating continuously, or quasi-continuously. Atoms will spend of order 10 ms in the region of the magnetic trap at the apex of the fountain and the number of atoms in the fountain overlapping with the trap at any one time is $\sim 10^6$. For a magnetic trap with a lifetime of 200 seconds, this is a reasonable method for accumulating atoms and increasing the phase space density. Obviously, as the number of trapped atoms increases, the ratio $N_t : N_b$ will increase and the thermalisation process will slow down.

3.4 Conclusion

A continuously operating optically guided fountain can be used to transfer laser-cooled atoms from a MOT to a conservative trap, conserving phase space density. The conservative trap can then be loaded directly, without the need for a second magneto-optical trap. Multiple loading can be used to accumulate a large number of atoms, which would be useful for improving signal to noise ratios in precision measurements or for creating larger Bose-Einstein condensates.

Conservative traps include magnetic traps and far-off resonant light traps. We have described three methods for loading magnetic traps - optical pumping from an untrapped to a trapped state, loading using a time-dependent potential and buffer gas loading, where the buffer gas is provided by atoms in an untrapped state delivered by the optical fountain. Trapping a large number of atoms in an optical dipole trap would be advantageous for spectroscopic and collisional studies. In addition, the accumulation of a large number of atoms in an optical dipole trap would be a first step towards an all optical route to BEC [89]. Of the loading methods discussed, the time-dependent potential is most suitable for loading an optical dipole trap. This is investigated experimentally in chapter 7.

Chapter 4

Experimental Setup

The foundation of nearly all experiments on cold atoms is a magneto-optical trap (MOT). This chapter describes the components of the MOT, including the lasers, the vacuum system, the magnetic trapping potential and the computer controlled timing and data acquisition system.

The main aims of the experiment - demonstrating a continuous beam of cold atoms guided over a short distance and the loading of a second atom trap at the apex of the fountain - influenced certain aspects of the design.

Firstly the quartz cell was chosen to have two regions, one of which would act as a vapour cell to give fast loading of a MOT, whilst the other could be differentially pumped giving a lower pressure and longer lifetimes for a second atom trap. In addition the cell has good optical axis, allowing for the possibility of large diameter cooling beams and study of an atomic beam anywhere along its path.

The magnetic field coils were designed to give an anisotropic trapping potential, giving weaker confinement along the vertical direction. The resulting magneto-optical trap is elongated and therefore well mode-matched for loading into a tubular guide, such as a laser beam.

4.1   The Vacuum System

The vacuum system is shown in figure 4.2. The cell is made from 6 mm thick amorphic quartz plates which have been polished to a flatness of order 100 nm. It consists of two regions connected by a hole of 1 mm diameter, the lower chamber measuring 16 cm × 9 cm × 9 cm and the upper chamber 3 cm × 3 cm × 10 cm. The large cells give nearly unlimited optical axis, but are not anti-reflection coated. Both ends are
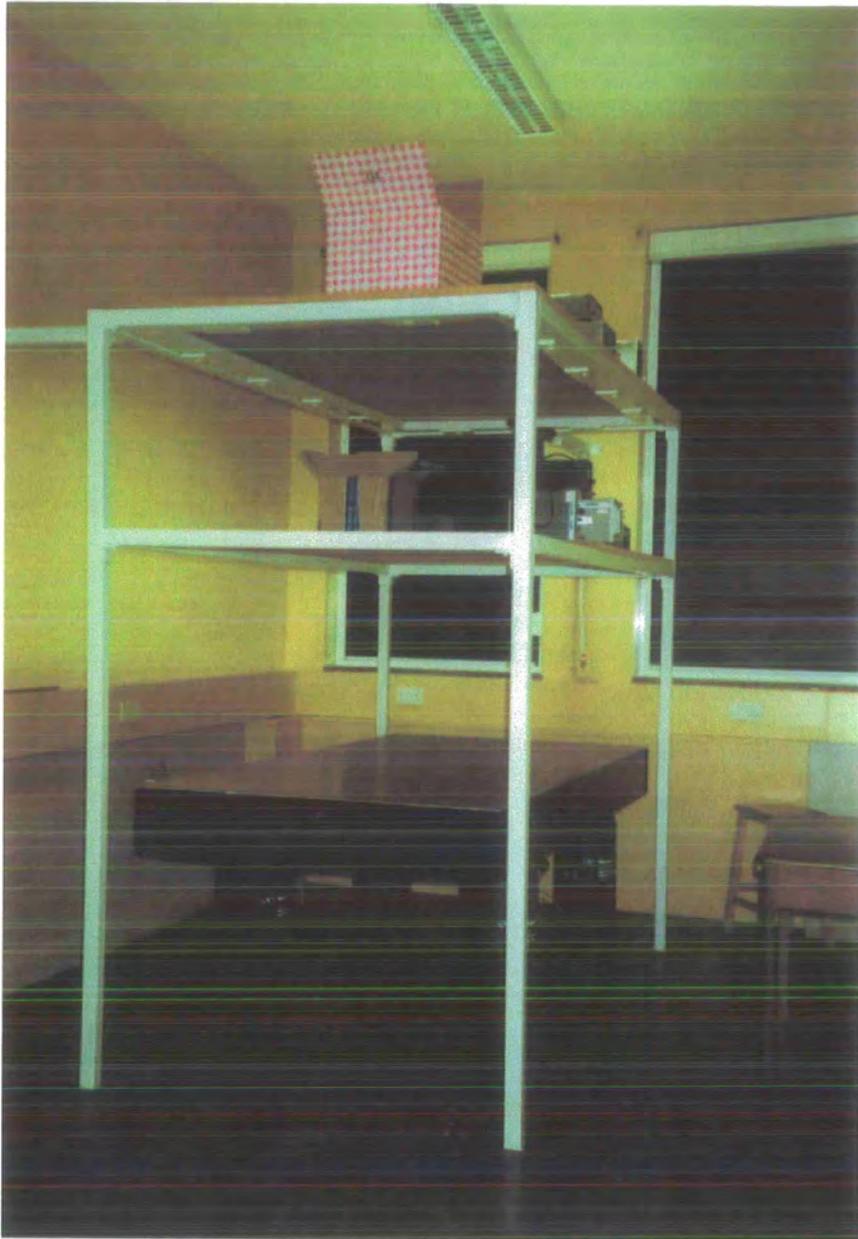
Figure 4.1: A photograph of the lab. in April 1997.
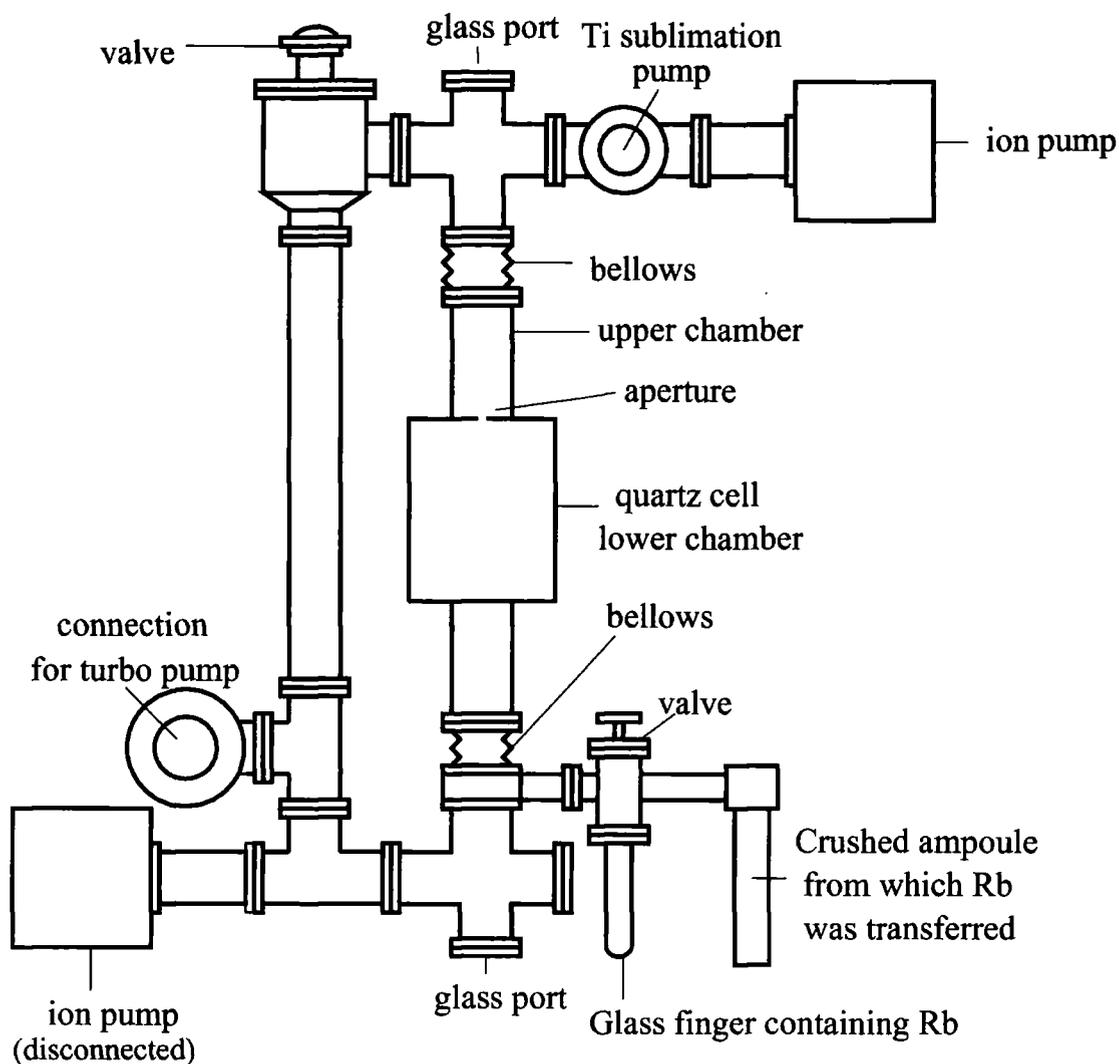
Figure 4.2: The vacuum system

mounted via bellows to avoid stressing the cells.

The pressure in the smaller of the two vapour cells was 3×10^{-10} Torr as measured on an ion gauge (AIG 17). Initially, the system was pumped using a turbo pump and baked at 200°C for two weeks giving a pressure of 3×10^{-7} Torr, which decreased to a pressure of 3×10^{-10} Torr when the system was cooled back down to 20°C. After switching off the turbo pump, an ion pump near the top of the system was turned on to give a pumping rate of 25 l/s. The lower ion pump in the figure has not been connected. Ion pumps can be damaged by alkali metal atoms and therefore graphite tubes were inserted into the vacuum chamber directly in front of the lower ion pump to absorb rubidium atoms.
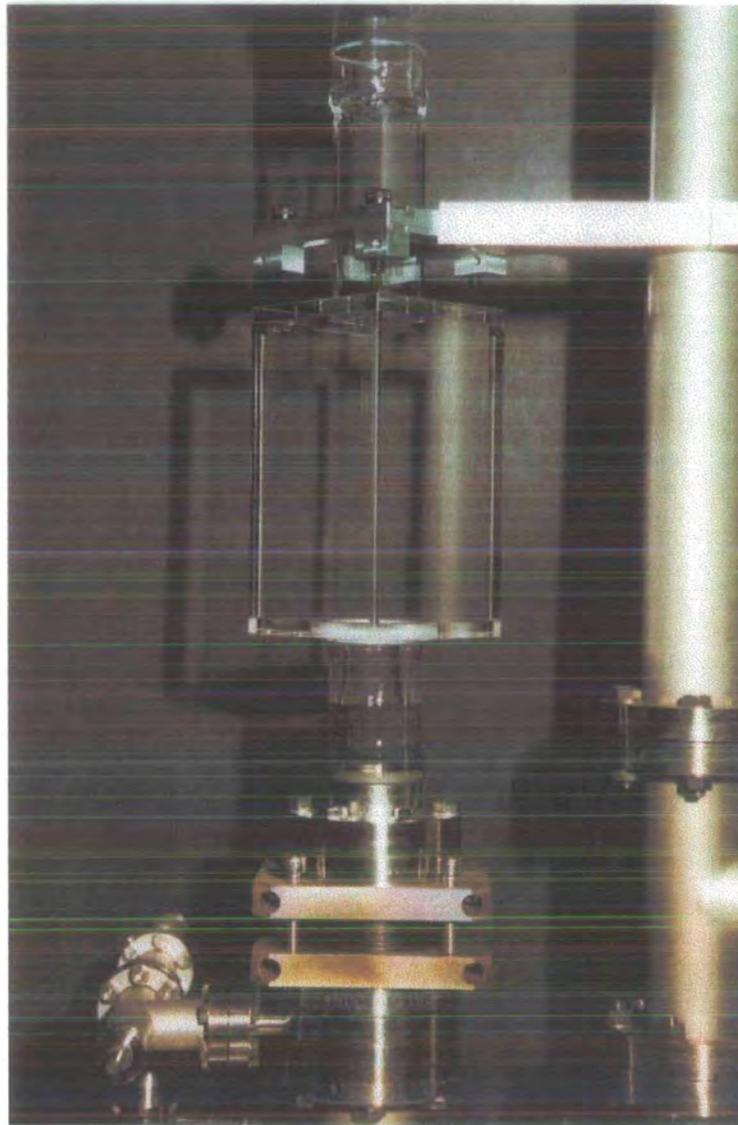
Figure 4.3: A photograph of the quartz cell, showing the two chambers connected by a small aperture. The cell is mounted at both ends using bellows. Photograph courtesy of Vicki Greener, Physics Audio Visual Department.
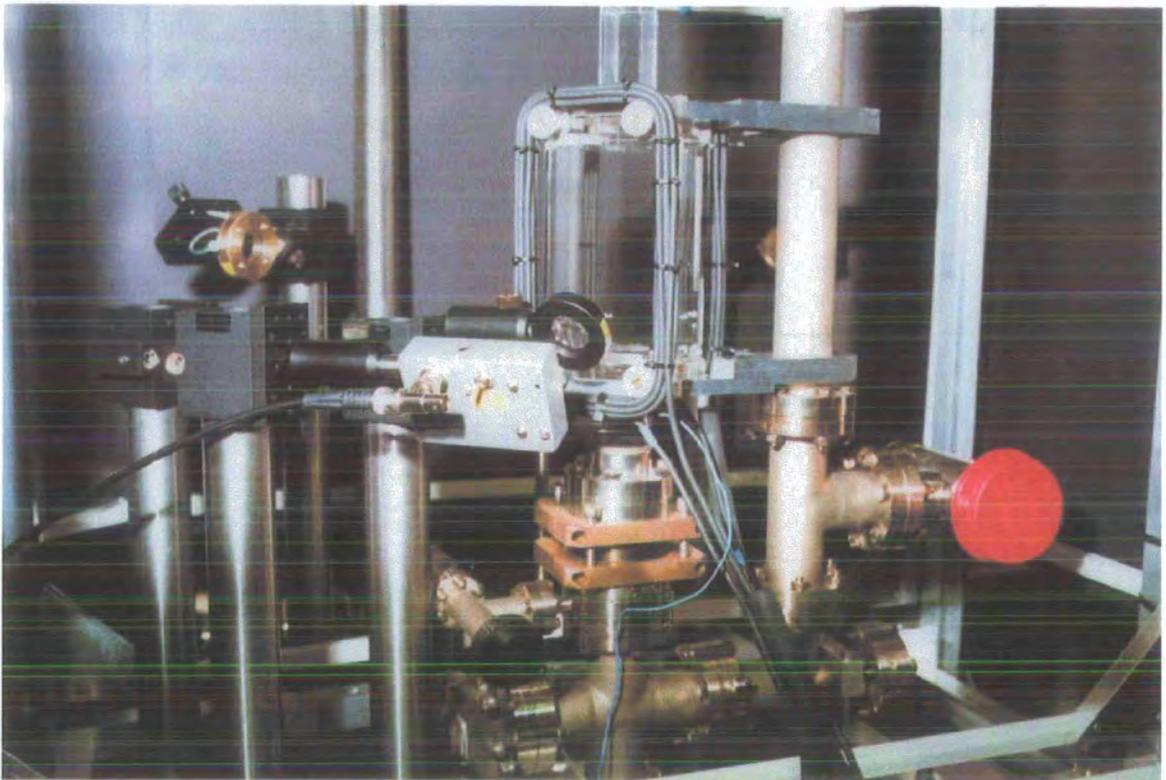
Figure 4.4: A photograph showing the magnetic field coils and the vacuum chamber. Photograph courtesy of Vicki Greener, Physics Audio Visual Department (June 1998)
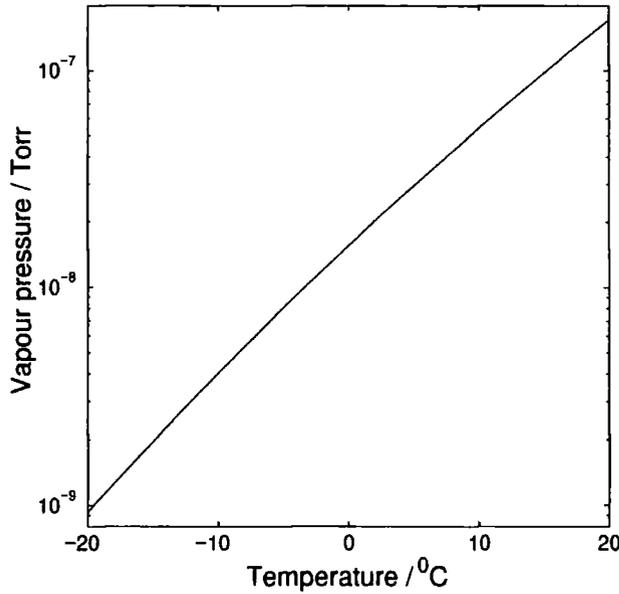
Figure 4.5: Vapour pressure of rubidium as a function of temperature.

The Rb pressure in the lower chamber can be varied by temperature controlling the glass finger containing Rb. The vapour pressure is expected to vary with temperature as below [91]:

$$\log(p/Torr) = A - \frac{B}{T/K} + C(T/K) + D\log(T/K), \qquad (4.1)$$

where A = −94.04826, B = 1961.258, C = −0.03771687, D = 42.57526 and T is the absolute temperature of the Rb reservoir. The vapour pressure is plotted in figure 4.5. The pressure increases by approximately an order of magnitude for a temperature increase of 20°C. Since there is no direct line of sight from the rubidium reservoir to the vapour cell it is necessary to heat both the reservoir and the vacuum chamber en route to the vapour cell in order to achieve high vapour pressures (e.g. 10^{-7} Torr).

4.2 The Lasers

4.2.1 Extended Cavity Diode Lasers

Semiconductor diode lasers have become very popular in atomic physics in recent years [92, 93, 94, 95, 96] because they are relatively cheap, compact and convenient to run. A free-running diode laser has a linewidth of several MHz and can be tuned

by varying either the current (3 GHz/mA) or the temperature (30 GHz/K). Neither of these methods give continuous tuning because of mode hops of the laser cavity. A well established technique for both narrowing the linewidth (from 1 MHz to 100 kHz) and for tuning the laser, is to build an external cavity by feeding back the first order diffracted beam from a grating (the Littrow configuration). The zeroth order light is used as the output, see figure 4.6.

The wavelength of the feedback light is given by the grating equation:

$$n\lambda = 2d\sin\theta, \tag{4.2}$$

where d is the grating spacing. Since the wavelength of the laser is determined by the wavelength of the feedback light, the extended cavity diode laser (ECDL) can be tuned by rotating the grating with respect to the laser. The range over which the laser can be tuned is limited by the additional standing wave criterion :

$$m\frac{\lambda}{2} = L \tag{4.3}$$

i.e. only an integer number of half wavelengths is allowed in a cavity of length L. By careful choice of the pivot point about which the diffraction grating is rotated, L and θ can be changed to fulfil equation 4.2 and 4.3 over a range of several hundred GigaHertz. For a full discussion of this consideration see [97]. However, if a tuning range of only a few GHz is required, as in this work, the position of the pivot point is not critical.

Good alignment of the feedback light into the laser cavity is vital. The threshold current is minimised for good alignment and this proved to be a good diagnostic for aligning the feedback.

The ECDL system built for this experiment used a SDL GaAlAs, 50 mW diode laser, with a wavelength specification of 781 nm at 25°C. The output beam is collimated using an aspheric lens with focal length of 4.4 mm. A diffraction grating is mounted on a standard Thorlabs mirror mount such that its angle relative to the laser can be changed. A piezo placed at one corner of the mirror mount enable the laser to be scanned over a few GigaHertz by applying a voltage. The external cavity has a length of 1.5 cm and the holographic grating has 1800 lines per mm. Two levels of temperature stabilisation are employed; one for the laser itself and the other
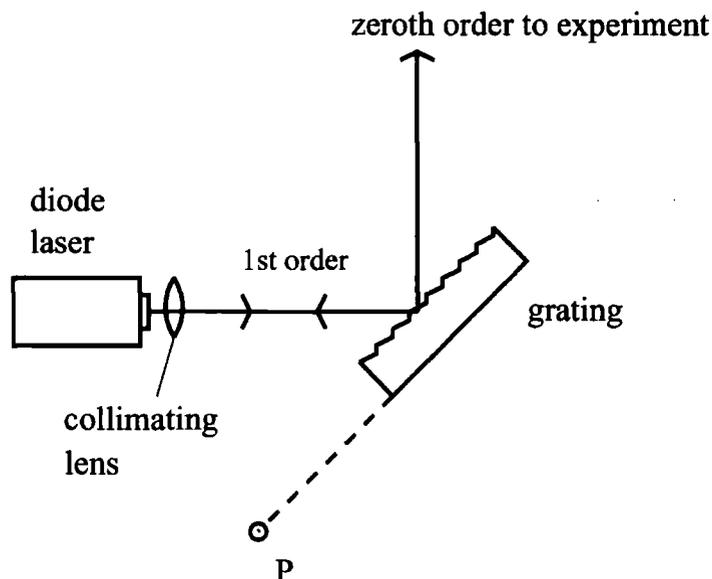
Figure 4.6: A diagram of the Littrow configuration for an extended cavity diode laser (ECDL). The first order light from a diffraction grating is reflected back into the laser diode. The zeroth order is the ouput of the ECDL. The grating can be rotated about a pivot point P, by use of a piezo electric element.

for the external cavity to prevent change of the cavity length. This eliminates large drifts in the frequency so that the laser can be locked by feedback to the current only. The laser is isolated from vibrations transmitted through the optical table by a foam base, approximately 15 mm thick. Air currents are also excluded using a perspex box. A diagram of the laser system is shown in figure 4.7.

4.2.2 Saturated Absorption Spectroscopy

The laser was used to perform spectroscopy on Rb vapour (containing both [85]Rb and [87]Rb isotopes) in a cell (figure 4.8). A pump beam was aligned through the cell to saturate the $5S_{1/2}$ to $5P_{3/2}$ transitions in the Rb vapour. The pump beam has a power of ~ 0.8 mW and is expanded to a beam of diameter 8 mm to give an intensity of 16 Wm^{-2} (c.f. I_{sat} is 16.3 Wm^{-2}). The absorption spectrum is Doppler-broadened because thermal atoms moving with a velocity v see the laser frequency shifted by kv, where k is the wavevector of the light. The beam was then attenuated and retro-reflected. Atoms that have non-zero velocity see the counter-propagating beams with different detunings and if the beams are not too intense, the absorption of one beam will not affect the absorption of the other. However, for atoms with $v = 0$, there is no Doppler shift so the presence of one beam reduces the absorption of the other. Figure 4.9 shows a typical saturated absorption spectrum obtained by
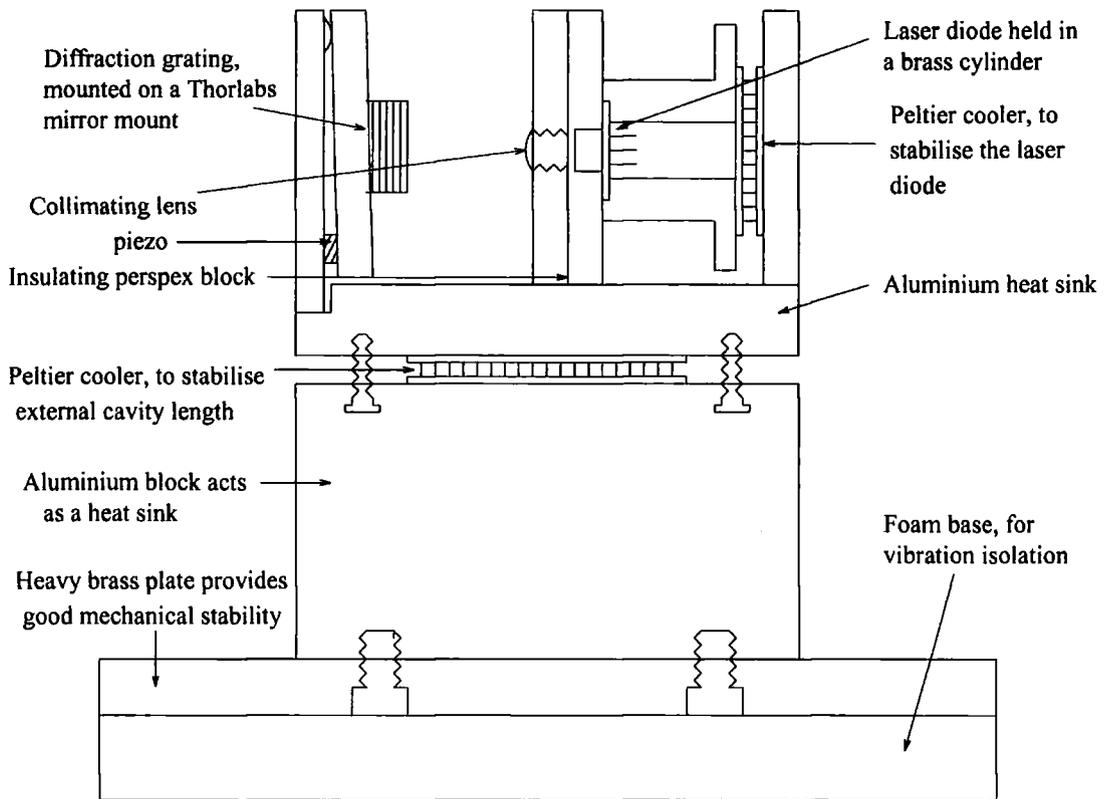
Figure 4.7: Showing the mounting of the extended cavity diode laser used to drive the repumping transition. The entire structure is surrounded by a perspex box (not shown) which excludes air currents.
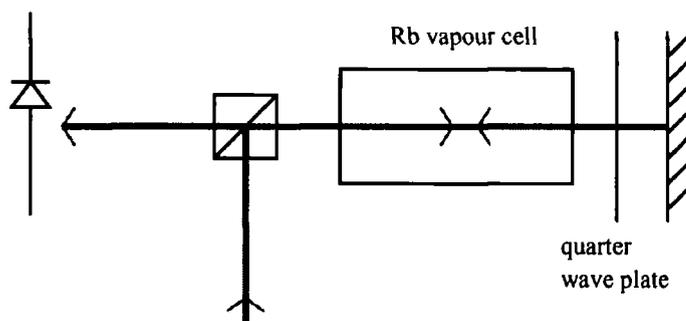
Figure 4.8: Saturated absorption spectroscopy in a rubidium vapour cell. The pump beam passes through the cell and a quarter wave plate and is retro-reflected with an orthogonal polarisation. The orthogonally polarised probe beam is separated from the pump using a beam splitting cube and absorption in the cell is detected on a photodiode.

scanning the laser through 7 GHz. The broad dips in the transmission show the Doppler-broadened transitions. Superimposed on this is the Doppler-free spectrum, showing the hyperfine structure. Figures 2.1 and 4.10 show the corresponding energy levels of ^{85}Rb and ^{87}Rb.

4.2.3 Locking the lasers

For a laser cooling experiment the laser frequency needs to be stabilised to better than the linewidth of the cooling transition i.e. better than a few MHz [93]. The lasers are locked to the appropriate hyperfine line of the Doppler-free saturated absorption signal using a dither lock.

For dither locking [98] the transmission through the Rb cell close to a frequency ω_0 is given by:

$$T(\omega) = T(\omega_0) + \frac{\mathrm{d}T}{\mathrm{d}\omega}(\omega - \omega_0) + \frac{1}{2}\frac{\mathrm{d}^2 T}{\mathrm{d}\omega^2}(\omega - \omega_0)^2 + \cdots \qquad (4.4)$$

Thus if the laser frequency is modulated such that $\omega - \omega_0 = \delta\sin(\omega_m t)$ (in our case the laser current was modulated at 32.5 kHz), the error signal is proportional to the first derivative of the transmission. Phase sensitive detection is used to extract the component oscillating at ω_m, isolating the signal from the noise. The error signal was generated by a EGG Brookdeal 9503-SC lock-in amplifier.

To lock the laser the integral of the error signal is fed back to the laser current. The integration is performed by a simple electronic circuit. Feedback to the laser current provides a fast response, but with a limited range. In many similar set-ups feedback is also sent to the piezo-electric element which controls the angle of the diffraction grating, to compensate for long term drifts of frequency. This was found to be unnecessary in our case because of the two levels of temperature stabilisation.

The Doppler-free absorption signal and the corresponding error signal for the $5S_{1/2}$, $F = 3$ to the $5P_{3/2}$ $F = F'$ of ^{85}Rb are shown in figures 4.11 and 4.12. In addition to the peaks for the $F \rightarrow F'$ transitions there are also extra peaks known as crossovers. These occur when the pump beam saturates, for example, the $F = 3 \rightarrow F' = 3$ transition for a particular velocity class and therefore the probe beam cannot drive the $F = 3 \rightarrow F' = 4$ transition for that velocity class. The crossover peaks lie half way in frequency between the two transitions. Figures 4.13
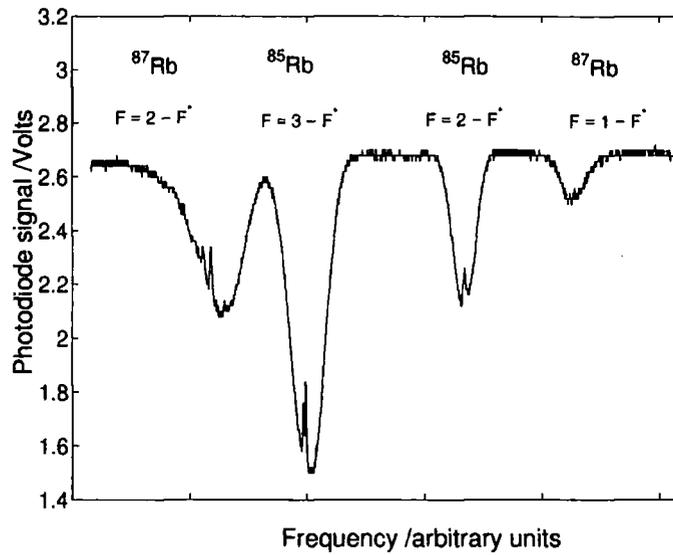
Figure 4.9: The Doppler broadened saturated absorption signal from a Rb vapour cell showing the $5S_{1/2}$ (two hyperfine levels) to $5P_{3/2}$ transitions for both [85]Rb and [87]Rb. The hyperfine structure of the $5P_{3/2}$ level can be seen in the Doppler-free reduced absorption features. For this data the ECDL was scanned without mode hops over more than 7 GHz.
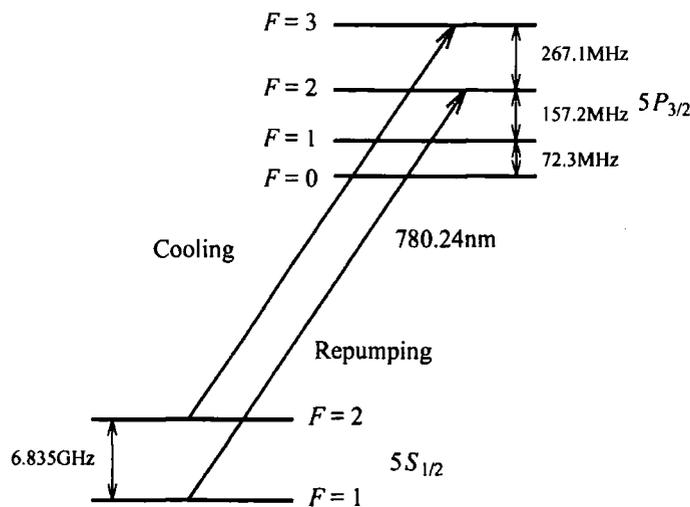
Figure 4.10: The $5S_{1/2}$ and the $5P_{3/2}$ energy levels of [87]Rb [20]. The cooling and repumping transitions are marked.
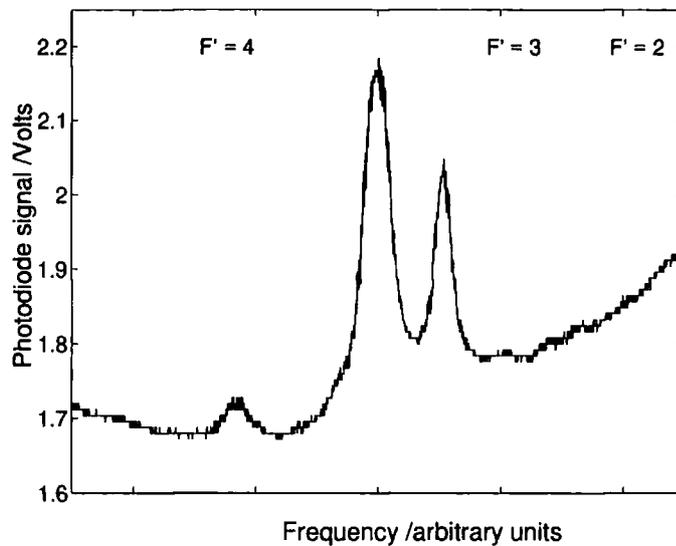
Figure 4.11: A Doppler-free saturated absorption spectrum of the ^{85}Rb $F = 3 \rightarrow F'$ transitions. The large peaks between the $F' = 4$ and the $F' = 3$ transitions are the crossovers between the $F' = 4$, $F' = 3$ and the $F' = 4$, $F' = 2$ transitions from left to right, respectively.
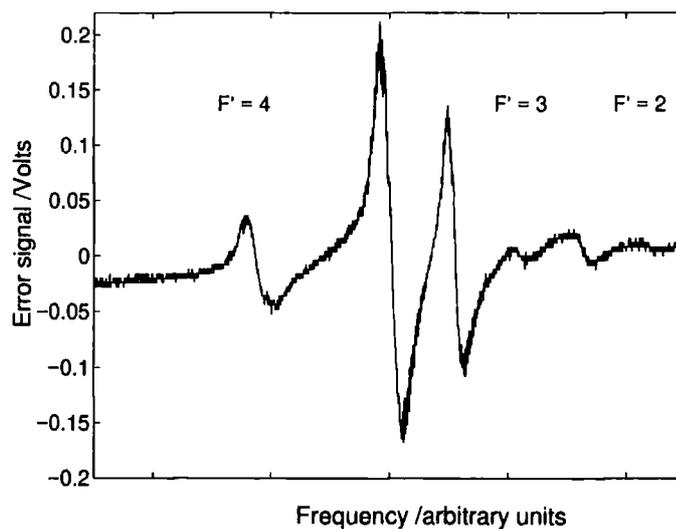
Figure 4.12: The error signal for locking the cooling laser, corresponding to the spectrum shown in figure 4.11.
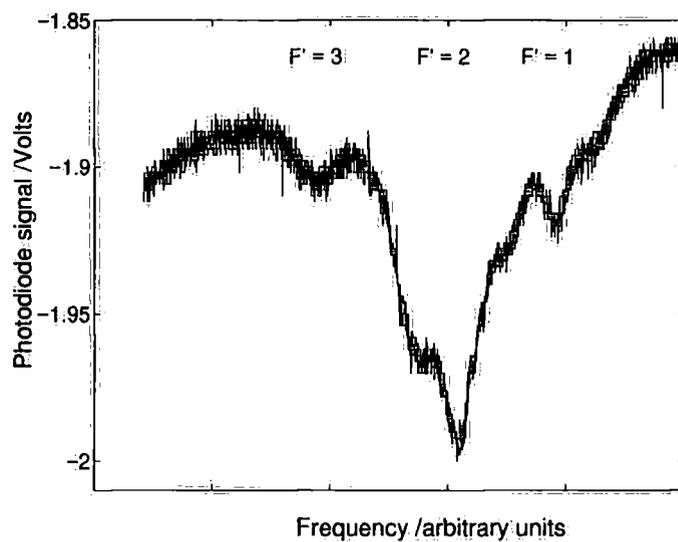
Figure 4.13: Saturated absorption spectrum for the ^{85}Rb $F = 2 \to F'$ transition. The repumping transition is $F = 2 \to F' = 3$.
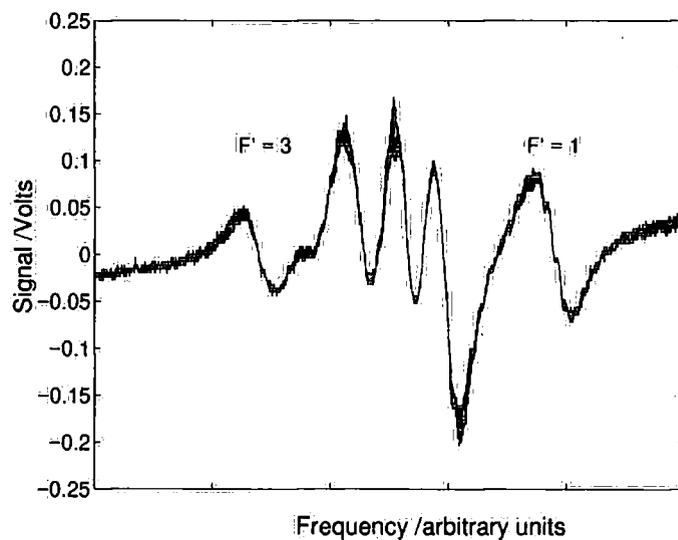
Figure 4.14: Error signal for the repumping lock, corresponding to the spectrum shown in figure 4.13.

and 4.14 show similar signals for the $5S_{1/2}$, $F = 2$ to the $5P_{3/2}$, $F = F'$ transition. The lasers can be locked to any zero-crossing of the error signal.

4.2.4   Repumping Laser

The extended cavity laser described above provided the repumping light for the MOT. The laser was locked to the $5S_{1/2}$, F = 2 to the $5P_{3/2}$, $F = 3$ transition and was stable to better than 1 MHz.

4.2.5   Cooling laser

The cooling laser was a commercial SDL TC40, 0.5W MOPA (master-oscillator power-amplifier) laser [99]. This laser relies on the injection-seeding of a tapered semiconductor laser/amplifier by a standard grating-tuned extended-cavity laser. This produces high output powers whilst retaining the advantages of a grating feedback diode laser such as a narrow linewidth, single spatial mode and a tunable frequency. The TC40 was locked to the $5S_{1/2}, F = 3$ to the $5P_{3/2}, F = 4$ transition using the error signal shown in figure 4.12, stabilising the laser to better than 1.5 MHz. The experimental set-up is shown in figure 4.15.

To optimise temperatures in magneto-optical traps it is necessary to have control of the frequency and the intensity of the light. This can be achieved using acousto-optic modulators (AOM). The first order light from the AOM is shifted by the frequency of a RF signal applied to the AOM. Our AOMs operate in the range of 60-110 MHz. They can also be used to control the intensity of the light by altering the amplitude of the RF signal which affects the efficiency of the diffraction into the first order.

An AOM is used in double pass configuration in order to provide a tunable offset for the lock. The double pass configuration has the advantage that the frequency can be changed without affecting the alignment of the experiment. The laser is thus locked around 200 MHz to the blue of the resonance. This shift is compensated for the cooling beams by using another AOM in double pass on the main beam, shifting the laser frequency to the red by around 170 MHz. Using this set-up the detuning of the cooling beams can be changed from 0 MHz to −55 MHz (i.e. red-detuned). The laser remained in lock if the detuning was ramped from −15 MHz to −55 MHz in 1 ms in steps of 4 MHz, during the molasses phase (see later). In addition the AOM in the cooling beam path could be used for fast switching of the cooling beams. No mechanical shutters were used.
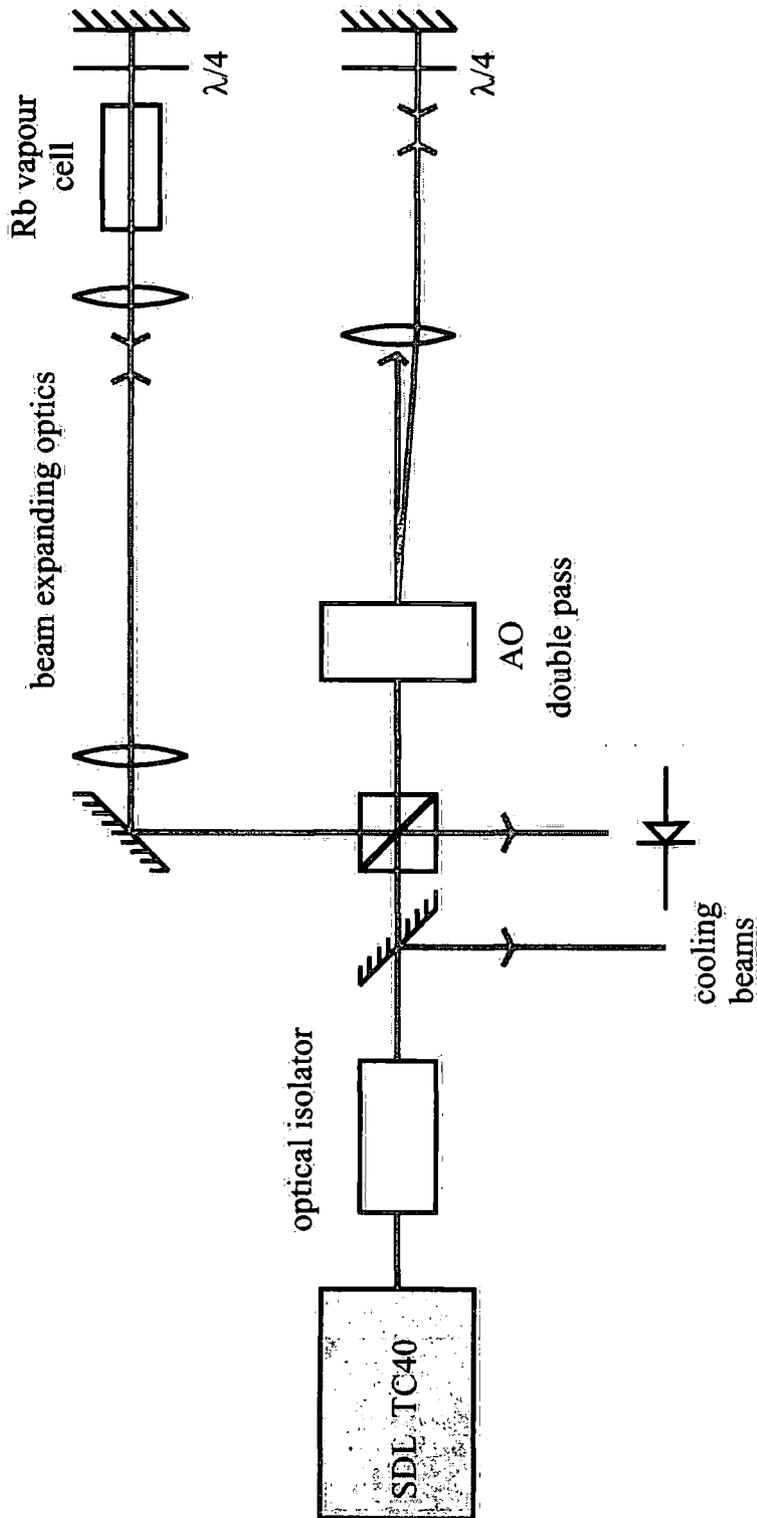
Figure 4.15: The experimental set-up for locking the TC40.

4.3   The Magnetic Field Coils

Two rectangular coils in an anti-Helmholtz configuration provide the magnetic field gradient for the MOT. The coils have dimensions of 17 cm and 9 cm, have 9 turns each and are separated by a distance of 9.5 cm. For a typical current of 60 A (supplied by a Hewlett Packard, 6671 A dc power supply) through the coils the magnetic field gradient along the axis of the coils at the midpoint is of order 6 G/cm and the gradient in the vertical direction is approximately 1.5 G/cm. Thus the confinement of the atoms in the MOT is approximately 4 times weaker in the vertical direction, leading to an elongated MOT. The coils were made of 3 mm diameter copper with a 1 mm diameter hole in the centre for water cooling. The cooling water was provided by a chiller system, at a temperature of 1.5 °C. With water cooling a maximum current of 165 A could be sustained continuously.

The coils were mounted to allow translational adjustment in both horizontal directions, but not in the vertical direction.

The decay time of the field on switching the current was 20 ms. For initial experiments the field was allowed to decay for this time before initiating the sub-Doppler cooling phase. Later, a MOSFET switching method was implemented and the field could be switched in 100 μs. The timescale of the switching was then limited by the decay of eddy currents in the coils.

Stray magnetic fields, due mainly to the earth's magnetic field are compensated by three orthogonal sets of coils in Helmholtz configuration. The ion pumps, situated to the top left and bottom right of the vapour cell produced a field gradient of order 0.1 G/cm in the region of the MOT. This gradient was not compensated but was found to be tolerable. In a poorly compensated field atoms experience a drift velocity in the optical molasses phase. The final values of the compensation fields were optimised to give the lowest temperature.

4.4 Timing and Data Acquisition

Timing for the experiment was controlled from a Pentium 150 MHz computer. The details are given in appendix A and only a brief overview will be given here.

The graphical interface is provided by Matlab. Pushbuttons toggle between the various modes (pulsed, continuous, temperature measurement etc.). Various parameters can be changed interactively. For each mode there is a matlab **.m** file which writes appropriate values for the intensity, detuning etc. to a *waveform buffer*.

Matlab communicates with NIDAQ (National Instruments Data Acquisition) cards via MEX-files which are c files for Matlab. A timing card, PC-TIO-10, generates pulses for the various timescales involved. An analogue output card, the AT-AO-10 is triggered by the PC-TIO-10 and updates voltages sent to the component parts of the experiment. The relevant voltages for each analogue output are read from the waveform buffer.

Data acquisition is performed by a Matrox Meteor frame grabber which records data from a CCD camera (CV-M50 from Alrad Instruments Ltd.) and transfers it to a Matlab array. Both the CCD camera and the frame grabber are triggered by the PC-TIO-10.

Controlling the timing from the computer is very convenient for the purposes of data acquisition. A particular sequence can be repeated many times and the results averaged or processed by the computer. The main limitation of the timing system was the time for data transfer from the CCD camera (around two seconds) which imposed a minimum time for each cycle.

Chapter 5

Characterising the MOT

A good understanding of the capabilities of our system was essential before continuing with the work. In particular the number and temperature of the atoms must be optimised with respect to the intensity and detuning of the cooling light and the magnetic field gradient. The optical set-up for the MOT is described and then the methods of measuring the temperature and number of atoms are discussed. These methods were implemented to optimise the MOT.

5.1   6-beam MOT

The 6-beam MOT is formed by six independent beams, two in the horizontal and four in a perpendicular plane at 45° to the horizontal. The beams can be well described by gaussians, with a $1/e^2$ diameter of 1.5 cm and equal intensities. The alignment of the beams is de-coupled from the laser by use of polarisation conserving fibres. This eliminates changes in the alignment of the experiment due to the beam pointing error of the laser. In addition the fibres perform spatial filtering, giving a near-gaussian output. Even with polarisation conserving fibres there can be a rotation of elliptical polarisation with small temperature changes. However, a pure linear polarisation is preserved if the input is aligned along the birefringence axis of the fibre. The maximum possible transmission through the fibre is of order 80%, assuming that the waist of the input beam is equal to the waist of the fibre. If not, the transmission goes as:

$$T = A \left(\frac{2w_1 w_2}{w_1^2 + w_2^2} \right)^2,$$ (5.1)

where w_1 and w_2 are the fibre diameter and the input beam diameter respectively and A a constant specified by the manufacturer ($A = 0.8$ in our case). Our best transmission after experimenting with different input beam diameters was of order 65%.

The acousto-optic modulators were sensitive to temperature changes on switching between operating modes. For example, the efficiency of one of the AOMs changed by about 10% on switching between operating the MOT continuously or in pulsed mode. This affected the beam balance.

The optics set-up is shown in figure 5.1. A typical CCD camera image of the MOT, taken from a side view, is shown in figure 5.2. The aspect ratio of the atom cloud is approximately 4:1 as expected from the ratio of the axial and radial magnetic field gradients. Fringes are clearly visible due to the interference between reflections of the laser beams from the uncoated quartz windows.

A typical time sequence for a cycle to produce a cloud of cold atoms is sketched in figure 5.3. Initially, in the MOT phase, both the magnetic field and the cooling light are on. The laser light has a high intensity and is red-detuned. Approximately one second is allowed for this phase. The magnetic field is then switched off. The cooling laser remains on for a further three milliseconds to allow a molasses phase to further cool the cloud. During this phase the intensity is decreased and the detuning is increased to allow polarisation gradient cooling. Both are ramped from their initial to final values over 1 ms. The repumper remains at full power for the entire cycle. After this short molasses phase the cooling laser is also switched off and the cloud of atoms expands ballistically. A resonant acquisition pulse is used to detect the atoms after a variable delay.

5.1.1 Temperature Measurement

Measurements of temperature of gases of cold atoms in the microKelvin range and below all rely on the fact that the temperature is an expression of the velocity spread of the atomic distribution. If the cooling and trapping fields are turned off instantaneously, then the cloud of atoms expands ballistically and the width of the cloud at subsequent times can be used to infer the velocity distribution and thus the temperature.

Figure 5.4 shows how the width of the cloud varies with the delay of the detection
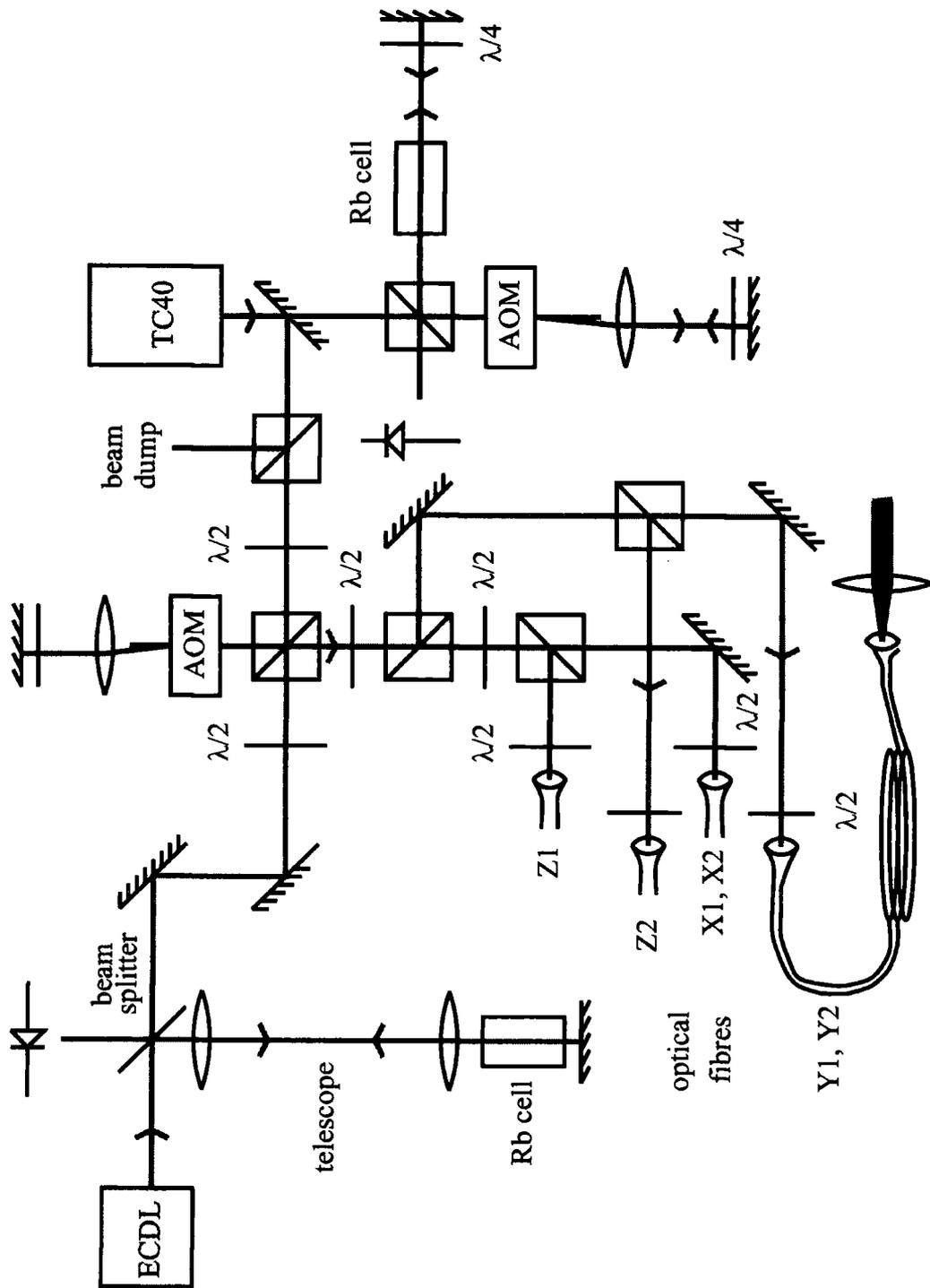
Figure 5.1: The optical set-up for a six-beam MOT, showing how the 6 independent beams are formed.
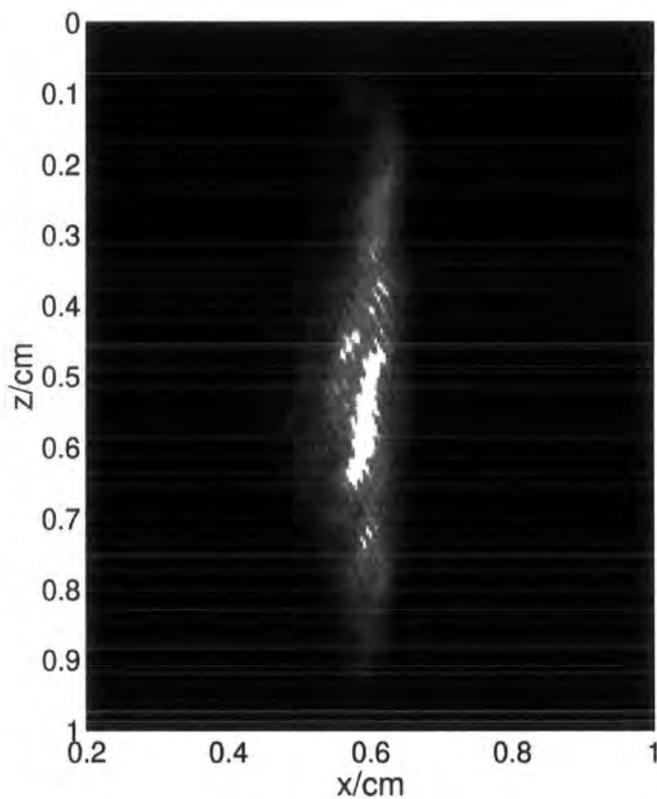
Figure 5.2: A CCD camera image of the MOT. The grey scale has been chosen so as to best show the structure of the cloud. Fringes with a period of 100 μm are visible running diagonally from top left to bottom right of the image. There are also fringes at around 10 degrees to the vertical with a period of 0.5 mm.
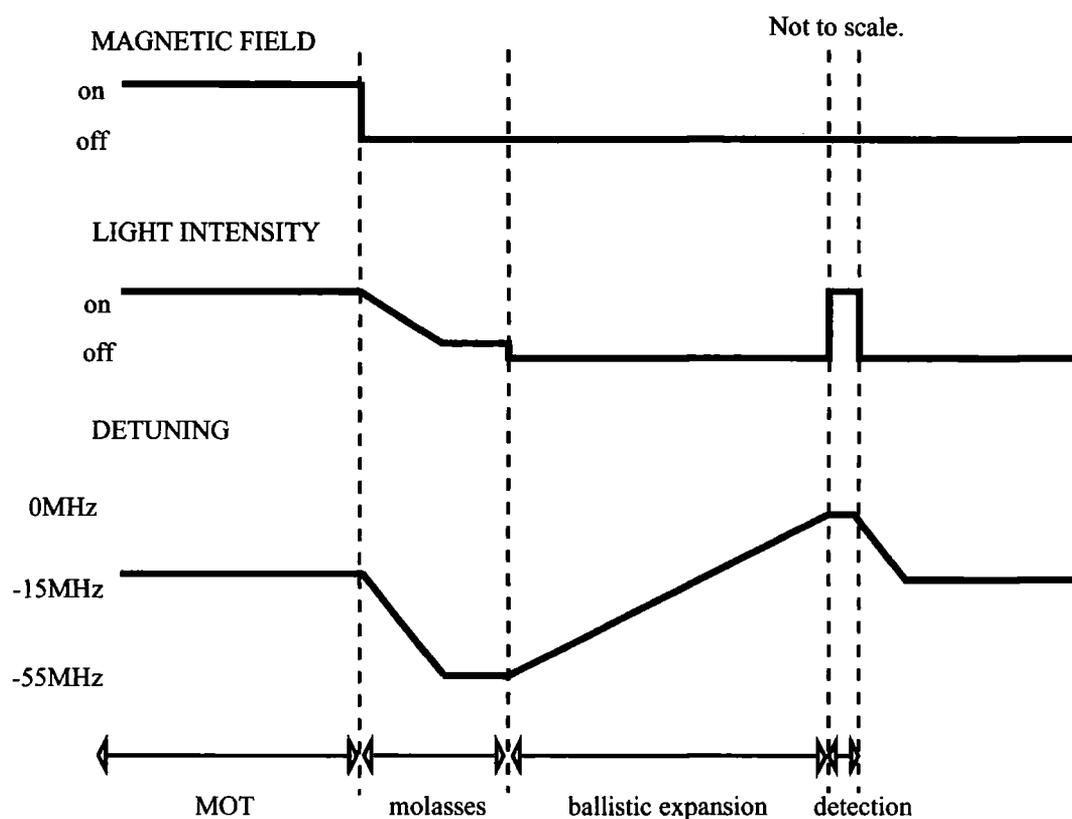
Figure 5.3: The pulse sequence for a temperature measurement. During the MOT phase both the light and the magnetic field are on, for 1 s. The MOT detuning is chosen to maximise the collection efficiency. The magnetic field is then turned off and the detuning increased whilst the light intensity is simultaneously decreased. After this molasses phase the light is also turned off and the atoms expand ballistically. A detection pulse of resonant light of duration 1.0 ms is used to image the expanding cloud.
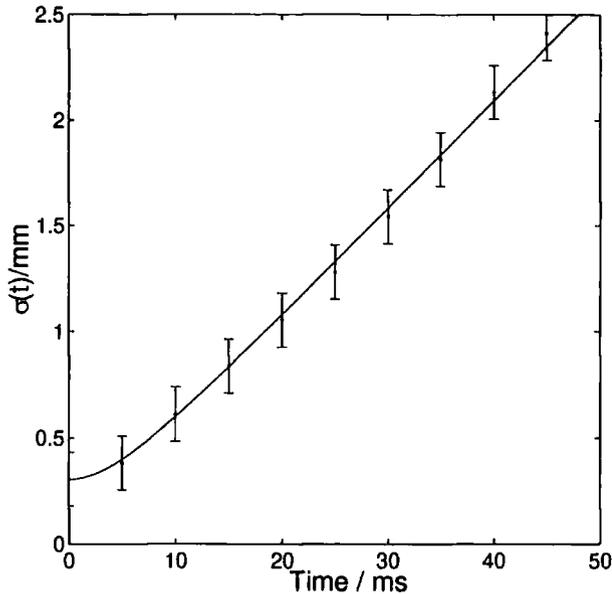
Figure 5.4: Graph showing measured widths of the atom cloud after ballistic expansion and a fit to the data. The fit gives a value of $u^2 = 0.00267$ m^{2}s^{-2} which implies a temperature of 27.5 μK using equation 4.6. The error bars are the statistical error from 5 measurements.

pulse. For initial gaussian position and velocity distributions, the width of the cloud is expected to vary as:

$$\sigma^2 = \sigma_0^2 + u^2 t^2, \tag{5.2}$$

where

$$u^2 = k_B T/m, \tag{5.3}$$

and σ_0 is the initial rms width of the gaussian position distribution and σ is the width at time t. The data in figure 5.4 is fit by a curve of this form, giving a temperature of 27.5 μK.

Note that this expression is one dimensional only and a temperature measurement of this sort assumes that the temperature is isotropic. It was verified that this is indeed the case by comparing the expansion of the cloud along three orthogonal axes. In addition it is necessary to ensure that the detection beam is sufficiently large to image all the atoms. Otherwise the imaged distribution will be a convolution of the profile of the detection beam and the atomic cloud. The detection pulse

must be short enough to image a 'snapshot' of the distribution. For a 1 ms detection pulse, atoms with a temperature of 20 μK will travel $\sim$ 45 μm, which is the same order as the resolution of the CCD camera and considerably smaller than the size of an expanded atom cloud. Finally, we also ensured that the atoms were not heated significantly by the detection by comparing the effect of detection pulses of different duration.

5.1.2 Number Measurement

The measurement of the number of atoms is based on the intensity of the spontaneously emitted light. This depends on the fraction of time which each atom spends in the excited state. Solving the optical Bloch equations, for a single laser beam of intensity I and detuning Δ, the rate of scattering of photons is given by:

$$\langle \frac{\mathrm{d}N}{\mathrm{d}t} \rangle = \frac{\Gamma_n}{2} \frac{p}{p+1} \tag{5.4}$$

and p is the saturation parameter, $p = (I/I_{sat})/(1 + 4\Delta^2/\Gamma_n^2)$ (Γ_n is the natural linewidth of the excited state, Δ is the detuning of the cooling light from resonance and I_{sat} is the saturation intensity).

For the initial number measurements, a 3.2 cm lens of one inch diameter was mounted 7 cm from the MOT in order to image the fluorescence onto a calibrated photodiode. To obtain the total fluorescence of the MOT, the solid angle of the collected light, and the quantum efficiency of the photodiode must be included in the calculation. This result was then used to calibrate the signal from the CCD camera.

The above method of measuring the number of atoms assumes that the cloud is optically thin, i.e., that a photon emitted by an atom at the centre of the cloud escapes without reabsorption. If this is not the case the measurement will be an under-estimate of the real number. In addition, equation 5.4 assumes a two-level atom, and does not account for slightly different saturation intensities for different transitions. The intensity is the absolute intensity, calculated by summing the individual intensities of the cooling beams. The intensity is measured before entering the vapour cell, using a calibrated photodiode.

5.2 Optimising the MOT

The remaining sections describe how the temperature and number of atoms in the MOT are optimised. The number of atoms depends on the loading rate into the MOT and therefore is determined by the high intensity trapping phase. The lowest temperatures are only obtained after the final molasses phase, which allows orientational cooling mechanisms.

5.2.1 Optimising the Number of Atoms

5.2.2 Loading Rates

In a vapour cell MOT the loading rate, R, is determined by the flux of atoms entering the cooling region with a velocity below the capture velocity, v_c (the largest velocity from which an atom can be brought to rest whilst crossing the laser beam). The steady state number of atoms occurs when R is equal to the loss rate due to collisions with the background gas. The number of atoms as a function of time ($t \geq 0$) is given by:

$$N(t) = \frac{R}{\gamma}[1 - \exp(-\gamma t)], \qquad (5.5)$$

where R is a loading rate into the MOT and γ is a loss rate that is assumed to be independent of N. Two and three body collisional losses are neglected.

A typical loading rate curve is shown in figure 5.5 for the case where the rubidium reservoir has been cooled to 1.2°C. The number of atoms in the MOT saturates after approximately 4 seconds, $\gamma = 0.6$ s^{-1}. With a steady state number of atoms of 4×10^8, $R = 2.4 \times 10^7$ s^{-1}.

5.2.3 Steady State Number of Atoms

The steady state number of atoms is given by R/γ (equation 5.5). For a vapour cell MOT, the main losses arise from collisions with the background vapour. For the following measurements the vapour pressure was a constant so the steady state number of atoms is proportional to R.

Dependence on Intensity of the Cooling Light

First consider the variation of the number of atoms with the intensity of the cooling light, as plotted in figure 5.6. For each measurement the MOT was loaded to
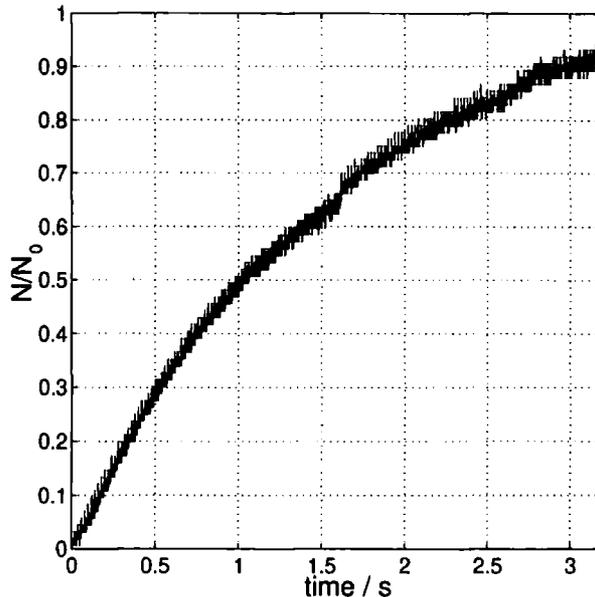
Figure 5.5: Number of atoms in the MOT as a function of time after switching on. The rubidium reservoir is at a temperature of 1.2°C. The signal is recorded by monitoring the fluorescence from the atoms on a photodiode. The data can be fitted by a curve of the form given in equation 5.5.

saturation, for different intensities of the cooling light, keeping the diameter of the beams constant. The number of atoms was determined by measuring the integrated signal obtained by a CCD camera for a resonant detection pulse of maximum laser intensity. The number of atoms increases linearly for single beam peak intensities of up to around 7.5 mW/cm^2 and then levels off. Atoms can only be loaded into the magneto-optical trap if they have an initial velocity below the capture velocity when they enter the cooling beams. For constant beam diameter but variable intensity, $R \propto (dN/dt)^2$ [101], where dN/dt is the rate of scattering photons, given by equation 5.4.

The photon scattering rate, dN/dt increases linearly with intensity for a saturation parameter $p \ll 1$. When $p \gg 1$, the transition is saturated and the scattering rate is constant. In this case the number of photons that can be scattered will be limited by the lifetime of the excited state since far above saturation atoms spend half of their time in the excited state. The data was taken for $\Delta = 2\pi \times 15$ MHz and for ^{85}Rb, Γ_n is $2\pi \times 5.9$ MHz and I_{sat} is 1.63 mW/cm^2. So with six beams, $p = 1$ when the single beam peak intensity, I_0, is 12 mW/cm^2, assuming that the absolute intensity seen by the atoms is a sum of the individual intensities of the cooling beams. This agrees well with the data in figure 5.6.
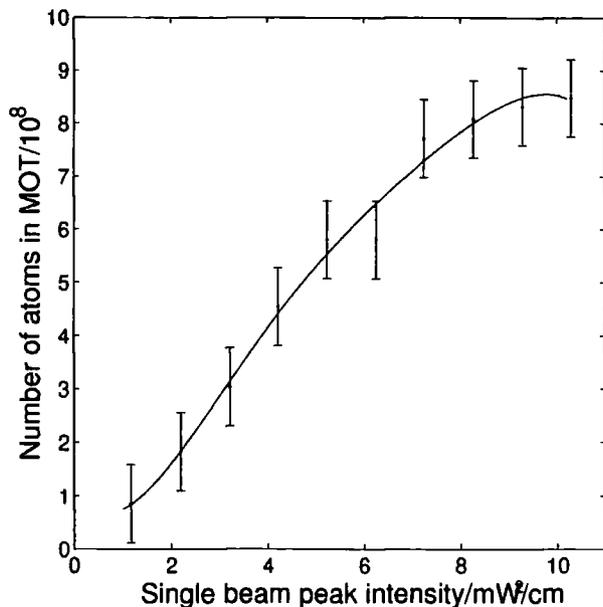
Figure 5.6: Variation of the number of atoms in the MOT with the single beam peak intensity, I_0. The data is taken for a detuning $\Delta = 2\pi \times 15$ MHz and a current, $I_B = 60$ A. The solid line is a fit to the data for $N = AI_0/(I_0 + B)$, where A and B are constants. The error bars are the statistical error on five measurements.

Dependence on the Magnetic Field Gradient

The effect of the magnetic field gradient is shown in figure 5.7. For increasing field gradients the steady state number of atoms at first increases, then levels off for currents through the coils, I_B, between 45 A and 90 A and finally decreases again. For low magnetic field gradients the main issue is a lack of trap depth. When the trap is deep enough to confine all atoms that can be slowed by the cooling light the steady state number of atoms saturates. The fall in the number of atoms for high magnetic field gradients occurs for $I_B > 80$ A. The gradient taken along a line through the centre of the coils is around 10 G/cm for $I_B = 100$ A. We can estimate the Zeeman shift at the edge of the beams to be 7×10^{-27} J (10.5 MHz in frequency units). This is comparable to the detuning of the cooling beams from resonance (10^{-26} J or 15 MHz), suggesting that for these field gradients the cooling mechanism is degraded by the large Zeeman shift.

Dependence on Detuning

A similar argument can be employed to explain the fall in the number of atoms for small detunings (figure 5.8). For large detuning the scattering rate falls and the capture velocity will be lower. The optimum detuning for a current of 60 A through
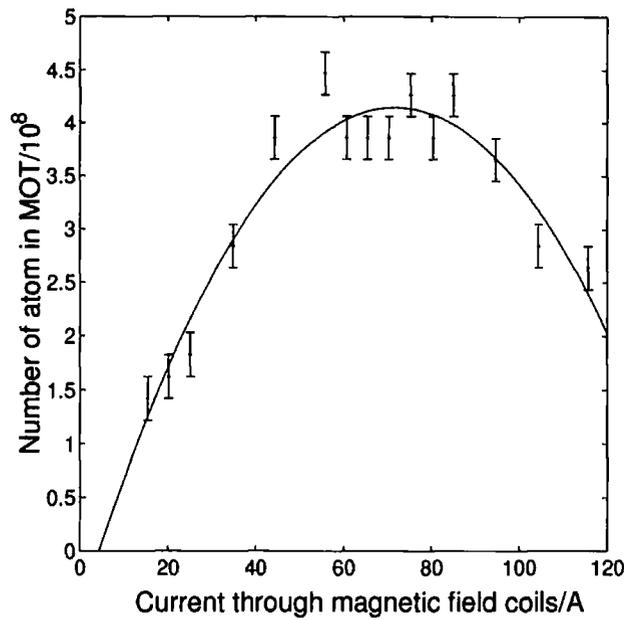
Figure 5.7: Variation of the number of atoms in the MOT with the current through the magnetic field coils, I_B. The data was taken with a detuning $\Delta = 2\pi \times 16$ MHz and $I_0 = 4.0$ mW/cm^2. The solid line is a second order polynomial fit to the data. The error bars are the statistical error on five measurements.
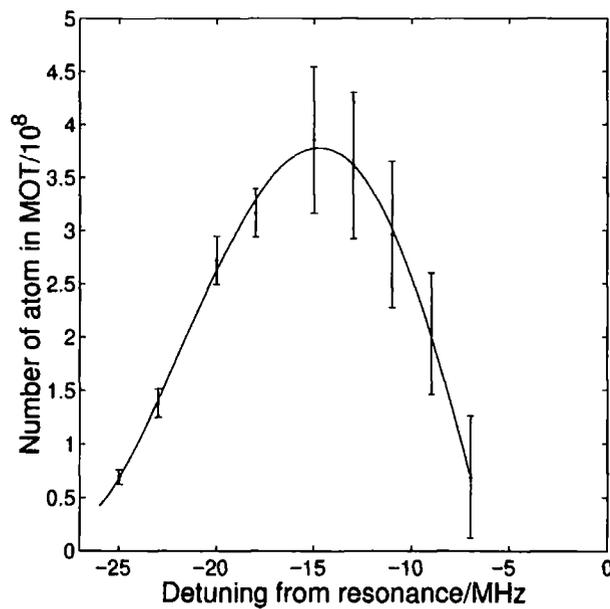
Figure 5.8: Variation of the number of atoms in the MOT with the laser detuning. The data was taken with $I_B = 60$ A and $I_0 = 4.6$ mW/cm ^{2}. The solid line is a polynomial fit to the data. The error bars are the statistical error on five measurements.

the anti-Helmholtz coils is around 15 MHz.

5.2.4   Optimising the Temperature

Whilst the main collection of atoms occurs during the MOT phase, the final cooling phase in which the magnetic field is turned off is important for reaching the lowest temperatures. During this phase, where a polarisation cooling mechanism is operating, the beam quality and good magnetic field compensation are important. Our lowest temperature is around 13 μK, comparable to the 10 μK obtained by Wallace *et al.* [102]. However, recently Fertig and Gibble have observed 1.8 μK and collected 5×10^{10} atoms [103] for an experiment with a Rb clock.

The molasses phase was optimised for a final detuning of 50 MHz (8.5Γ, where Γ is 5.9 MHz) and a final single beam peak intensity of 2.0 mW/cm^2. The MOT values were ramped to these final values over 1 ms and a further 2 ms of molasses was sufficient to reach the final temperature. Figure 5.9 shows the variation of temperature with detuning in the molasses phase and figure 5.10 shows the variation of temperature with intensity of the cooling light. The temperature varies linearly with the intensity, for $I_0 > 2$ mW/cm^2 and linearly with inverse detuning for $\Delta > 50$ MHz (c.f. equation 2.2). For lower intensities and larger detunings, the polarisation gradient cooling mechanism is not efficient.

5.2.5   Optimised Trapping and Cooling Sequence

In summary, the final sequence is an initial trapping phase with the current through the magnetic field coils set at 60 A, the detuning of the cooling light at -15 MHz and the intensity at its maximum value $I_0 = 10.7$ mW/cm^2. The temperature is then optimised by switching off the magnetic field, ramping the intensity down to 2.0 mW/cm^2 and ramping the detuning to -50 MHz.
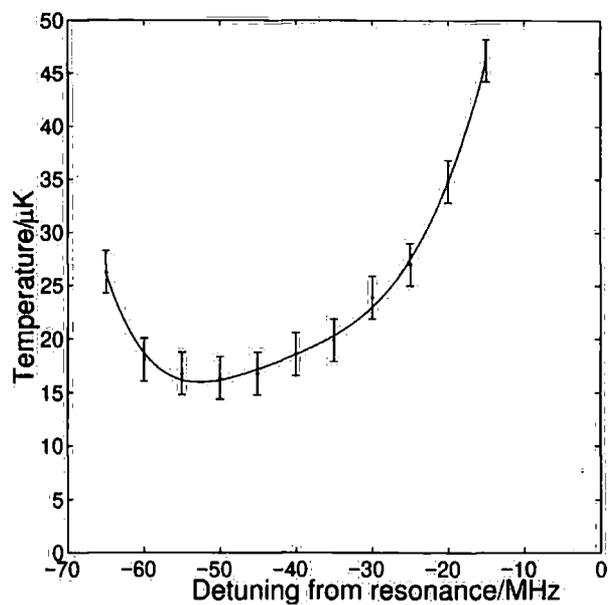
Figure 5.9: Temperature in molasses as a function of detuning. I_0 is 2 mWcm^{-2}. The solid line is a polynomial fit to the data.
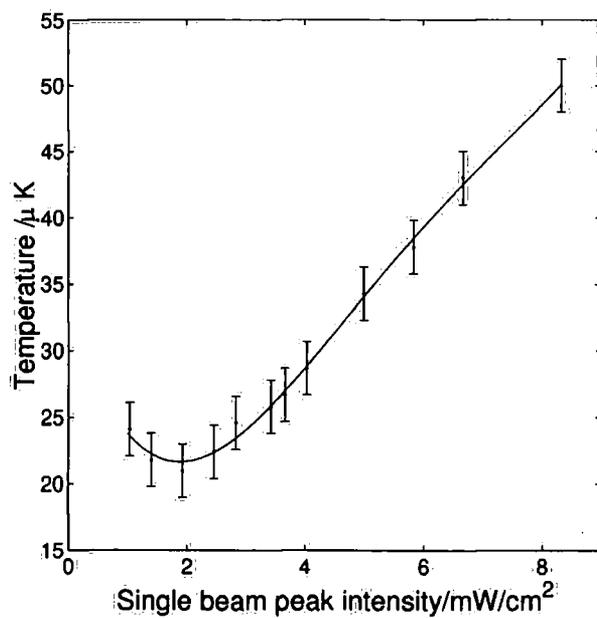
Figure 5.10: Temperature in molasses as a function of intensity. The detuning is -15 MHz. The solid line is a polynomial fit to the data.

Chapter 6

The Guided Atomic Fountain

6.1 Introduction

The technology for atomic fountains is now well developed for use in the new generation of atomic clocks. The fountain is an ideal geometry for providing relatively long interaction times in a perturbation free environment. An additional advantage for a clock was recognised by Zacharius [104] in 1954 - in the fountain geometry atoms pass twice though the same region of space. In Ramsey's technique of separated oscillatory fields [105] the frequency of an atomic resonance is measured by observing fringes produced by applying two $\pi/2$ pulses to an atom passing through rf cavities. In a fountain a single cavity can be used for both pulses, eliminating errors due to phase shifts between two separate cavities.

The atomic fountain as a frequency standard was only successfully demonstrated after the development of laser cooling. Launching techniques for the cold atoms have evolved over time. The simplest is to apply a short pulse of light to push the atoms upwards by the radiation force [2]. The disadvantage here is that the atoms are heated in the transverse direction. A more successful technique (but also more involved experimentally) is known as 'moving molasses' [3, 106] where the atoms are cooled in a moving frame by shifting the frequencies of the upward and downward propagating beams by equal amounts, but in opposite senses.

In this chapter we consider how to convert the MOT described in the previous two chapters into an atomic fountain, using a 'moving molasses' method. Fountains used for atomic clocks are typically 1 - 2 metres high. In contrast, our fountain is designed for loading an atom trap and therefore it is important that the cloud has not spread out too much by the time it reaches the apex. Therefore, a small fountain ($\sim$ 10 cm or less) is an advantage. With the addition of a far-off resonant

red-detuned guiding laser beam to confine the atoms in the horizontal direction, the density of the atoms at the apex of the fountain can be maximised. Section 6.2.1 describes the moving molasses technique. Section 6.3 describes how the loading into the guide can be optimised and how the guided fountain improves the efficiency of transfer of the atoms from a vapour cell MOT to an UHV chamber [107].

Most fountains operate in a pulsed fashion - the MOT is loaded for several hundred milliseconds and then a cloud of cold atoms is launched by switching to moving molasses for the last couple of milliseconds. However, by continuously extracting atoms using moving molasses it may be possible to obtain a higher flux. With the guiding laser beam one could envisage accumulating a column of cold atoms with a high density at the apex, similar to the results of the simulation presented in chapter 3. The extension to continuous operation is discussed in section 6.4.

6.2 The Atomic Fountain

6.2.1 Moving Molasses

For a standard magneto-optical trap the frequencies of all the cooling beams are equal and atoms are cooled isotropically in the laboratory frame of reference. However, in order to produce a beam of cold atoms, the atoms can be cooled in a moving frame. The frequencies of two counter-propagating cooling beams are set to be:

$$\omega_1 = \omega_0 + \Delta\omega, \tag{6.1}$$

$$\omega_2 = \omega_0 - \Delta\omega, \tag{6.2}$$

where ω_0 is the normal MOT frequency. The atoms will be cooled about a velocity v such that atoms travelling at v see both beams with equal frequencies. In the moving frame the frequencies are:

$$\omega_1' = \omega_1 - kv = \omega_0 + \Delta\omega - kv, \tag{6.3}$$

$$\omega_2' = \omega_2 + kv = \omega_0 - \Delta\omega + kv, \tag{6.4}$$

where k is the wavevector of the light. So the velocity of the moving frame is:

$$v = \frac{\Delta \omega}{k}.$$ (6.5)

6.2.2 Generation of Frequencies for Launching

In chapter 3 we discussed the use of acousto-optic modulators for switching and controlling the frequency of the cooling light. These AOMs operate in double pass at 86 MHz. By using separate AOMs for different sets of laser beams, a small frequency difference can be introduced which can be used to generate a moving molasses. For example, launching the atoms to a height of approximately 10 cm can be achieved by generating $\nu \pm 1.4$ MHz. The frequency difference must be stable to at least a few kilohertz to prevent heating and give a consistent launching speed. In addition, for the pulsed fountain, it is necessary to be able to switch between the central frequency (86 MHz) and the shifted frequencies over the course of a single cycle. The scheme for generating these frequencies using electronic components purchased from Mini Circuits is outlined below.

6.2.3 Mini Circuits

The central 86 MHz signal is generated by a sine-wave generator (Tektronix SG503). A 5-way rf-splitter (Mini Circuits ZFSC-5-1) divides the signal into 5 parts of equal amplitude. Three of the outputs may be fed directly into amplifiers and subsequently to AOM drivers to provide the MOT frequencies. Each of the two other outputs are combined with the $\Delta \omega / 2$ signal using frequency modulators (Mini Circuits ZFMIQ-70ML). The output from one modulator is 86 MHz $+ \Delta \omega / 2$ and that from the other is 86 MHz $- \Delta \omega / 2$ (the drive frequency is $\Delta \omega / 2$ as the AOMs operate in double pass). We can gain an understanding of how the modulator works by using some simple trigonometry.

First the rf input is split into 2 components with a 90° phase difference.

$$2 \cos(\omega_1 t) \rightarrow \cos(\omega_1 t) + \sin(\omega_1 t).$$ (6.6)

Each modulator has additionally two inputs for the low frequency $\Delta \omega / 2$ signal, in phase and in quadrature (produced by Mini Circuits PSCQ-2-0.455). Multiplying the cosine terms together and the sine terms together gives:

$$\cos(\omega_1 t)\cos(\frac{\Delta\omega}{2}t) + \sin(\omega_1 t)\sin(\frac{\Delta\omega}{2}t), \tag{6.7}$$

Using trigonometric identities this can be re-written as:

$$\frac{1}{2}\cos\left[(\omega_1 + \frac{\Delta\omega}{2})t\right] + \frac{1}{2}\cos\left[(\omega_1 - \frac{\Delta\omega}{2})t\right]$$
$$+\frac{1}{2}\cos\left[(\omega_1 - \frac{\Delta\omega}{2})t\right] - \frac{1}{2}\cos\left[(\omega_1 + \frac{\Delta\omega}{2})t\right], \tag{6.8}$$

i.e.

$$\cos\left[(\omega_1 - \frac{\Delta\omega}{2})t\right]. \tag{6.9}$$

By subtracting rather than adding the second term in equation 6.7, we obtain the other sideband:

$$\cos\left[(\omega_1 + \frac{\Delta\omega}{2})t\right]. \tag{6.10}$$

In practice the modulators produce a 30 dBm suppression of the carrier and the other sidebands. An rf switch enables these frequencies to replace the 86 MHz for the launch phase. The chip generating the in-phase and quadrature signals works efficiently between 250 kHz and 750 kHz. Since the AOMs are operating in double pass this gives $\Delta\omega$ between 500 kHz and 1.5 MHz. Assuming that the beams propagate along the vertical direction, this corresponds to fountain heights of up to 7 cm. Larger fountain heights can be realised by replacing PSCQ-2-0.455 by a chip operating at higher frequencies.

All the outputs are amplified sufficiently to saturate the AOM driver and thus give no change in the laser power being used for the experiment. Figure 6.1 shows the components and their connections. Figure 6.2 shows a typical Fourier transform of the frequency spectrum input to the AOMs, for both the moving molasses and the MOT case. The frequency of the carrier is 86 MHz and that of the sidebands is 450 kHz. For the moving molasses case it can be seen that the carrier and the upper sideband are suppressed by 30 dBm.

As an aside, it is interesting to note the importance of deriving the central frequency for all six molasses beams from the same source. If, for example, the
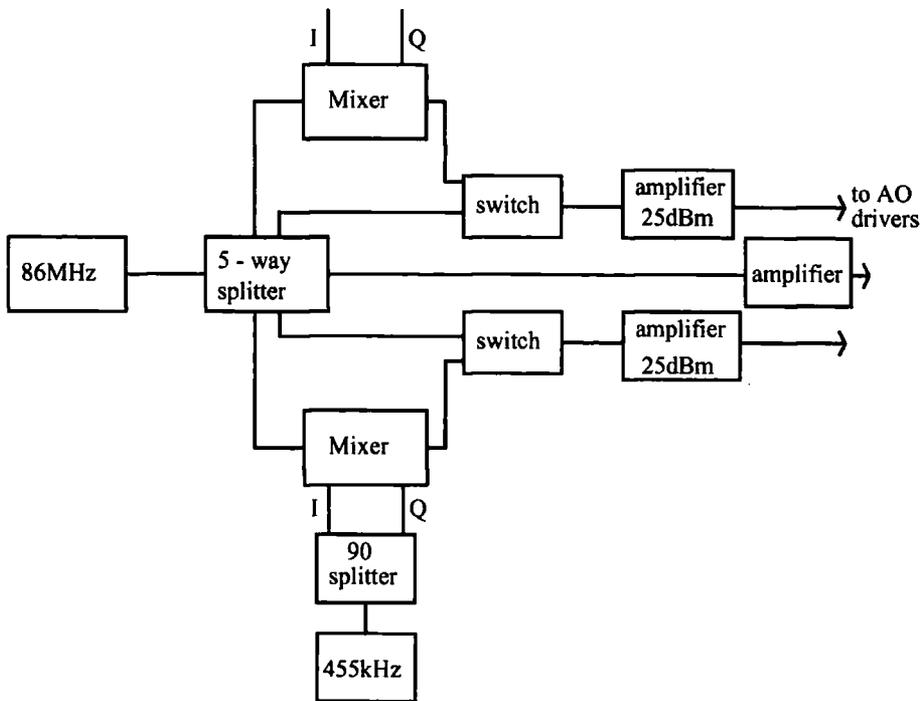
Figure 6.1: Schematic of the electronics for generating the launching frequencies.
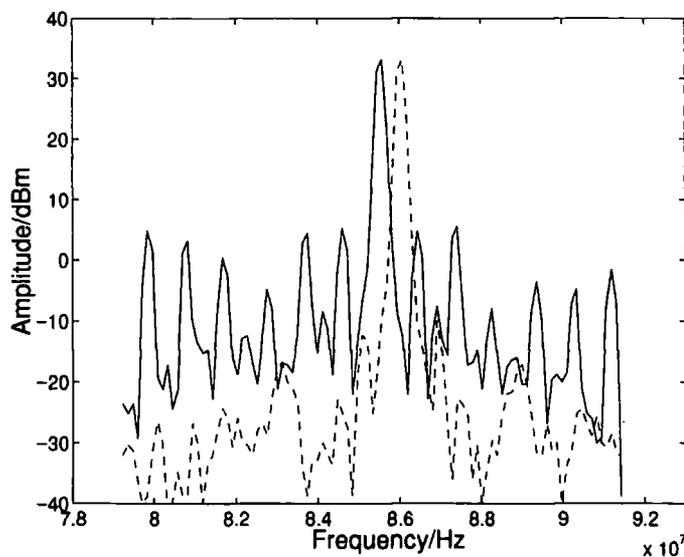
Figure 6.2: Fourier transform of the rf signal applied to the acousto-optic modulators. The dashed line shows the pure rf signal at 86 MHz and the solid line shows the spectrum when a 450 kHz signal is added using a frequency modulator. For the latter case the carrier and upper sideband are suppressed by 30 dBm.
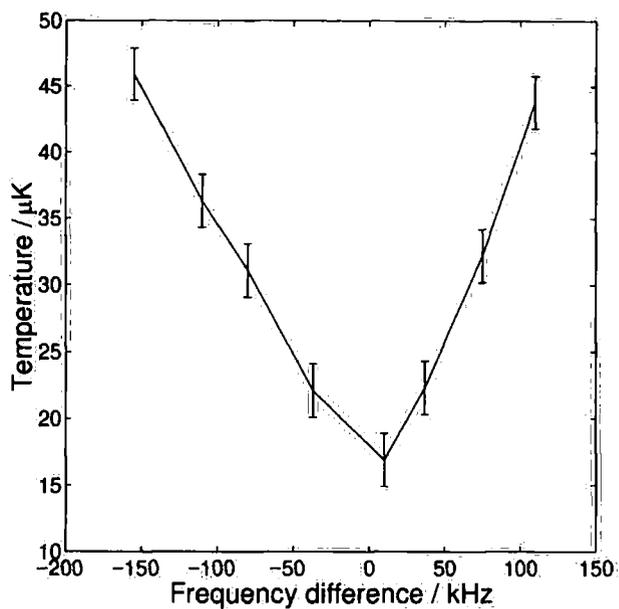
Figure 6.3: Temperature of the molasses as a function of frequency difference between horizontal and vertical cooling beams.
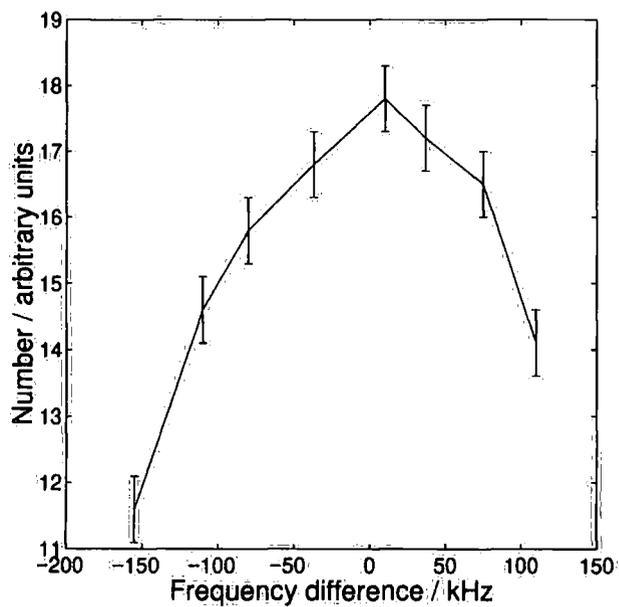
Figure 6.4: Number of atoms in the MOT as a function of the frequency difference between the horizontal and vertical cooling beams.

horizontal and the vertical beams differ in frequency by a few hundred kHz, the effect on the temperature of atoms in the molasses can be seen in figure 6.3. This data was taken by sending the horizontal and vertical beams through AOMs driven by different voltage controlled oscillators and noting the beat frequency between the beams. The order of magnitude increase in temperature of the molasses is consistent with equation 6.5. A corresponding plot of the number of atoms in the MOT is shown in figure 6.4. The number of atoms decreases by 34% for a frequency difference of 155 kHz.

6.2.4 Operation of the Fountain

The atomic fountain is built using 6 beams, two counter-propagating horizontal and two pairs of counter-propagating beams in a perpendicular plane at 45° to the horizontal as illustrated in figure 6.6. The 45^0 geometry is important for the extension to continuous operation since it allows the atoms to propagate freely along the vertical direction after leaving the MOT. The frequency difference of the launching beams must be a factor of $\sqrt{2}$ smaller than for a vertical beam geometry (i.e. $v = \sqrt{2}\Delta\omega/k$). Separate AOMs are used to provide control of three different frequencies - one AOM controls the horizontal beams, another the downwards propagating beams and a third controls the upward propagating beams. Each beam has a $1/e^2$ diameter of 1.5 cm and a peak intensity of 10 mW/cm^2. For the pulsed fountain, the repumping beam is aligned vertically through the MOT and retro-reflected with orthogonal polarisation. It operates continuously. The MOT is loaded for approximately one second. The MOT was optimised for the lowest temperatures and for the measurements described below, the cloud is roughly cylindrical with a diameter of 0.4 mm (FWHM) and a long axis of 2 mm.

The pulse sequence is identical to that of figure 5.3 except that the frequencies are switched to the launching values 500 μs before the intensity decrease. After the initial MOT phase, a sub-Doppler cooling phase is initiated; the magnetic field is switched off; the intensities of the molasses beams are reduced by a factor of 4 and the detuning increased from -3Γ to -10Γ for 2 ms. After launching, all light is switched off using the AOMs, giving an extinction ratio of better than 10^{-3}.

In order to observe the atoms during their ballistic flight, a detection beam is aligned vertically through the MOT, overlapping with the repumping beam and also retro-reflected with an orthogonal polarisation. The detection beam is switched with an independent AOM and is off all the time except during detection. The detection
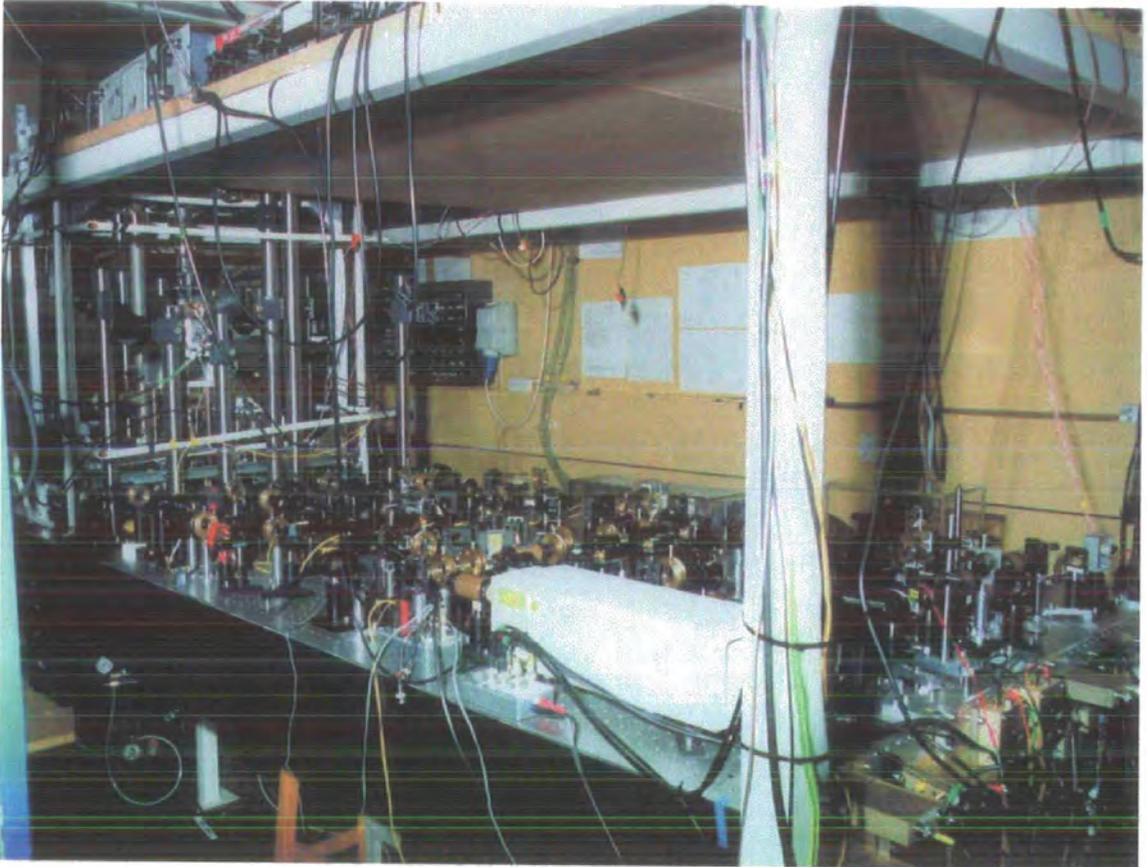
Figure 6.5: Photograph of the optics for the atomic fountain. Photograph courtesy of Vicki Greener, Physics Audio Visual Department.
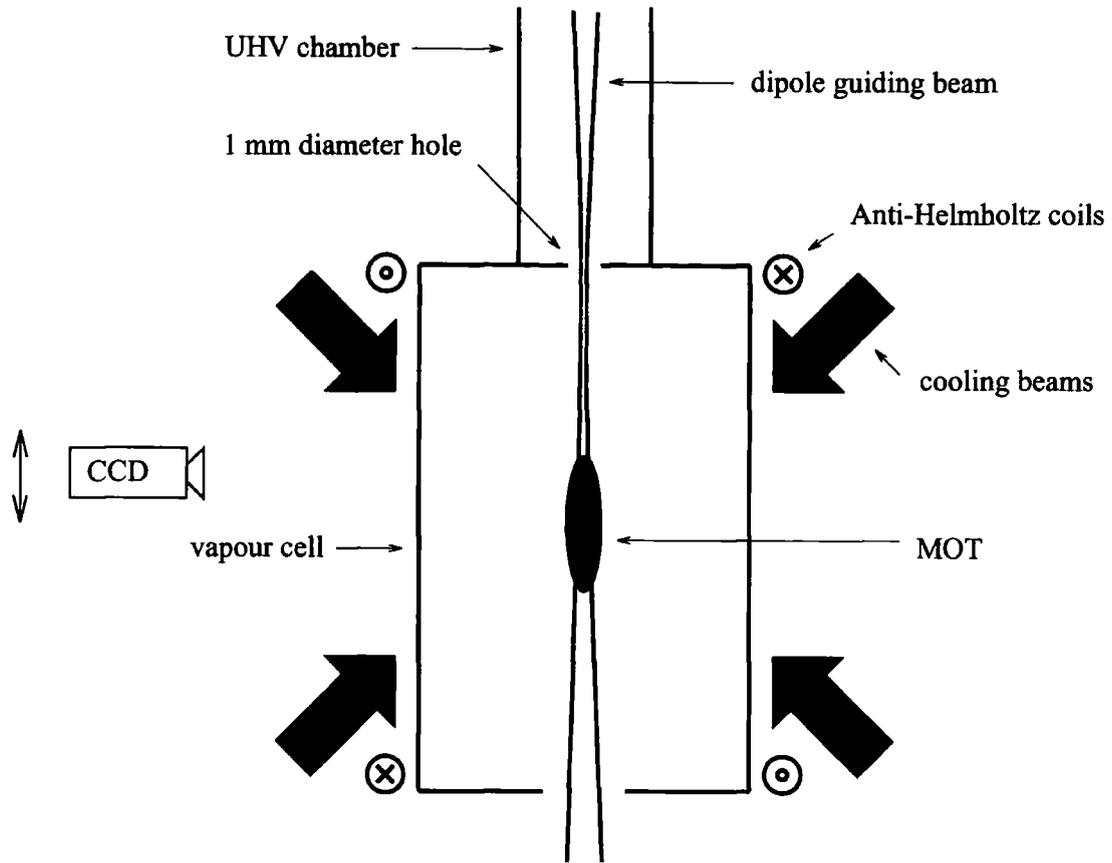
Figure 6.6: Schematic of the experiment. A vapour cell MOT loads cold rubidium atoms into a far-off resonant, red-detuned laser beam. The atoms are launched using moving molasses and guided in the beam through a 1 mm diameter hole into an UHV chamber. Fluorescence from the atoms can be imaged onto a CCD camera.

pulse duration was varied to produce sufficient signal without significantly disturbing the distribution.

We compared the temperature of a cloud of atoms launched in the fountain with that of atoms simply dropped when the MOT is turned off and found that they were the same within error. Thus the moving molasses cooled the atoms as efficiently as cooling in the laboratory frame.

6.3 The Pulsed Guided Atomic Fountain

With the atomic fountain working reliably it is possible to study the effect of adding a guiding potential, in our case a red-detuned, far-off-resonant focused laser beam. The dipole guiding laser is a 12 W, diode-pumped, continuous wave, Nd:YAG laser. The central wavelength is 1064 nm and the linewidth is 5 GHz.

The beam, focused to a waist of radius w_0 is aligned vertically through the MOT and operates continuously. It is retro-reflected, with the orthogonal polarisation. The retro-reflected power measured with a calibrated power meter is only approximately 8.5 W before re-entering the vacuum chamber and 6 W afterwards. Therefore, we can estimate the total power in the MOT region to be approximately 19 W. We found that the easiest alignment procedure involved overlapping a resonant beam with the guide beam in order to give a visible reference and then moving the magnetic field coils until the MOT was overlapped. Finally, the alignment of the laser beams were re-optimised to collect the maximum number of atoms and the compensation fields were adjusted to yield the lowest temperatures.

6.3.1 The Guiding Potential

Figure 6.7 plots the trap depth in microKelvin along the axis of a 19 W laser beam, detuned 284 nm from resonance, focused to w_0 at $z = 0$, for three different values of w_0 (50, 100, 200) μm. The trap depth is given by equation 2.9 and the Rayleigh range, z_R (the distance from the focus at which the trap depth is halved) is:

$$z_R = \frac{\pi w_0^2}{\lambda}. \tag{6.11}$$

From the figure we can easily see that the choice of focus will be a trade-off between trap depth and Rayleigh length; the trap depth gives an indication of the percentage loaded into the trap and the Rayleigh length is related to the distance over which the atoms can be guided. An additional factor to consider is the overlap of the guide with the MOT, since only atoms which are spatially overlapped with the guide can be loaded. Obviously good mode matching of the shape of the MOT with the guiding potential is important, hence the choice of an elongated MOT.

6.3.2 Loading into the guide beam

The percentage of MOT atoms loaded into the guide can be studied by imaging the atomic cloud after it has been released from the MOT and allowed to ballistically
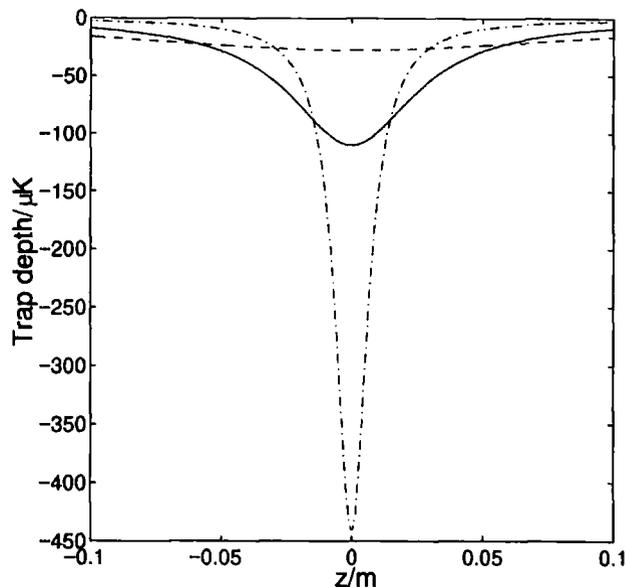
Figure 6.7: Trap depth along the axis of a focused laser beam, with beam radius at the focus, w_0. $w_0 = 50 \ \mu$m (dot-dashed), $w_0 = 100 \ \mu$m (solid) and $w_0 = 200 \ \mu$m (dashed).

expand for a variable time delay, typically between 20 and 30 ms. The guided atoms can be seen as a sharp peak superimposed on top of the gaussian distribution of the unguided atoms. The percentage loaded into the guide can be estimated by integrating over the number in the narrow peak and comparing it to the integral over the whole cloud.

Figure 6.8 shows experimental data on the fraction loaded into the guide for different values of w_0, with the guide focused in the MOT. The values of w_0 were calculated from the measured divergence of the beam. For each measurement the alignment of the MOT was optimised for maximum overlap with the guide and the temperature of the atoms was also optimised (the lowest temperature observed was 13 μK, but a temperature of approximately 20 μK is obtained easily without any optimisation). A maximum of 20% were loaded into the dipole guide beam. We attempted to improve this percentage by ramping up the magnetic field to compress the cloud, for a short period before the molasses phase, but this was unsuccessful.

Also shown on the figure are the results of a simulation of the percentage loaded into the guide from a MOT for different values of w_0 and different positions of the focus. For the simulation the density of atoms in the MOT was assumed to be gaussian in all directions, with $\sigma_x = \sigma_y = 0.2$ mm and $\sigma_z = 1$ mm, which are similar

to the parameters for our MOT. The power of the guide laser is taken as 19 W, with a detuning of 284 nm from resonance.

The first three data points agree well with the theoretical curve for atoms of temperature 13 μK. The final two points do not agree, most likely due to fluctuations in the temperature and that for larger foci it is more difficult to be certain of the precise position of the focus.

Loading the atoms below the focus and then launching them upwards avoids loss during the guiding. For example, if the position of the focus is shifted to 6 cm above the MOT (focusing through the aperture connecting the vapour cell and the UHV chamber) then all the atoms loaded from the MOT into the guide can be guided over a distance of at least 12 cm. Figure 6.8 shows that the optimum focus shifts to a larger value if the guide is focused 6 cm above the MOT. The Rayleigh range of 6 cm corresponds to a beam focused to 142 μm and for more sharply focused beams the trap depth in the MOT region falls off rapidly so very few atoms are loaded into the guide.

The dependence of the loading on trap depth can be simply studied by decreasing the power of the guiding laser (trap depth $\propto$ power) as shown in figure 6.9. The two sets of data correspond to the case where the guide is focused to 120 $\pm$ 25 μm in the MOT (circles) and 6 cm above the MOT (squares). There is a linear dependence as predicted by equation 2.9.

6.3.3 Temperature of Guided Atoms

The temperature of the guided atoms can be measured by considering the expansion of the guided atoms along the vertical axis. Dropping the atoms, we measured a temperature of 20 μK, consistent with a measurement of the temperature of the unguided atoms for the same alignment. This indicates that the sub-Doppler force is similar inside and outside of the guide, as would be expected for a light shallow trap, where the light shift is less than the optical molasses detuning. In our case, the ground state light shift is $\sim$ 6 MHz, i.e., the same order as the linewidth.

6.3.4 Importance of the Molasses Phase

For loading atoms into a dipole guide the molasses phase serves a dual purpose. Firstly, as usual, the molasses phase lowers the temperature of the MOT atoms by enabling the polarisation gradient cooling mechanisms. Secondly, the molasses
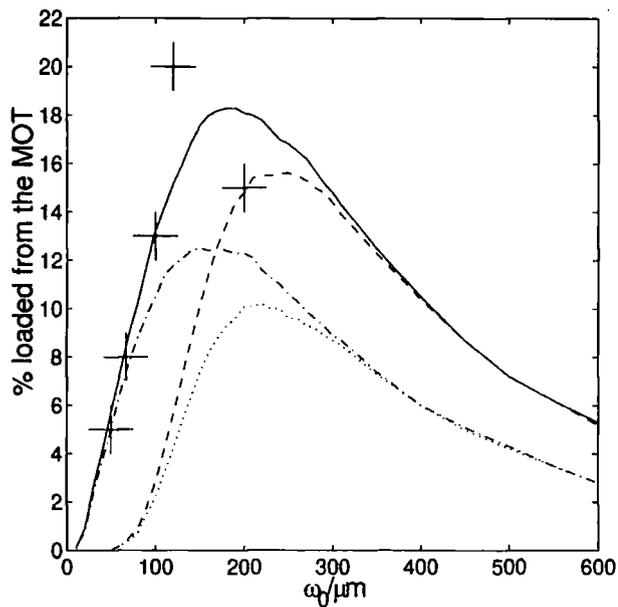
Figure 6.8: Fraction of atoms loaded as a function of laser spot size, w_0. The curves correspond to Monte Carlo simulations where the density of atoms in the MOT is gaussian with $\sigma_x = \sigma_y = 0.2$ mm and $\sigma_z = 1$ mm. The power of the guide laser is 19 W, with a detuning of 284 nm from resonance. Solid: Temperature of atoms $T = 13$ μK, guide focused in the centre of the MOT; dashed: $T = 13$ μK, guide focused 6 cm above the MOT; dot-dashed: $T = 20$ μK, guide focused in centre of MOT; dotted: $T = 20$ μK, guide focused 6 cm above the MOT. The data points correspond to experimental data.
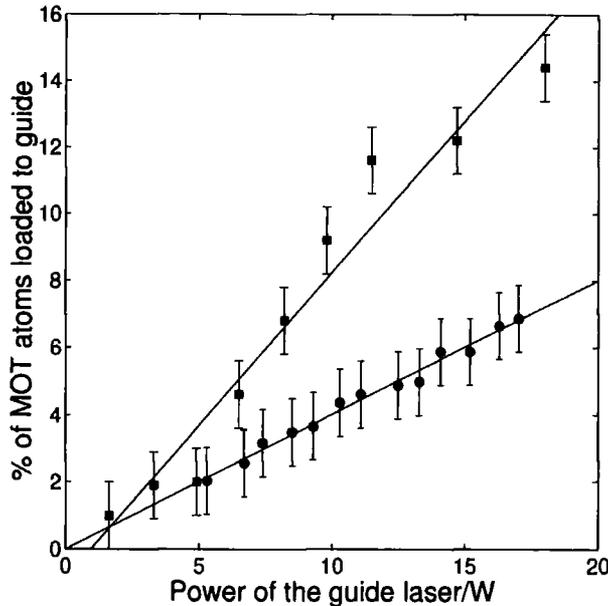
Figure 6.9: Percentage of atoms loaded into the dipole guide beam as a function of laser power. The guide is focused to 200 μm either in the centre of the MOT (circles) or 6 cm above the MOT (squares). The temperature of the cold atoms is 20 $\pm$1 μK.

phase estalishes a quasi-equilibrium temperature distribution across the atom cloud, including the region overlapped with the dipole guide beam. Without this phase, if the dipole guide is not exactly aligned along the zero of the magnetic field, atoms are loaded to one side and the percentage loaded will be smaller.

In fact, if the magnetic field was left on for the duration of the low intensity, large detuning phase, the loading to the guide remained very similar indicating that the guide was well aligned with the zero of the magnetic field. Very close to zero magnetic field the polarisation cooling mechanism is not made ineffective by Zeeman shifts and the temperature of the atoms is similar to that obtained in optical molasses [108]. If the intensity and the detuning were kept at the MOT values the loading into the guide decreased by a factor of four due to the increased temperature of the atoms. This is important if one wishes to operate the fountain continuously.

6.3.5 Launching the Atoms Within the Guide

Typical images of the cloud as it travels upwards are shown in figure 6.10. The guided atoms are at the same vertical displacement as the unguided ones after launching. Thus both cooling and launching light forces act similarly inside and outside the

guide.

From the data in the figures it can be seen that for the launching and guiding parameters that were used, i.e., a hole of diameter 1 mm, 6 cm above the source and a launch velocity of 1.25 m/s, the guiding increases the number of atoms coupled into the UHV chamber by a factor of 50. This enhancement factor is a function of the speed of launch and hence the size of the unguided atomic cloud when it reaches the hole. For the slow launch speeds and small fountains that are important for this work, guiding the atoms is very important to improve the transfer to the UHV chamber.

The width of the atomic cloud as it is guided through the aperture is shown in figure 6.11. The data illustrates the focusing effect of the laser beam discussed in chapter 3.

6.3.6 Flux from the Pulsed Guided Fountain

With the rubidium reservoir at a temperature of $1.2°C$, approximately 10^8 atoms can be collected in one second, giving a flux from the 3D MOT of 1×10^8 s^{-1}. Assuming a loading percentage of 15% in to the dipole guide beam, the flux of atoms through the aperture into the UHV chamber is 1.5×10^7 s^{-1} or 4.8×10^{10} s^{-1}cm^{-2}. By operating with the rubidium reservoir at 40 °C, $\sim 10^8$ atoms can be loaded in 150 ms, giving a corresponding flux from the MOT of 6.7×10^8 s^{-1}. The flux of atoms into the UHV chamber is then 10^8 s^{-1} or 32×10^{10} s^{-1}cm^{-2}.

6.4 Extension to Continuous Operation

To obtain a higher flux of atoms it would be advantageous to operate the fountain continuously. The obvious choice for the generation of a continuously operated atomic beam is a 2D MOT, with no trapping along the axis of propagation of the beam, but cooling in all three dimensions. Then, only damping forces of the cooling light have to be overcome in order to extract atoms. Section 6.4.1 compares coil arrangements for producing a 2D trapping potential. Section 6.4.2 discusses the two-dimensional magneto-optical trap, including the modifications that were necessary to the magnetic field coils and a summary of some characterisation measurements. Section 6.5 describes the operation of the 2D MOT as a funnel, in which atoms are continuously extracted along the axis of zero magnetic field using moving molasses. The effect of the guiding potential is considered.
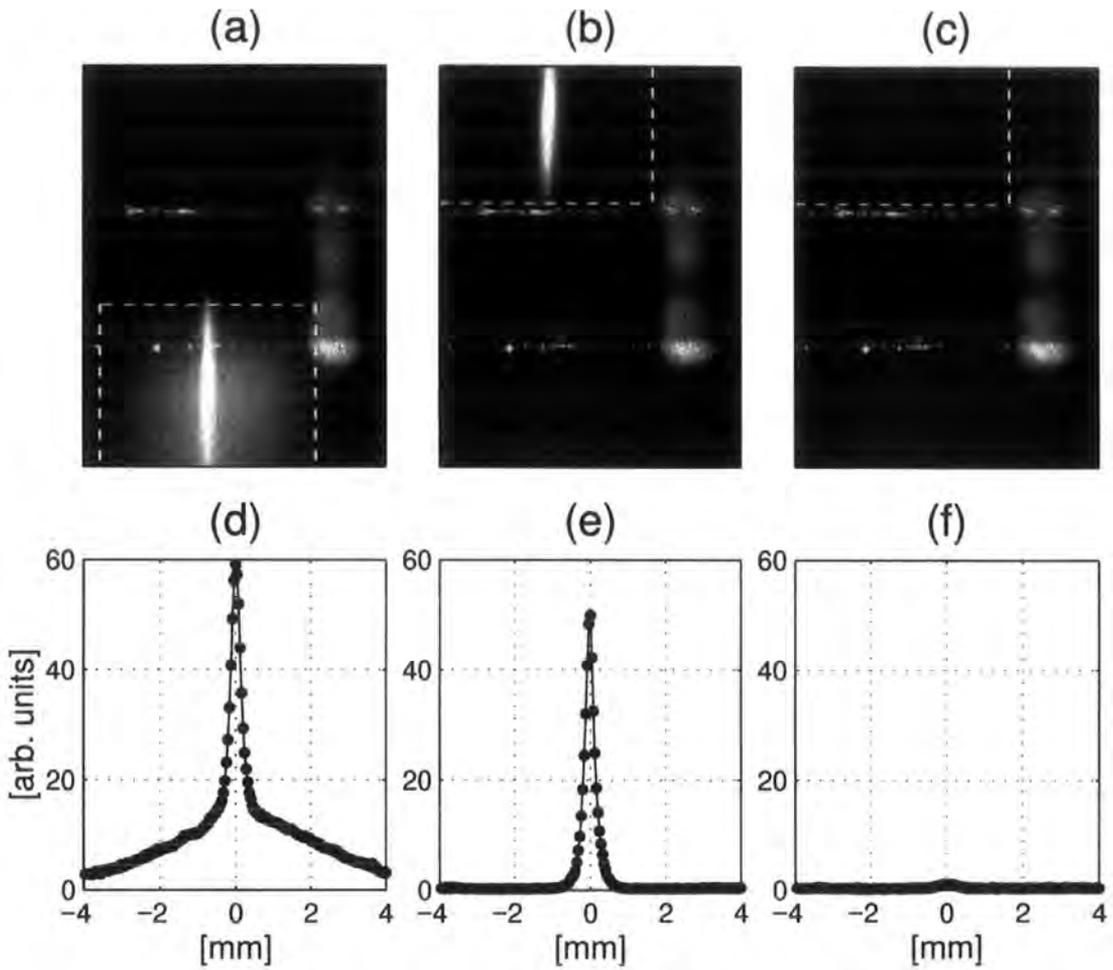
Figure 6.10: Atomic distribution at various delays after launching. The upper and lower surfaces of the quartz plate and the aperture between the two chambers are also visible in the figures due to scattered light. The relative position of the atomic cloud and the aperture is distorted due to refraction in the quartz. a) the distribution 55 ms after launch when the cloud is 6 mm below the lower surface of the quartz plate; b) the distribution 84 ms after launching, when the atoms are 4 mm above the upper surface of the quartz plate; c) image at 84 ms with no guide laser. For this last case very few atoms are coupled into the upper chamber. The lower figures show the corresponding integrated CCD signals, where the integrated area is indicated by a dotted line on the images. Scattered light has been subtracted. A comparison of d) and e) shows that all the guided atoms are transferred through the aperture, but comparing e) and f) shows that hardly any of the unguided atoms pass through.
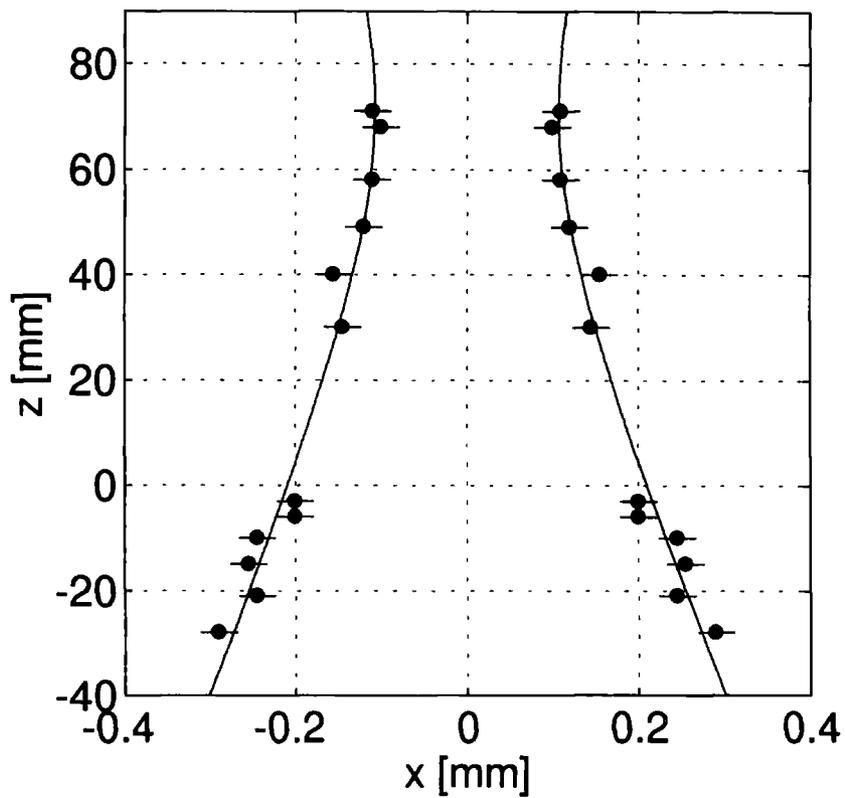
Figure 6.11: The width of the atomic distribution as a function of height, illustrating the focusing effect of the laser guide. The MOT and the aperture are at 0 and 60 mm respectively. The widths below 0 mm correspond to the atoms falling below the MOT position.

6.4.1 Design of the Magnetic Field Coils

A number of different coil geometries can be used to create a field which confines the atoms in two dimensions and not in the third. Two potential arrangements are considered here, both of which have been used in other experiments on two-dimensional traps [53, 49]. Both give a good 2D trap at the centre of the coils but differ mainly in the behaviour of the field outside of the region surrounded by the coils.

In order to compare the fields for each we have calculated both the z component of the field and the resultant field along a line parallel to the z axis, 1 mm away from the centre of the coil arrangement, using the Biot-Savart law.

The first option is that of 4 rectangular coils placed around the cell, to form a cuboid, which we will call the 'racetrack' configuration after [53] (figure 6.12). The coils would be positioned on the sides of the lower cell of our vacuum chamber, which therefore determines the length of the short side to be 9 cm. The long side is chosen to be 18 cm. The axes and origin of coordinates are shown in the figure. The z component of the field and the resultant field 1 mm off-axis are shown in figure 6.13. From this we can see that the radial magnetic field gradient near the origin for coils with 9 turns and a current of 60 A is around 20 G/cm. This falls to zero about 2 cm above the top of the coils and then increases again. It decays to 3% of the maximum value, 10 cm outside the coils. The z component of the field is zero for most of the length of the coils but there is a small increase to 0.5 G/cm at the top of the coils.

The second option which we shall consider is that of four rectangular coils placed at the corners of a square, pointing outwards, i.e., aligned along the lines of the diagonals of the square (figure 6.14), which we shall call the 'diagonal' geometry. The coils again measure 9 cm by 18 cm. Figure 6.15 shows the z component and the resultant field again for a distance of 1 mm away from the z-axis. The most obvious point is that the resultant field is less than half the value of that for the racetrack configuration, for the same current and number of turns. If the current is increased to give the same resultant field at the centre of the arrangement, the z-component also increases and becomes equivalent to the other case. The advantage of the diagonal arrangement over the racetrack, however, is that the resultant magnetic field decays away more quickly outside the coils. It decays smoothly to 3% of the maximum value over a distance of 5 cm outside the coils.

A commonly adopted geometry for 2D fields is the hairpin arrangement, formed
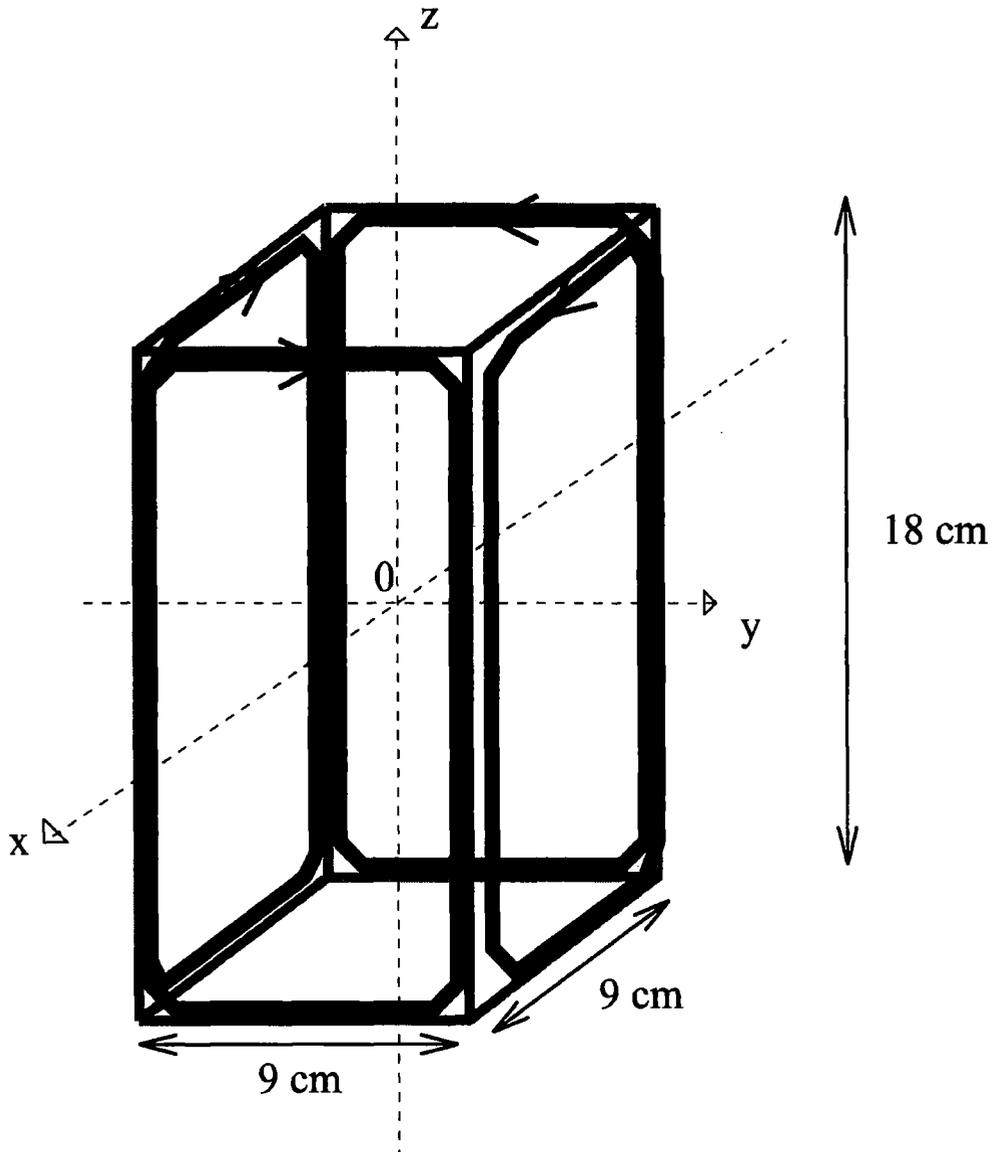
Figure 6.12: The racetrack coil geometry: four coils placed around the walls of the vacuum cell in a cuboid arrangement. The current in each is indicated by arrows. The axes and origin of coordinates are marked on the figure.
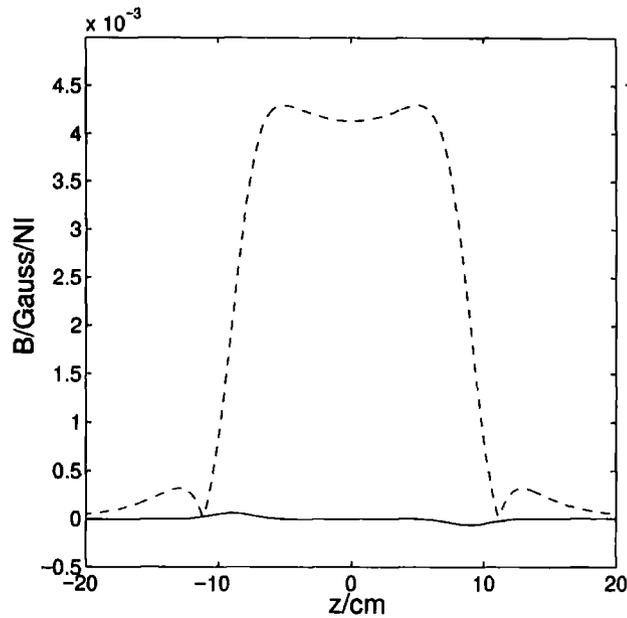
Figure 6.13: Racetrack configuration: magnetic field strength calculated from the Biot-Savart law, 1 mm away from the centre. The coils measure 9 cm by 18 cm and have N turns and carry a current I. The solid line shows the z-component of the magnetic field and the dashed line is the total resultant field.

from a single coil but with a similar resultant shape to that of figure 6.14. The resultant fields are also similar. However, separate coils can be more efficiently cooled in parallel rather than in series. For good cooling the coils should also be as small as possible. Figure 6.16 shows the effect of reducing the dimension a on the size of the resultant field near the centre of the coils. The current which travels in the opposite direction in the outer arm reduces the field at the centre of the coil arrangement. For an arm length of 8 cm, the field gradient at the centre is $\sim 90\%$ of its maximum value.

6.4.2 The 2D MOT

The magnetic field coils for the 2D MOT consisted of four coils, each measuring 12 cm by 8 cm, with 9 turns each. As for the 3D MOT coils, water cooling was necessary and the same technology was used, with the water cooling in parallel and the current in series through the coils. The coils were mounted on a single block with translation stages machined accurately at 45^0 outwards from the corners of the cell, giving only a single degree of freedom of movement, along the line connecting two coils at opposite corners. Mounts for the coils consisted of clamps which held the lower third of the coils. The clamps ensured that the coils remained rigid and
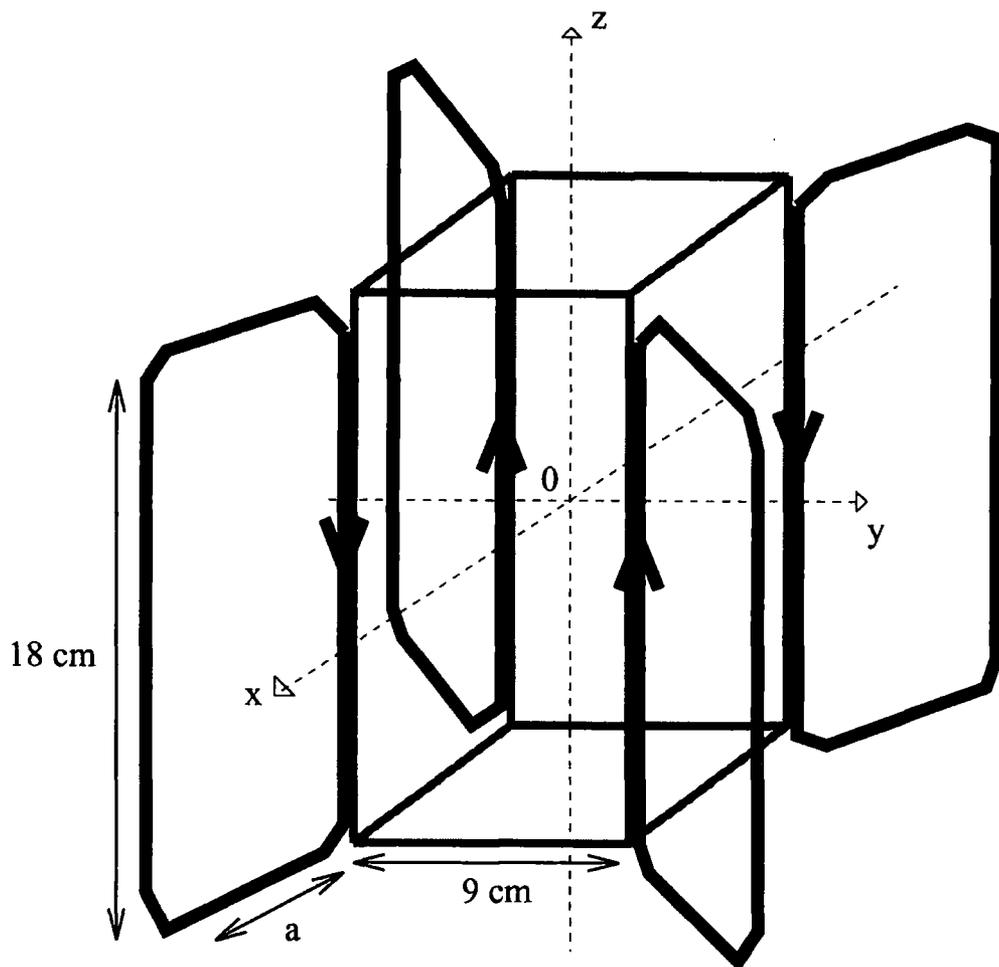
Figure 6.14: Diagonal geometry: coils placed around the vacuum cell aligned along the diagonals of the cell. The current in each is indicated by arrows. The axes and origin of coordinates are marked on the figure.
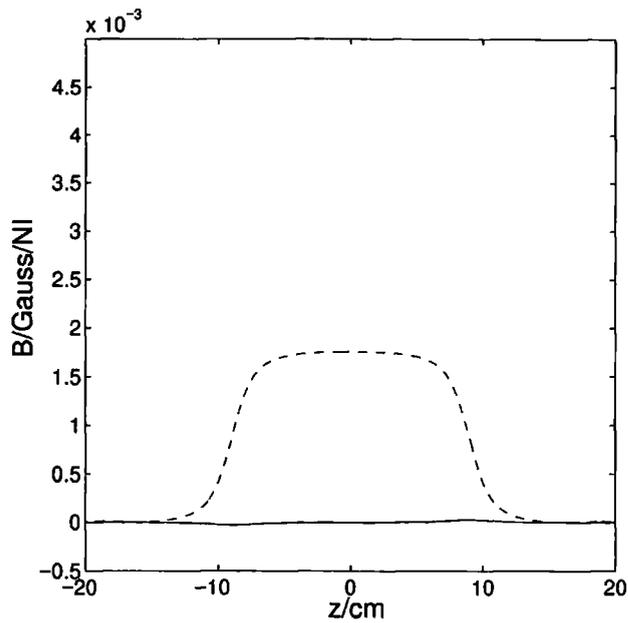
Figure 6.15: Diagonal configuration: magnetic field strength calculated using the Biot-Savart law, 1 mm away from the centre. The coils measure 9 cm by 18 cm and have N turns and carry a current I. The solid line shows the z-component of the magnetic field and the dashed line is the total resultant field.
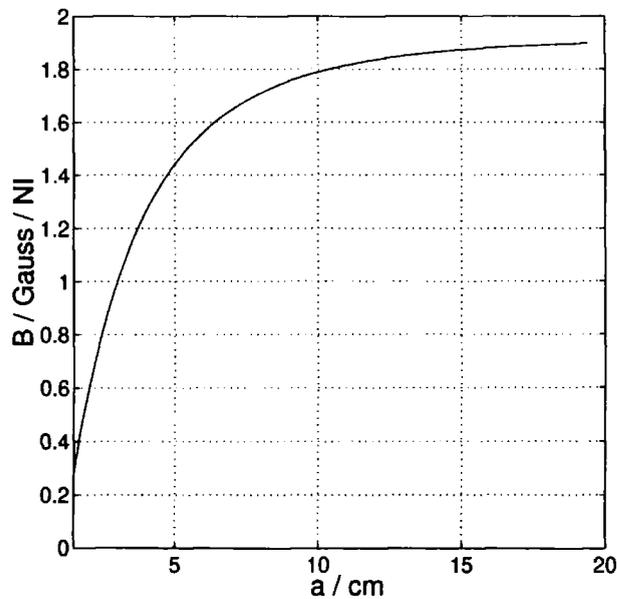
Figure 6.16: Resultant magnetic field 1 mm from the centre of the coils, as a function of the length a, marked in figure 5.14.
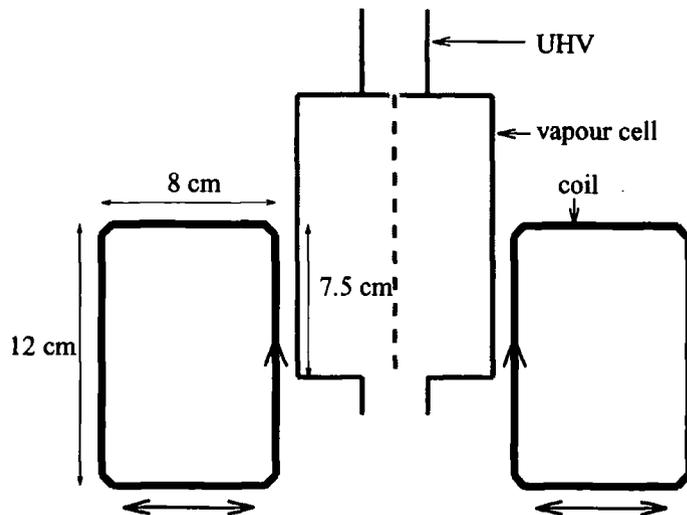
Figure 6.17: Schematic showing the vapour cell and magnetic field coils for the 2D MOT. The vapour cell measures 9 cm by 13 cm and the coils each measure 8 cm by 12 cm. The top of the coils is 1 cm above the centre of the vapour cell. Arrows on the diagram indicate the direction of movement along the translation stage. Arrows on the coils indicate the direction of the current.

upright. Figure 6.17 is a vertical cross-section showing the position of the coils relative to the vapour cell, with arrows indicating movement along the translation stage. The MOT beams cross at the centre of the cell and the height of the top of the coils is set to be approximately 1 cm above this point. Figure 6.18 is a horizontal cross-section. To avoid part of the vacuum system, the coils had to be rotated round by a few degrees from the corners of the cell, slightly restricting optical access. However, this did not prove to be a problem.

The beam alignment for the 2D MOT was the same as that for the 3D MOT. Figure 6.19 shows a CCD camera image of the two dimensional MOT. The MOT extends for the entire width of the laser beams in the vertical direction. Again the fringes imposed on the laser beams by interference at the uncoated windows are clearly visible.

6.4.3   Loading Rates

Since the 2D MOT has no confinement along one direction, it has a lower collection efficiency than the 3D MOT. The loading rate, R, into the 2D MOT is approximately 4 times lower than into the 3D MOT at the same Rb reservoir temperature. The intensity for both measurements is high enough to saturate the number of atoms in the MOT and the loading rate is a maximum. R_{2D} at 19°C was equal to R_{3D} at 13°C.
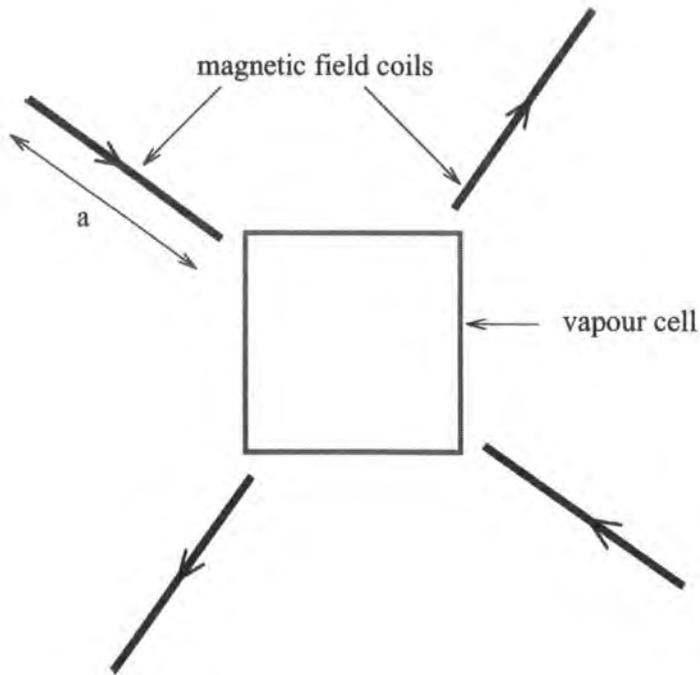
Figure 6.18: A horizontal cross-section through the vapour cell and magnetic field coils. The coils are mounted along the diagonals of a square and rotated from round a few degrees from the corners of the vapour cell. The arrows on the coils indicate the direction of the current.
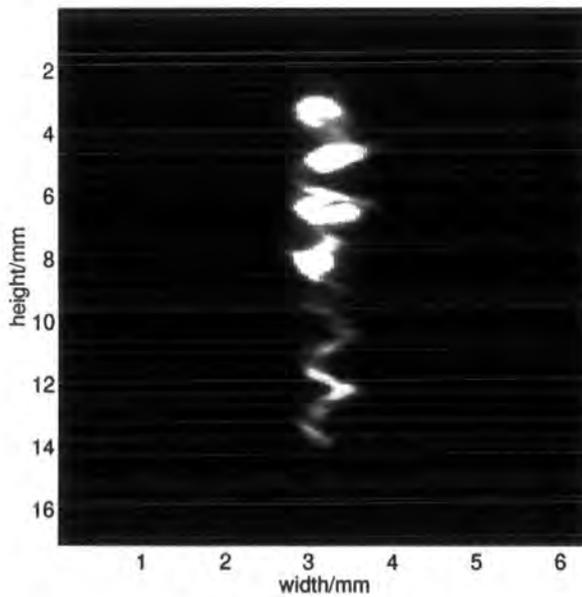
Figure 6.19: A CCD camera image of the 2D MOT.
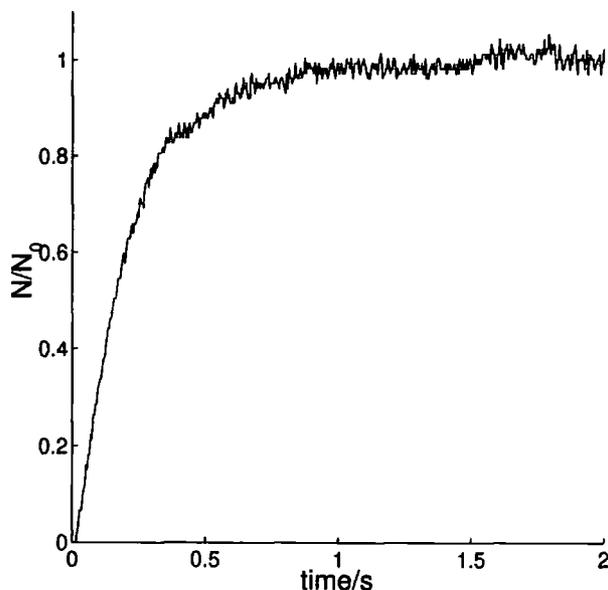
Figure 6.20: Loading rate into the 2D MOT with the Rb reservoir heated to 38^0C and the vacuum chamber en route to the vapour cell heated to 85^0C. The time constant is 160 ms.

For continuous extraction from the MOT it is obviously important to obtain a good loading rate in order to get a good flux. Figure 6.20 shows the loading rate if the Rb reservoir is heated to 38°C and the vacuum chamber en route to the vapour cell is heated to 85°C. In this case the time constant is of order 160 ms.

6.4.4 Comparison of number and temperature with 3D MOT

As with the 3D MOT it was necessary to optimise the number and temperature of the atoms. Figures 6.21, 6.22, 6.23 show the variation of the number of atoms with intensity, detuning and current through the magnetic field coils. Comparison with the results of chapter 4 shows that intensity and detuning are optimised for the similar parameters as for the 3D case, i.e., maximum intensity of 9 mW/cm^2. and a red detuning of 13 MHz. The dependence on the current through the coils is different to the 3D case, due to the different coil arrangement. The number of atoms maximised for a current of 90 A. In fact the coils begin to get hot for this current, so most of the work was performed using a current of 70 A.

In continuous operation the magnetic field is always on and there is no low intensity, high detuning molasses phase. The lowest temperature obtainable for an intensity of 9 mW/cm^2 and a detuning of -13 MHz is 55 ± 5 μK. This is still considerably lower than the Doppler temperature for rubidium (141 μK). With a low
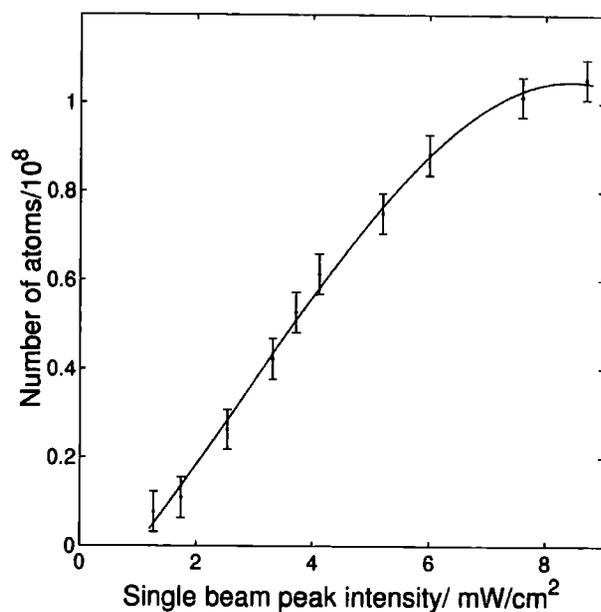
Figure 6.21: Number of atoms in the 2D trap as function of intensity of the cooling beams. The solid line is a fit to the data.
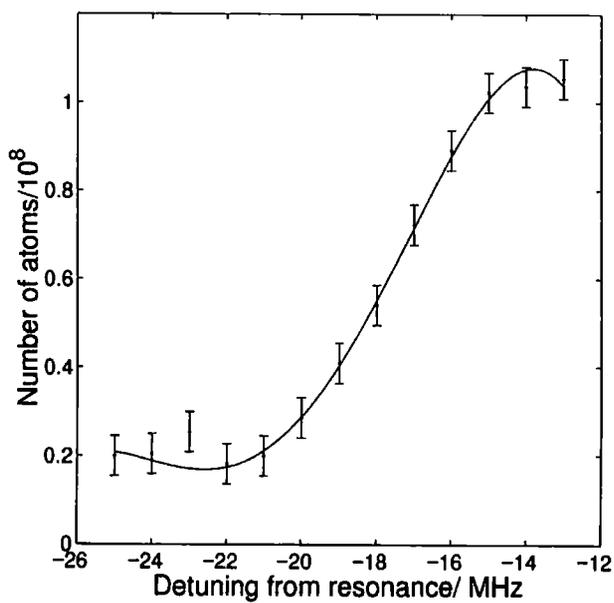
Figure 6.22: Number of atoms in the 2D trap as a function of detuning in the MOT. The solid line is a polynomial fit to the data.
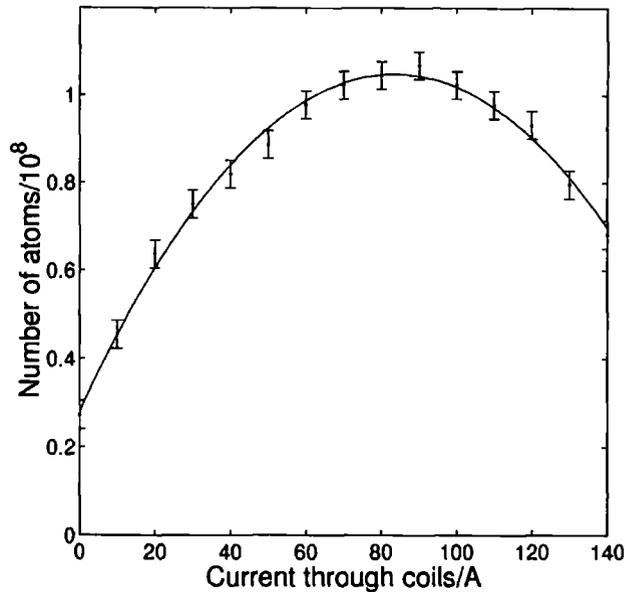
Figure 6.23: Number of atoms in the 2D trap as a function of current through the magnetic field coils. The solid line is a polynomial fit to the data.

intensity, far detuned molasses phase, the temperatures were comparable to those obtained in the 3D MOT.

6.4.5 Guiding

The loading into the guide from the 2D MOT depended in a similar fashion to the 3D MOT on the beam waist at the focus, the position of the focus and the temperature of the atoms loaded in. The actual percentage loaded was the same as the 3D MOT, within error, for similar temperatures and cloud sizes. However, since the 2D MOT can be longer in the vertical direction than the 3D MOT, the overlap with the guide is also improved. Therefore a loading percentage of 10% was observed for temperatures as high as 55 μK for a cloud measuring approximately 1.2 cm in the vertical direction.

6.5 The Guided Atomic Funnel

The 2D MOT can be simply converted into a 'funnel' by using the moving molasses frequencies continuously. Since the efficiency of the AOMs and the angle of deflection of the first order beam depends on their operating frequency, some small alignment adjustments are also necessary to switch between MOT and funnel. A CCD camera image of the funnel is shown in figure 6.24. Again, the funnel extends
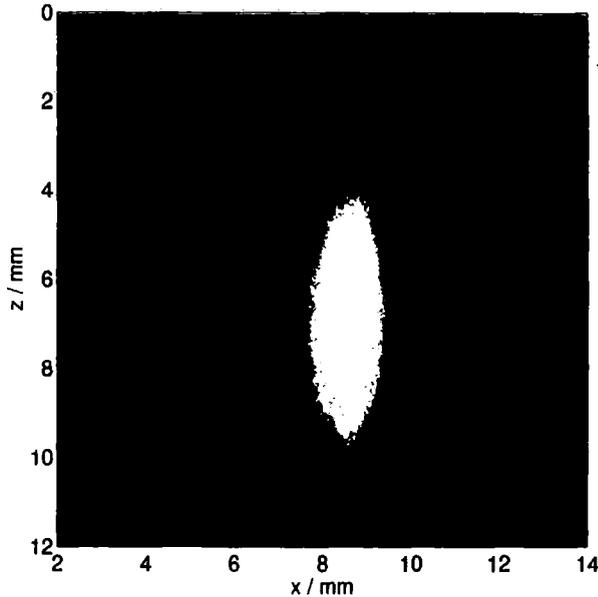
Figure 6.24: CCD camera image of the funnel.

for the entire length of the beams. In this case the fringes are not visible since the atoms are moving at ~ 1 m/s. There is a high background fluorescence because the vapour pressure has been increased by heating the reservoir to 40°C and the vacuum chamber enroute to the cell to 85°C to give a good loading rate.

6.5.1   Depumping atoms using a spatial method

One of the main problems of creating a continuous beam of atoms is that, as the atoms leave the region of the cooling light they are strongly affected by intensity imbalances which cause heating. Temperatures of a few hundred microKelvin are typical for atomic funnels [49, 50].

The guiding is particularly sensitive to any intensity imbalance of the beams. By allowing the guided atoms to be launched and then return to the MOT region it is possible to isolate the guided atoms from the unguided ones and use the guided atoms as a diagnostic of the effect of the intensity imbalance. Figure 6.25 shows the guided atoms after a 240 ms flight time. The cloud now has a vertical width of over 2 cm. Figure 6.26 shows the effect of a low intensity, high detuning molasses pulse of 1 ms. Comparing the two figures it is clear that some atoms are knocked out of the guide by the short molasses pulse since the molasses beams do not balance perfectly in all places. The imbalance is particularly significant at the top and bottom of the
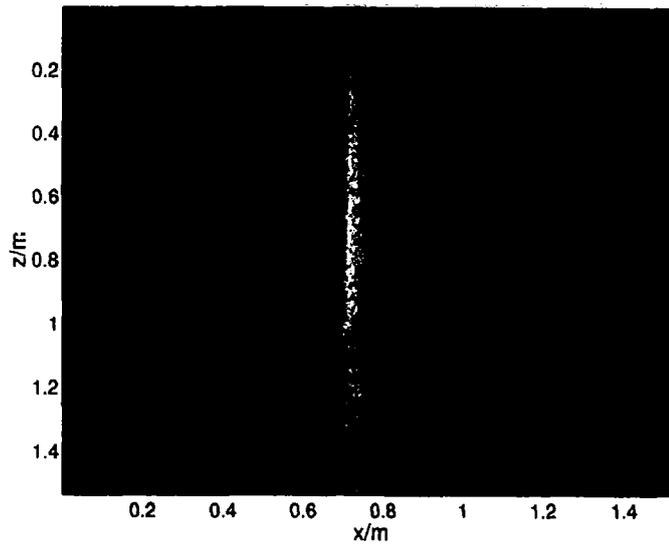
Figure 6.25: CCD camera image of the guided atoms returning to the MOT region after 245 ms.
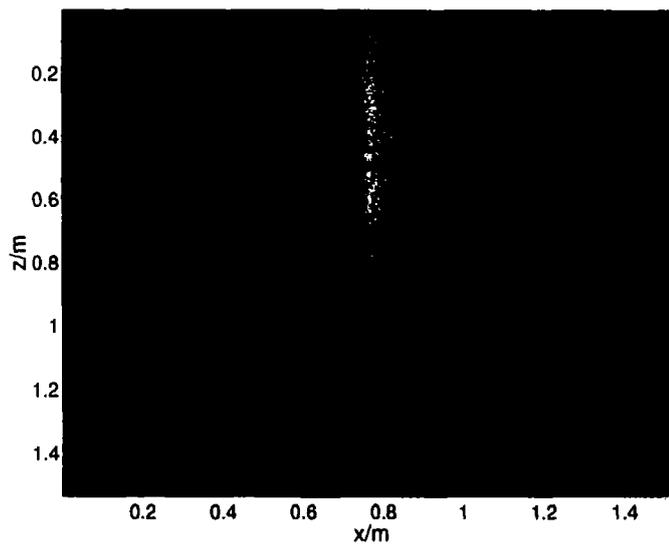
Figure 6.26: CCD camera image of the atoms returning to the MOT region after 240 ms. For this data a 1 ms low intensity, high detuning molasses pulse was applied before taking the image. By comparison with figure 6.25 it can be seen that atoms have been knocked out of the guide beam at the bottom of the figure due to an imbalance of the molasses beams in this region.

cooling region.

One method of reducing this problem is to pump the atoms into the lower hyperfine state before they leave the cooling region so that they are not heated on leaving the funnel. Using a horizontally aligned repumping beam that is smaller than the cooling beams or a beam with a sharp edge, the atoms will pass through a region of cooling light and no repumper as they leave the funnel and will be pumped to the lower hyperfine state. To create a sharp edge to the repumping beam at the top end of the funnel, the repumper was cut with a razor blade. Using this method the temperature of the atoms leaving the funnel was 55 ±5 μK, in agreement with the temperature of atoms in the 2D MOT, operating without a low intensity, far-detuned molasses phase.

6.5.2 Guiding

A maximum guiding of order 1% was observed for the funnel as compared to 10% for the 2D MOT for optimum guide beam parameters (note that the 2D MOT for these measurements extended for the length of the cooling beams i.e. 1.2 cm, giving a larger overlap with the guide beam and therefore a good loading percentage, despite temperatures of 55 μK). The lower guiding percentage arises because the atomic spatial distribution leaving the funnel is broader than that leaving the 2D MOT, even though the temperatures of the atoms are similar. A gaussian fit to the images obtained from the CCD camera and shown in figures 6.24 and 6.19 gives $\sigma = 170$ μm for the 2D MOT and $\sigma = 475$ μm for the funnel.

The broader width of the atomic distribution in the funnel can be explained by considering the various timescales involved. Atoms continuously leave the funnel at a speed of 1 m/s and for a funnel of length ~ 1 cm the average time spent in the cooling region is 10 ms. The motion of atoms in a magneto-optical trap is well approximated by damped simple harmonic motion:

$$F = -\kappa x - \alpha v, \qquad (6.12)$$

where the spring constant, κ, is:

$$\kappa = \frac{\alpha g_e \mu_B b}{\hbar k}, \qquad (6.13)$$

with g_e is the g-factor of the excited state, μ_B is the Bohr magnetron, b is the magnetic field gradient and α is the friction coefficient in the laser field:
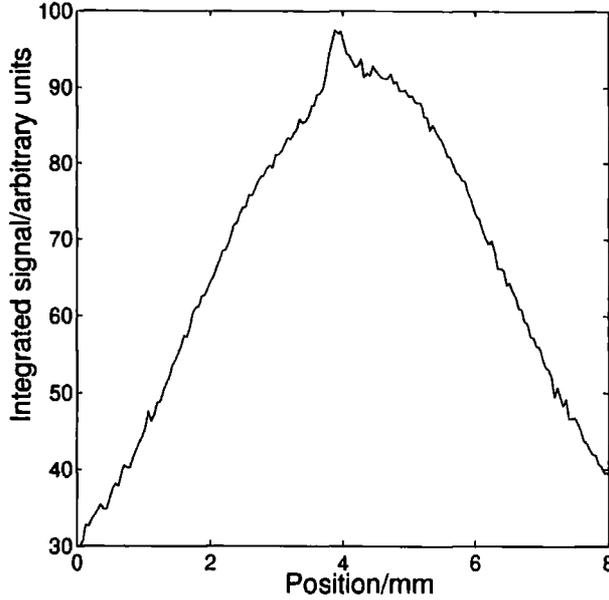
Figure 6.27: Cross-section through atomic cloud leaving the funnel with the dipole guide switched on. The percentage of atoms guided is 0.5%.

$$\alpha = -12\hbar k^2 \frac{I}{I_{sat}} \frac{2\Delta/\Gamma}{[4\Delta^2/\Gamma^2 + (1 + 6I/I_{sat})]^2} \qquad (6.14)$$

I is the single beam intensity. The expression for α can be simply derived from Doppler cooling theory [14]. For our parameters $\alpha \approx 0.09 \ \hbar k^2$.

The condition for critical damping of simple harmonic motion is $\alpha_c = 2m\sqrt{\kappa/m}$, where m is the mass of a rubidium atom. For a magnetic field gradient of 6 G/cm, we find $2m\sqrt{\kappa/m} = 0.0059 \ \hbar k^2$. Therefore, for our parameters, $\alpha \approx 15\alpha_c$ and the system is overdamped.

Finally the period of the simple harmonic motion, $T = 2\pi\sqrt{m/\kappa}$, is 29 ms. Therefore the atoms which only spend 10 ms in the funnel do not have time to reach the equilibrium spatial distribution and therefore the funnel is much broader than the 2D MOT.

6.5.3 Comparison of the flux from the funnel and the 2D MOT

By integrating over the number of atoms obtained from the funnel in one second we can compare the flux for the funnel and the 2D and 3D MOTs operating in a pulsed
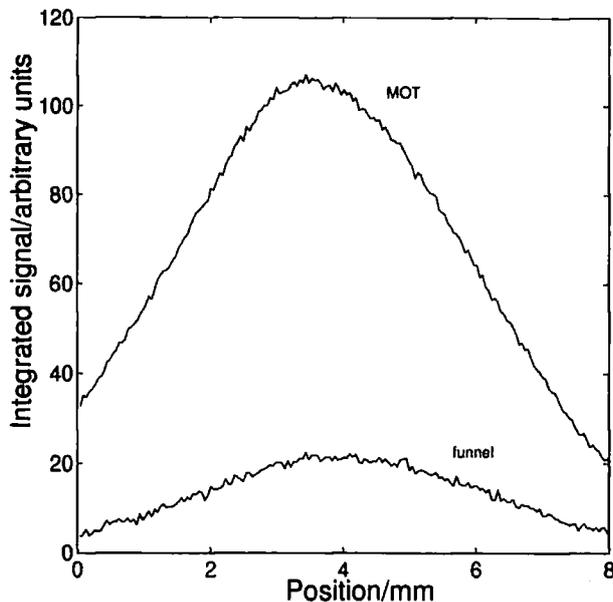
Figure 6.28: Flux of atoms, integrated over the vertical direction, obtained from the 2D MOT after 1 second loading time (upper curve) and from the funnel for the same vertical distance (i.e. implying a loading time of only 10 ms) (lower curve). The cooling light was switched off before taking the images.

fashion. The flux of atoms leaving the funnel was measured approximately 1 cm above the funnel, to avoid problems due to scattered light. Scattered light from the MOT knocked atoms out of the guide and also heated the unguided atomic beam after leaving the funnel.

If the 2D MOT is loaded for 150 ms, for a loading curve similar to figure 6.20, the flux is 1.7×10^8 s^{-1}. The funnel at the same vapour pressure gives a flux of 1.2×10^9 s^{-1}. Therefore for these parameters the flux obtained from the funnel in continuous operation is approximately 7 times higher than that obtained from the 2D MOT, operating in a pulsed fashion. The reason for this difference is that the 2D MOT has no confinement along one axis so that during the loading phase atoms are free to diffuse out of the MOT along this axis and therefore be lost. For the funnel, since atoms are continuously extracted there is no such loss. However, since the loading into the guide from the funnel is only of order 1%, compared to 15% for the 2D MOT and for the 3D MOT for similar guiding beam parameters, the flux into the UHV chamber is 1.2×10^7 s^{-1}, 2.6×10^7 s^{-1} and 10×10^7 s^{-1} respectively. The optimum configuration for our aim of transferring atoms efficiently at low velocity into the UHV chamber is therefore the 3D MOT, operating in a pulsed fashion, at high vapour pressures.

6.6 Summary

We have demonstrated an optically guided atomic fountain for efficient transfer of laser cooled atoms over a distance of order 10 cm. For a given laser power and detuning the percentage loaded in the guide laser beam is dependent on the temperature of the atoms, the beam waist at the focus, the position of the focus and the overlap of the guide beam with the MOT. For our beam parameters (P = 19 W, Δ = 284 nm), we loaded a maximum of 20% of MOT atoms in the the guide for a 100 μm beam focused in the MOT, corresponding to a guiding distance $\sim$ 3 cm. For a 200 μm beam focused 6 cm above the MOT, 13% were loaded and can be guided over a distance of more than 12 cm.

The transfer of atoms is very efficient. For a 20 μK cloud of atoms guided over 7 cm the phase space density decreases by a factor of around 4, compared to a decrease of a factor of more than 640 for a cloud of atoms ballistically expanding in free flight over the same distance. The guided cloud has a transverse dimension $\sim$ 200 μm, comparable to the dimension of a typical atom trap.

We have also compared the flux of atoms obtained from a 3D MOT with a 2D MOT and a funnel. The atomic flux obtained from the funnel is greater than that obtained from the 2D MOT or the 3D MOT. However, since the atomic beam leaving the funnel is broader, the loading into the guide beam is considerably less efficient. A guided fountain loaded from the 3D MOT delivers a factor of ten more atoms into the UHV chamber than a guided fountain loaded from the funnel and a factor of four more than from the 2D MOT. An additional problem in the funnel configuration is that any imbalance in the intensity of the cooling beams as the atoms leave the funnel tends to heat the atoms. This can be alleviated by blocking the repumper for the upper section of the funnel such that atoms are pumped into a dark state before they leave the cooling light. For continuous operation of the guided funnel, an opaque partition just above the exit of the funnel would be necessary to prevent scattered light from knocking atoms out of the guide.

Chapter 7

Loading an Atom Trap from the Guided Fountain

7.1 Introduction

Confining atoms in traps provides long interaction times and high densities, important for many studies of light-matter interaction and atom-atom collisions . There are various types of atom traps, including the magneto-optical trap (which we have already looked at in detail), magnetic traps, traps using oscillating electric fields[1] and optical dipole traps formed by far-off resonant light. Each has its own advantages and disadvantages. Amongst the issues that have to be considered are trap depth, method of loading and lifetime.

The magneto-optical trap combines the dissipative nature of near-resonant light with position dependent Zeeman shifts imposed by a magnetic field gradient to provide a trap a few Kelvin deep and the ability to load from a room temperature vapour. The presence of near-resonant light, however, sets a limit to the density achievable, as we have already discussed in chapter 2. For this reason, magneto-optical traps are often used as a preliminary to loading into a purely conservative trap, where the density limit can be exceeded.

Both the magnetic trap and the far-off resonant optical dipole trap are conservative traps. Conservative traps have limited depth and no intrinsic dissipative mechanism and therefore the atoms need to be precooled before they can be loaded. Magnetic traps can be a few hundred milliKelvin deep, but have the disadvantage that the trapping is dependent on the internal state of the atom, prohibiting certain

---

[1]Static electric fields cannot produce a trapping potential since it is impossible to obtain a minimum of the potential using static fields. A dynamic trap has been proposed by Riis and Barnett [109].

spectroscopic measurements and precision measurements.

The optical dipole trap is more flexible. Light traps provide easy control of the trapping potential, both spatially and temporally. Tighter confinement is possible and for sufficiently far detuned traps, where the Stark shift is much greater than the hyperfine level splitting for linearly polarised light (for circularly polarised light the detuning must be greater than the fine structure splitting), all the hyperfine levels move together [113] and therefore a number of different magnetic sub-levels can be trapped. These factors combine to make dipole traps ideal for spectroscopy and collisional studies [110, 111, 112]. However, the trap depth is only of order 1 mK.

Loading into either a magnetic trap or an optical dipole trap without the aid of near-resonant light could open up a route to overcoming the density limitations of the MOT. By multiple loading of atoms the number limit could also be exceeded. Any such scheme requires a method of delivering cold atoms (e.g. the guided fountain) and a technique for loading them into the trap.

In this chapter we shall investigate the possibility of obtaining a large number of atoms in an optical dipole trap. First we look at losses from optical dipole traps and existing methods of loading them. We then discuss schemes for loading an optical dipole trap from the guided fountain. In section 7.4 we demonstrate experimentally a method of loading an an optical dipole trap, spatially separated from the MOT, using the guided fountain. The trap is based on a time dependent potential and therefore can be loaded without any additional cooling. The idea is adapted for accumulation of atoms by multiple loading.

7.2 Loss Mechanisms from Optical Dipole Traps

Optical dipole traps are not truly conservative, as discussed in chapter 2 (section 2.4.1). A dissipative component arises from heating due to spontaneous emission. In the limit where $\Delta \gg \Gamma$, the scattering rate is given by:

$$\gamma_s = \frac{\omega_R^2 \Gamma}{4\Delta^2},\tag{7.1}$$

i.e., $\gamma_s \propto I/\Delta^2$. Heating due to scattering a large number of photons can lead to trap loss. Since the trap depth is proportional to I/Δ (equation 2.9), the scattering rate can be decreased and the trap depth maintained by increasing both intensity

and detuning.

Other losses arise due to collisions. The number of trapped atoms is expected to vary as:

$$\dot{N}(t) = -\alpha N(t) - \beta \int n^2(\mathbf{r}, t) d^3 r - \gamma \int n^3(\mathbf{r}, t) d^3 r. \qquad (7.2)$$

The first term is loss due to collisions with a background gas. As an indication of the size of this term, the $1/e$ lifetime, $\tau = 1/\alpha$, is around one second at a pressure of 3×10^{-9} Torr [113]. The second term is due to binary collisions. In the absence of resonant light, the most important of these is hyperfine structure changing collisions. β is typically of the order 5×10^{11} cm^{-3}s^{-1} [114, 115]. If there is any near resonant light present, excited state fine structure changing collisions, radiative redistribution and photoassociation [21] also become important. The final term, three body losses, only plays a role at very high densities, such as those for Bose-Einstein condensates trapped in optical traps [116].

7.3   Loading Optical Dipole Traps

The most common method of loading a dipole trap is directly from a MOT, by simply spatially overlapping the two traps. For focused laser beams a trap depth versus volume trade-off is necessary - the overlap with the MOT should be as large as possible whilst still maintaining a great enough trap depth to confine the atoms. Loading atoms directly from a MOT implies the same phase space density and number limits inherent in the MOT. The density in a dipole trap can be ramped up by adiabatically tightening the trapping potential, but the temperature will also increase keeping the phase space density constant [117].

7.3.1   Loading Directly from the MOT

We measured the characteristic lifetime of a crossed-dipole trap loaded by overlapping with our vapour cell MOT. The crossed-dipole was formed using the 12 W Nd:YAG beam aligned vertically and focused to a beam waist of 200 μm in the MOT region. The beam was retro-reflected to give a total power of 19 W. The retro-reflected beam (power 6 W) was recycled, focused to 60 μm and aligned horizontally to form the crossed trap in the MOT region. The resulting trap depth was 125 μK. The crossed-dipole trap was left on continuously.

The MOT was loaded for 750 ms and after a short molasses phase, which cooled the atoms to 20 μK, all cooling light was switched off and the atoms allowed to fall under gravity. Those overlapping with the crossed dipole trap remain trapped (figure 7.1). Imaging the trap after a variable delay, we obtained the lifetime. Since the imaging is destructive, each measurement was taken for a new load of atoms. A typical lifetime curve is shown in figure 7.2 where each point represents an average of six measurements. No data points were taken for the first 150 ms to allow the untrapped atoms to fall out of the detection region. The data can be fitted with a single exponential, giving a lifetime of 370 ms.

Possible loss mechanisms include heating due to spontaneous scattering, hyperfine state changing collisions and collisions with the background gas. The spontaneous scattering rate is only of order 1 s^{-1} and therefore negligible. The density in the trap should be too low for hyperfine structure changing collisions to be significant. This was confirmed by pumping atoms to the lower hyperfine state at the end of the molasses phase by switching off the repumper several milliseconds before the cooling light. No change of the lifetime in the crossed-dipole trap was observed. Therefore, we would expect that the lifetime measurement is dominated by loss due to collisions with a background gas. We have no way of measuring directly the pressure of the background gas in the lower vapour cell, but, from the vapour pressure of the rubidium reservoir we expect the pressure to be of order 10^{-8} Torr. A lifetime of 370 ms at this pressure agrees well with measurements of other groups [113].

A crossed-dipole trap loaded from a vapour cell MOT is the easiest way to load an optical dipole trap. The vapour cell MOT is much simpler than a MOT loaded from a Zeeman slower. However, the lifetime of the trap (370 ms) is relatively short - lifetimes of up to 200 s have been observed for far-off resonant traps [80]. To obtain longer lifetimes the background pressure must be reduced by trapping in an UHV chamber.

7.3.2 Loading a trap below the MOT

Atom traps loaded a small distance (a few millimetres) away from the MOT have been demonstrated [73, 118, 119, 120]. The traps are all variations on a gravito-optical trap (so named since the trap is closed from above by gravity) where the atoms fall a few millimetres onto a repulsive potential. Excess kinetic energy is removed by cooling of some form, most commonly a variation of Sisyphus cooling [25, 26]. Note that again near-resonant light is involved in the loading process. In
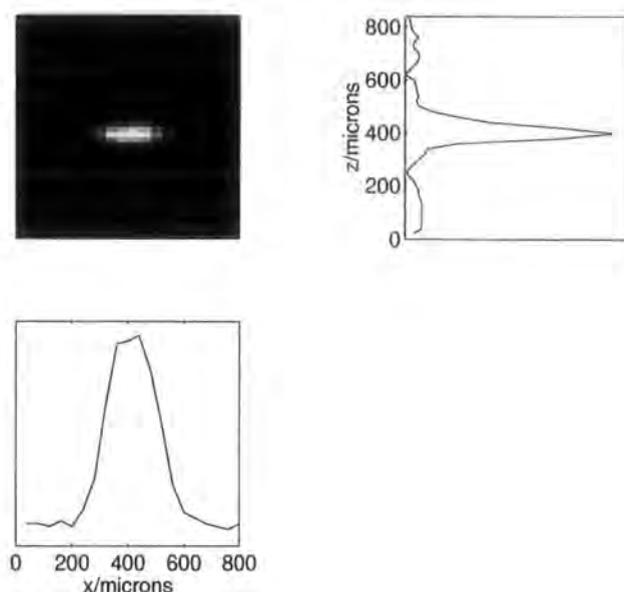
Figure 7.1: CCD camera image of the crossed-dipole trap together with horizontal and vertical cross-sections. The FWHM in the horizontal direction is 200 μm and 60 μm in the vertical direction. Note that the resolution of the CCD camera was only 44 μm in the horizontal direction and 22 μm in the vertical direction.
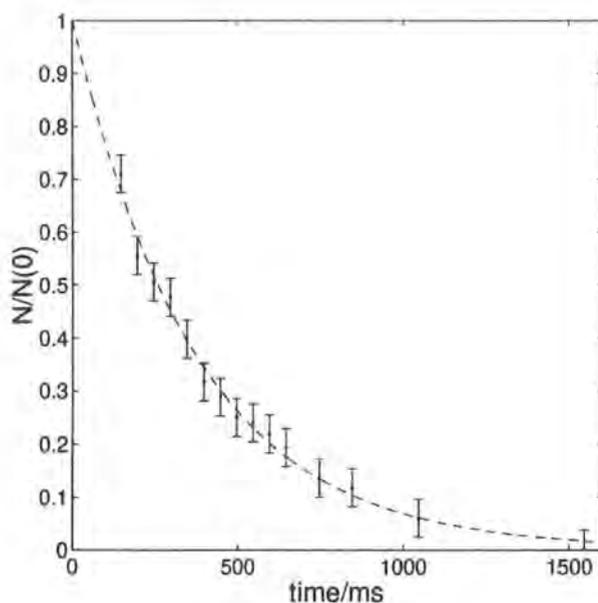
Figure 7.2: Number of atoms in the crossed-dipole trap as a function of time after switching off the MOT. The data has been fit with a single exponential, with a time constant of 370 ms.

addition, the traps are not sufficiently distant from the MOT to allow for the MOT to be reloaded whilst atoms are in the gravito-optical trap, preventing multiple loading schemes. A new technique is necessary to load an optical dipole trap spatially separated from the MOT without the aid of near-resonant light. One way is to use collisions to remove excess energy from the atoms delivered to the trap, similar to the idea of evaporative cooling [85]. An alternative is to use a time-dependent potential, where cold atoms are delivered to a particular region and then a trap is switched on to hold them there.

7.3.3 Crossed Dipole Trap at the Apex of the Fountain

In chapter 2 the results of a simulation of the density on axis of a guided atomic fountain with a crossed-dipole beam at the apex showed that in continuous operation a density enhancement in the crossed dipole region could be expected. Such a density enhancement could be useful for collisional loading of an atom trap. We have attempted to observe the density enhancement using the pulsed guided fountain.

The retro-reflected beam from the guide was focused to 60 μm and aligned to cross the guide, forming a cross-dipole trap in the UHV chamber, just above the aperture. Bunches of atoms were sent up from the MOT with the velocity chosen such that the apex of their trajectory coincided with the position of the crossed-dipole trap. Since the cloud is well spread out by the time it enters the vacuum chamber only a very small proportion of the atoms ($\approx$ 0.5%) turn around in the region of the crossed-dipole trap. Figure 7.3 is a cross-section through the atom cloud.

The most obvious feature is the dip in the originally gaussian profile. The dip arises when atoms moving upwards at velocities of a few tens of centimetres per second, pass the dipole trap, tend to be accelerated around it and are lost from the guide. There is also a small peak in the profile, but it is much broader than the width of the crossed-dipole trap. It appears that the atoms which do turn around in the region of the trap are slowed down, spending more time in the attractive potential. In continuous operation this should give rise to a large increase in density. This structure in the cloud is only visible for a short time period ($\sim$ 2 ms) indicating that it is due only to those atoms that turn around exactly in the region of the dipole trap. The broad dip is visible for around 10 ms since it arises when atoms with a range of velocities travel through the crossed-dipole region.

So, it is clear that it is difficult to obtain a significant density enhancement using
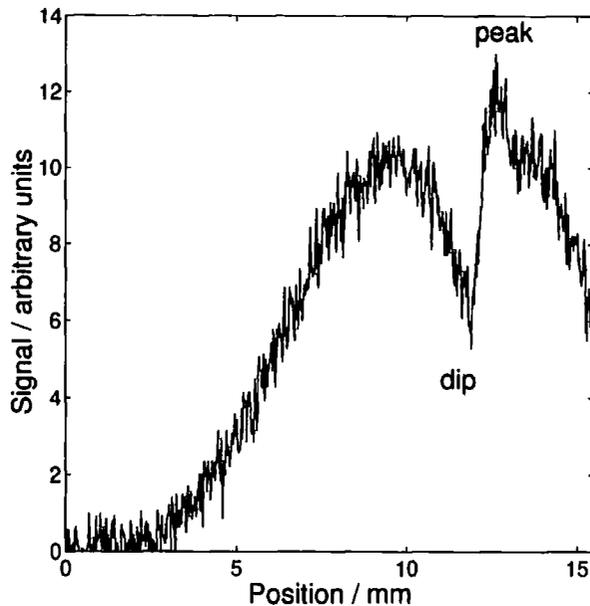
Figure 7.3: Vertical cross-section through the atom cloud as it turns around at the apex of the guided fountain in the region of a crossed-dipole trap.

a pulsed method. However, in continuous operation it may be possible to use the density enhancement to implement a collisional loading scheme.

Since the largest flux is obtained from the guided fountain operating in a pulsed fashion, a good alternative to collisional loading is a scheme using a time-dependent potential, as outlined in chapter 3. One example, the 'optical trap door' is outlined below.

7.4 The 'Optical Trap Door'

The idea of the 'optical trap door' is to create an optical dipole trap with a time-dependent potential that can be switched off to allow atoms to enter the trapping region and then on again to trap them. In our design we have chosen to use the red-detuned dipole guide beam to form the walls of a trap and an additional blue-detuned beam termed the 'trap door', aligned horizontally for the floor. The trap is closed from above by gravity. The trap is loaded several centimetres away from the MOT, in order to remove atoms spatially from the disruptive forces of resonant light. An efficient transfer technique is necessary. The optically guided fountain thus serves a dual purpose - it delivers cold atoms to a specific location and the guide beam also forms the walls of the trap itself. The scheme, then, is to launch

a cloud of atoms from the MOT with a velocity such that they turn around under gravity approximately 8 cm above the MOT. The atoms are guided through the aperture to an UHV chamber using the dipole guide beam. As they turn around under gravity, a blue-detuned trap door is switched on and the atoms fall back onto a repulsive potential and bounce, thus remaining trapped. Figure 7.4 illustrates the idea.

7.4.1   Quantum Monte Carlo Simulations

We can calculate typical atomic trajectories of atoms bouncing on the trap door beam using a Quantum Monte Carlo simulation [121]. The Quantum Monte Carlo method has been shown to be equivalent to the Optical Bloch equations and is computationally more efficient if a large number of atomic states are being considered. In this case, it is useful for gaining some physical insight into the bouncing process.

As the atoms fall onto a sharply focused laser beam, the number of photons scattered will depend on how far the atoms penetrate into the beam. Assuming that the atoms transfer adiabatically from a state $|g\rangle$ to dressed state $|2(N)\rangle$ as they enter the trap door beam potential, they will experience a repulsive potential. For light detuned by more than a few MHz, most atoms undergoing a spontaneous emission will fall into state $|2(N-1)\rangle$ and they will still feel a repulsive potential. The only change is then that due to the photon recoil. Occasionally, however, the atoms fall into $|1(N-1)\rangle$ and experience an attractive potential and thus tend to fall through the trap door. The relevant transition rates are given by equations 2.7. This process is modelled below.

First the initial position of the atom in the $x - y$ plane is chosen randomly from a gaussian distribution and the velocity of the atom is chosen randomly from a distribution corresponding to a temperature of 20 μK. Only atoms which are initially trapped in the dipole guide beam are selected. At the start of the calculation the atoms are a vertical distance of 30 μm above the blue-detuned trap door beam and are travelling downwards at a mean velocity of 0.485 ms^{-1}. The initial velocity is equivalent to that of atoms dropped from a height of 1.2 cm. The guide beam is focused to $w_0 = 100$ μm at $z = 0$, has a power of 19 W and a detuning of 284 nm. The trap door beam is focused to w_{0V} in the vertical direction and w_{0H} in the horizontal direction and has a power P and a detuning Δ. In the dressed state picture the atom remains in a single dressed state until a spontaneous emission occurs, when it is transferred to a new dressed state. The atomic trajectory is calculated by solving:
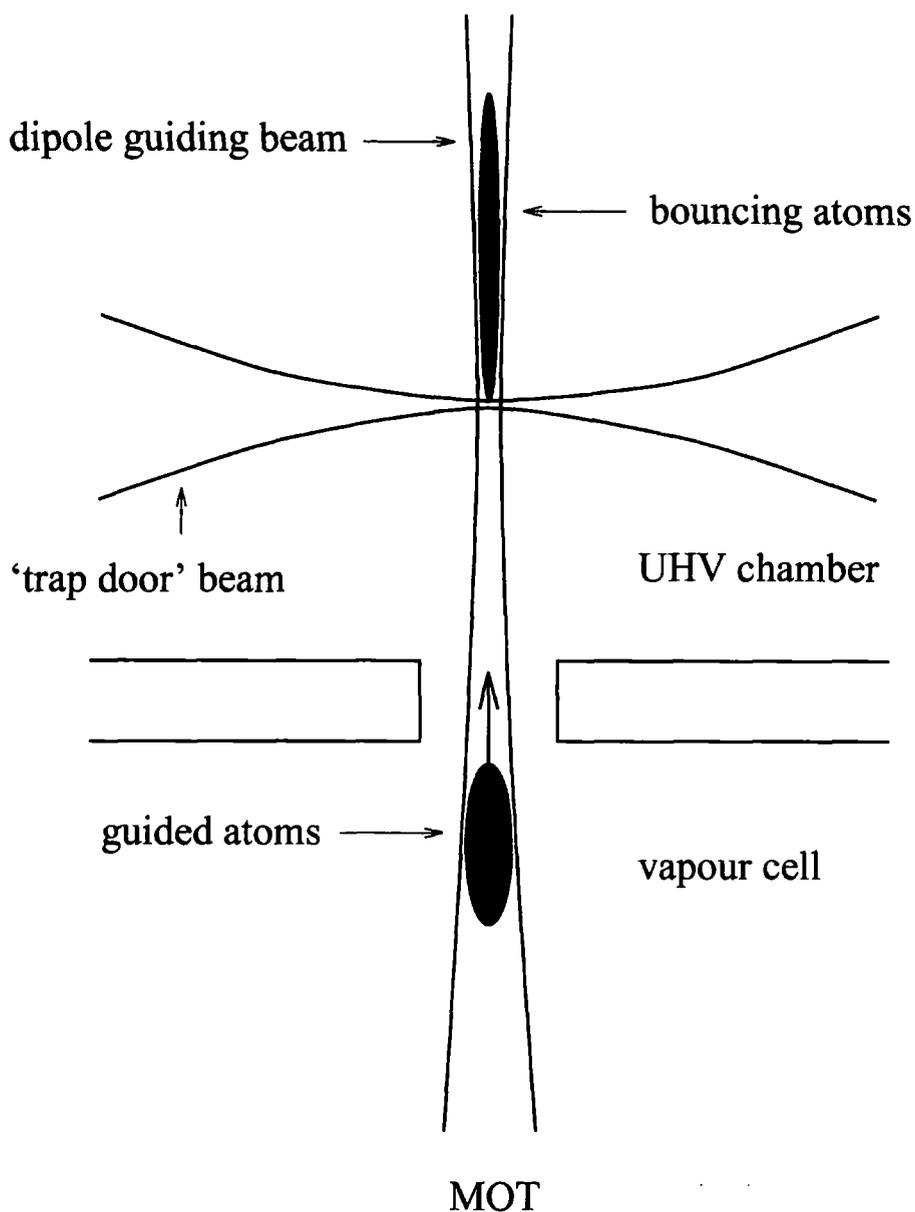
Figure 7.4: Schematic of the 'optical trap door'. Atoms are launched from a vapour cell MOT and guided into a UHV chamber using a far-off resonant red-detuned beam. As they turn around under gravity a blue-detuned 'trap door' beam is switched on. The atoms fall onto the beam and bounce.

$$m\ddot{\mathbf{x}} = -\nabla \mathbf{U}, \tag{7.3}$$

where $\mathbf{U}$ is the energy of the dressed state and includes the potential of the guide and trap door beams and gravity. The spontaneous emission process is modelled using a quantum Monte Carlo method [121, 122, 123, 124]. At each time step ($dt = (2\pi/100)\Gamma$) the probability for a spontaneous emission occurring is $dp = \Gamma dt |a_e|^2$ where $|a_e|$ is the normalised component of the excited state $|e\rangle$ in the dressed state. This is compared to a random number, α chosen between 0 and 1 and if $dp > \alpha$ then a photon is emitted. The choice of which state it falls into is again random, with probabilities weighted by the transition rates to the states $|1(N-1)\rangle$ and $|2(N-1)\rangle$.

The approximations made in the approach include the secular approximation: i.e. $\Omega \gg \Gamma$ so that the spontaneous emission occurs on a much shorter timescale than the Rabi oscillations and the photons of the laser field can be considered to be simply spectators during the spontaneous emission. The atom is treated as a pointlike particle. Collisions with other trapped atoms or the background gas are ignored. On a practical level the trap door beam is assumed to be perfectly gaussian and for most of the calculations scattered light is neglected.

Results

For the following calculations $w_{0V} = 5$ μm and $w_{0H} = 100$ μm.

Figure 7.5 shows a typical trajectory of an atom bouncing on the trap door beam. Figure 7.6 is a trajectory for the case where an atom emits a photon and falls into the wrong dressed state and is accelerated through the beam.

Figure 7.7 shows the percentage of atoms lost through the trapdoor beam as a function of trap depth for five different detunings. All the atoms fall through the trap door for trap depths less than 1.2 mK. For detunings of 14 GHz, 1.4 GHz and 140 MHz there is a sharp drop in the number of atoms lost at a trap depth of 1.2 mK. For trap depths of over 10 mK, less than 5% of the atoms are lost. The dependence is very different for detunings of 14 MHz. The drop in the number of atoms lost occurs for a higher trap depth (~ 4 mK) and the loss falls off more gradually.
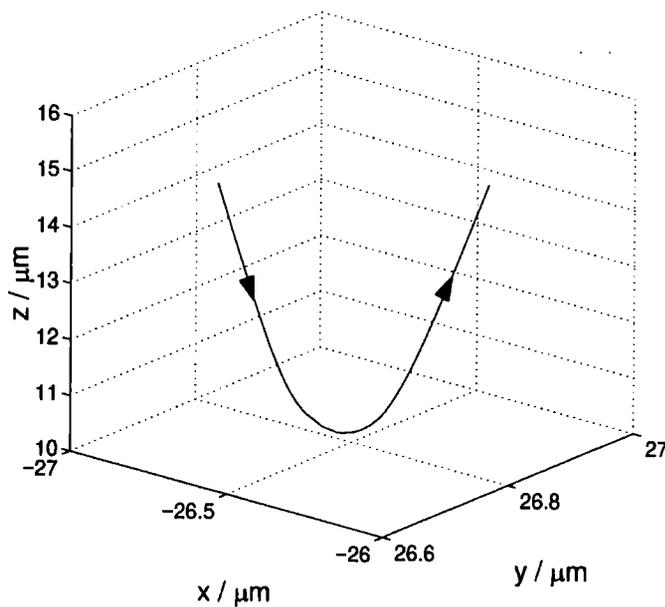
Figure 7.5: Typical trajectory of an atom bouncing on the trap door beam.
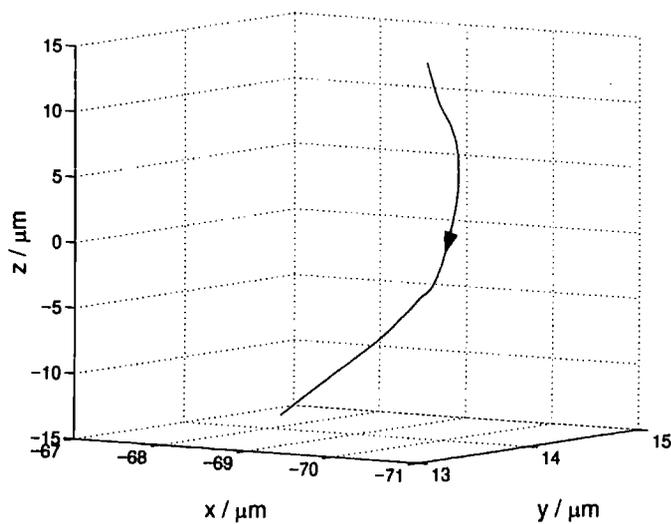
Figure 7.6: Trajectory of an atom that undergoes a transition to a dressed state which sees an attractive potential and falls through the trap door beam.
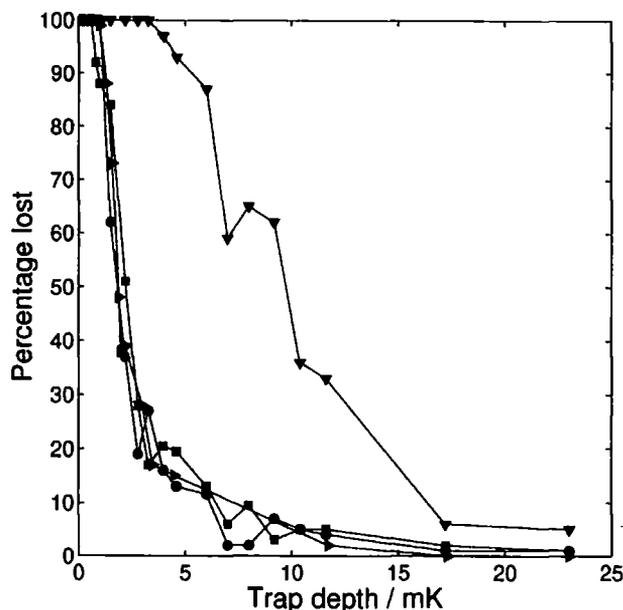
Figure 7.7: Percentage of atoms lost through the trap door beam as a function of trap depth for different detunings. Triangledown : 14 MHz; Square : 140 MHz; Circle : 1.4 GHz; Triangleside : 14 GHz.

Figure 7.8 shows the corresponding number of photons scattered. The number of photons scattered decreases rapidly as the detuning is increased. For detunings of greater than 140 MHz the photon scattering rate peaks for a trap depth of between 1 mK and 2.5 mK where the percentage of atoms falling through the beam is changing rapidly. Some atoms penetrate a long way into the beam before being reflected and therefore spend a long time in the light field and scatter a large number of photons. For detunings of less than 100 MHz the scattering rate continues to increase for trap depths up to 10 mK. This difference for smaller detunings can be explained by transitions to the dressed state $|1(N)\rangle$, in which atoms experience an attractive potential. Figure 7.9 shows the average time spent in the dressed state. The general shape closely follows the shape of the curves of the number of photons scattered.

In conclusion, over 95 % of atoms falling from rest from a height of 1.2 cm should bounce on the optical trap door beam for trap depths of over 10 mK, provided that the detuning is larger than 140 MHz. For a detuning of 14 GHz a 10 mK trap depth corresponds to a power of 8.6 mW (figure 7.10). For these detunings less than one photon is scattered for each bounce (figure 7.11) and scattering into a dressed state feeling an attractive potential is negligible.
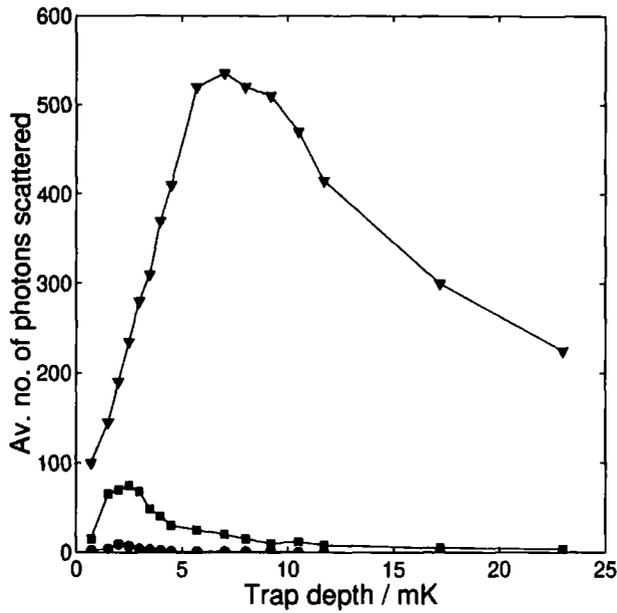
Figure 7.8: Average number of photons scattered by an atom bouncing on the trap door beam as a function of trap depth, for different detunings. Triangle : 14 MHz; Square : 140 MHz; Circle : 1.4 GHz.
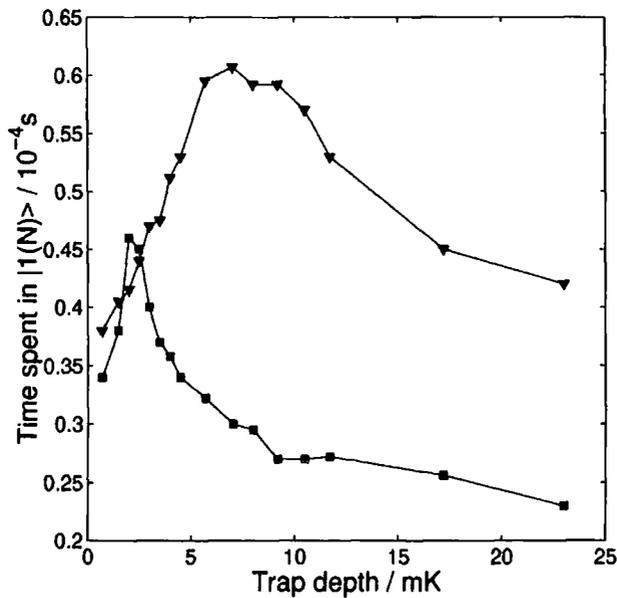
Figure 7.9: Average time spent in the dressed state $|1(N)\rangle$ (which experiences an attractive potential), as a function of trap depth for two different detunings. Triangle : 14 MHz; Square : 140 MHz.
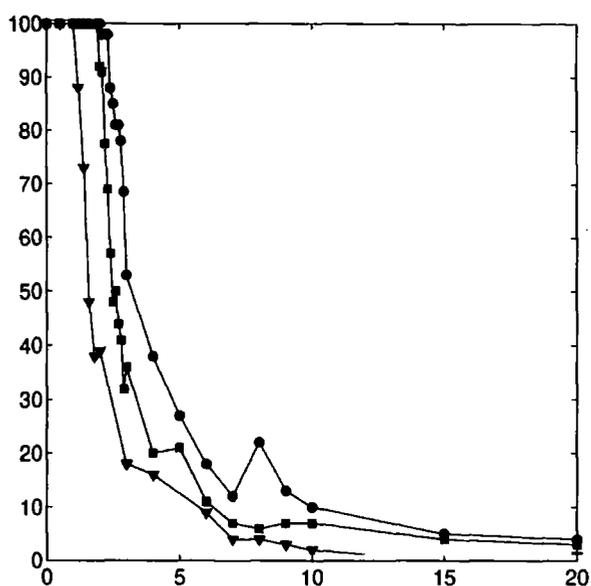
Figure 7.10: Percentage of atoms lost through the trap door beam as a function of power for different detunings. Triangle : 14 GHz; Square : 21 GHz; Circle : 28 GHz.
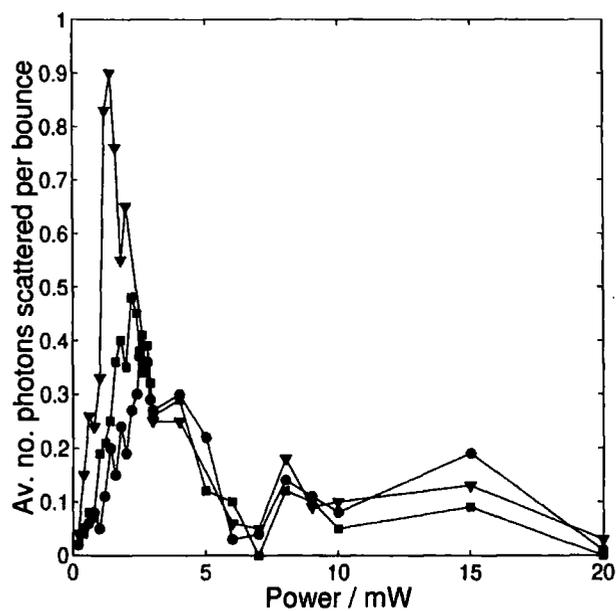
Figure 7.11: Average number of photons scattered by an atom bouncing on the trap door as a function of power for different detunings. Triangle : 14 GHz; Square : 21 GHz; Circle : 28 GHz.
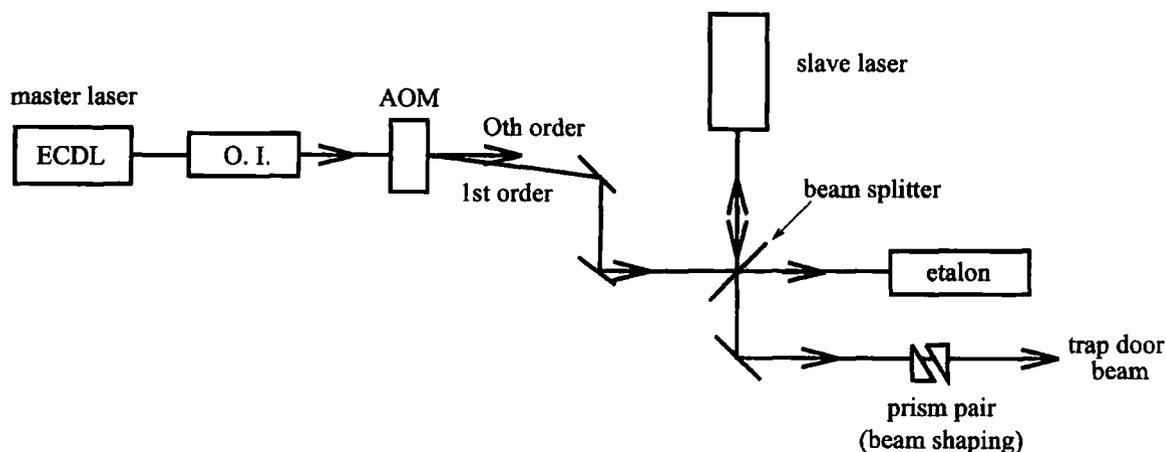
Figure 7.12: Set-up for generation of the trap door beam. A slave laser is injection locked by an ECDL. The injection lock can be switched on or off using an AOM.

7.4.2 The experimental set-up

The set-up for the trap door is illustrated in figure 7.12. The trap door beam is generated by a 70 mW Sanyo diode laser, injection locked [125, 126] by a master laser. The master laser is an extended cavity diode laser (ECDL) with a design similar to that of the repumping laser described in chapter 2 (section 4.2.1). In this case only a single level of temperature stabilisation is used, for the laser itself - the extended cavity is not temperature stabilised. The laser is not locked. The result is a laser with a linewidth of a few hundred kilohertz, stable to a few Megahertz. By changing the diode current or temperature, the laser can be blue-detuned from resonance in 7 GHz steps, up to 50 GHz, whilst monitoring the frequency with reference to the $^2S_{1/2}, F = 3 \rightarrow^2 P_{3/2}, F = 4$ transition on a scanning Fabry Perot etalon with a free spectral range of 70 GHz. The output of the master laser is passed through an optical isolator and then an acousto-optic modulator (AOM), which acts as a switch. When the trapdoor is 'on' the first order of the AOM can be used to injection lock the slave diode laser but when it is 'off' no light goes to the slave laser and the slave is free running. There is no shutter on the output of the slave laser so the beam is present even during the upward flight of the atoms, but at this time it is not injection locked. Since the free running frequency is 5 nm from resonance and the power is of order 50 mW, the light shift experienced by the atoms during their upward flight is equivalent to a few tens of microKelvin and therefore negligible to atoms travelling at a few tens of cm/s. Once the atoms have passed through the beam the injection lock is turned on and a repulsive barrier is created.

Stability of the injection locking of the slave was very important. Alignment of the injection lock is optimised by tuning the master to a rubidium absorption line and then monitoring the transmission of the slave beam through a Rb cell, whilst modulating the slave current. When the alignment of the injection lock is good the slave will injection lock over a range of a couple of milliamps and this can be seen as a decrease in transmission through the Rb cell. Figure 7.13 shows the current modulation applied to the slave laser and a corresponding transmission signal. When the injection lock is working well the transmission through the cell is a minimum. The flat portion corresponds to a locking range of around 1.5 mA. Injection locking mechanisms are discussed by Bouyer *et al* [127].

There are only certain combinations of temperature and current of the slave laser at which lasing behaviour is possible for the frequency of the injected light. By controlling the temperature of the slave the injection lock current can be set to give maximum output power. The stability of the injection lock was monitored during the experiment on another etalon.

The output beam from the slave is passed through anamorphic prisms to give a beam measuring approximately 1.5 mm by 9 mm. By a combination of spherical and cylindrical lenses the beam is focused a thickness of 10 μm and a width of 200 μm and aligned horizontally just above the aperture, crossing the dipole guide beam. The width of the focus can be confirmed by measuring the divergence of the beam over a couple of metres. The Rayleigh range of a beam focused to $w_0 = 5$ μm is only around 100 μm, so the translational alignment is critical and the final lens was mounted on a translation stage for easy adjustment of the focal plane.

7.4.3 Bouncing Atoms

Atoms are delivered to the region above the trapdoor beam by the pulsed guided fountain, which is described in the previous chapter. In this section we discuss the dynamics of an atom cloud bouncing on the 'trap door'. The observed distribution differs significantly from those of previous atom bouncing experiments [128, 129, 130] since in our case the spread in potential energy of the initial cloud is of the same order as the mean potential energy. In other bouncing experiments the potential energy spread is significantly less than the mean potential energy.

The flight time of atoms to the apex of the fountain is around 110 ms and in this time a cloud with an initial vertical size of 2 mm has expanded to 1.2 cm due
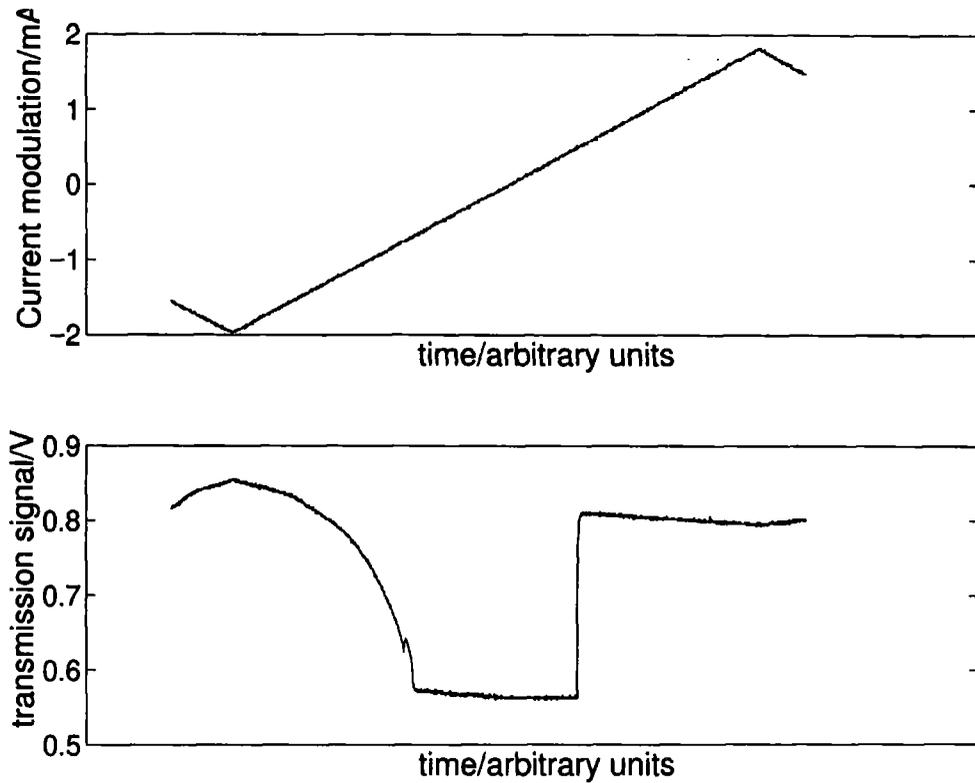
Figure 7.13: The upper figure shows the current modulation applied to the slave laser with a peak to peak amplitude of 4 mA. The lower figure show the corresponding tranmission of the slave beam through a cell containing rubidium vapour. The master laser is tuned to a rubidium resonance, such that when the slave is injection locked the transmission through the Rb cell falls. The lower level flat region indicates that the injection lock works well over a slave current range of more than 1.5 mA.
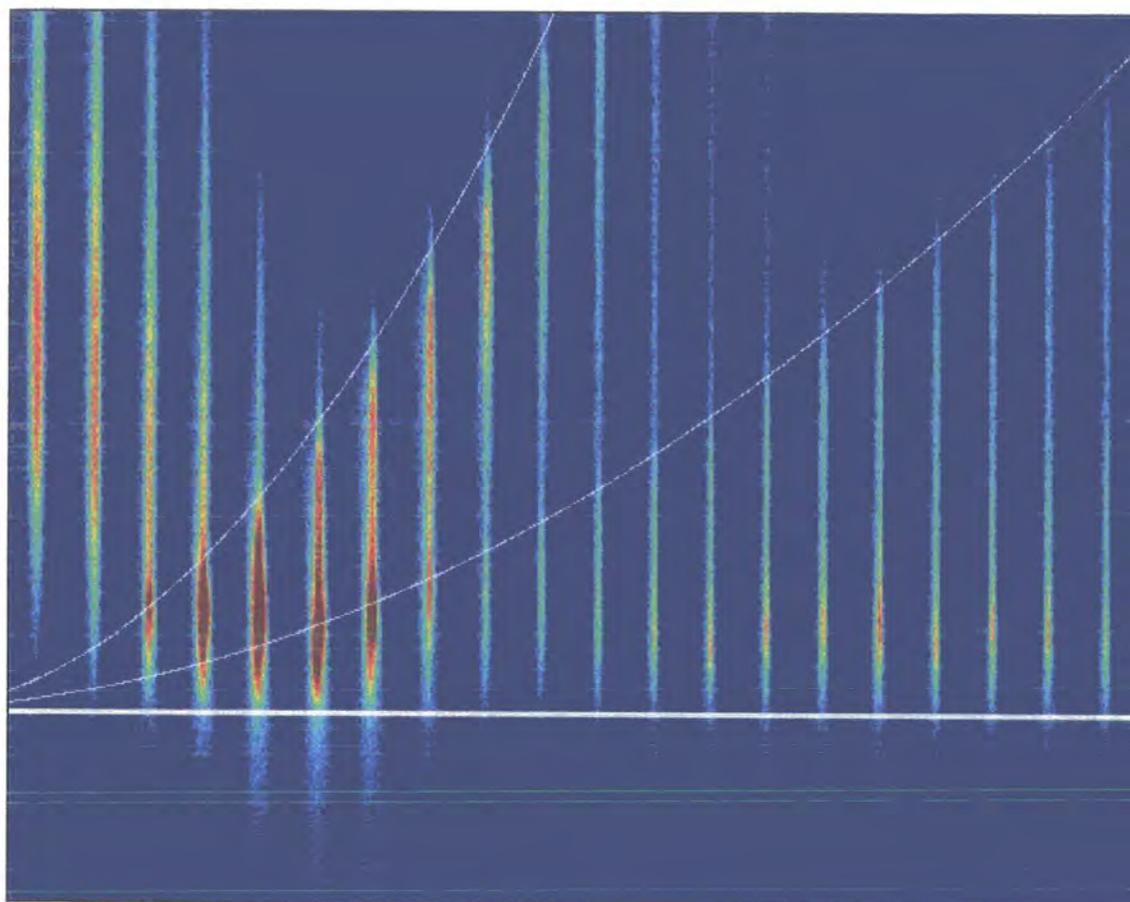
Figure 7.14: CCD camera images of atoms bouncing on the trap door beam, whilst guided in a far-red-detuned beam. The images are taken every 10 ms and the height of each image is 17 mm. Since the imaging technique is destructive each image is taken with a new cloud of atoms. The position of the trap door is indicated by a solid white line. Two parabolas are superimposed on the images as a guide to the eye (see text).
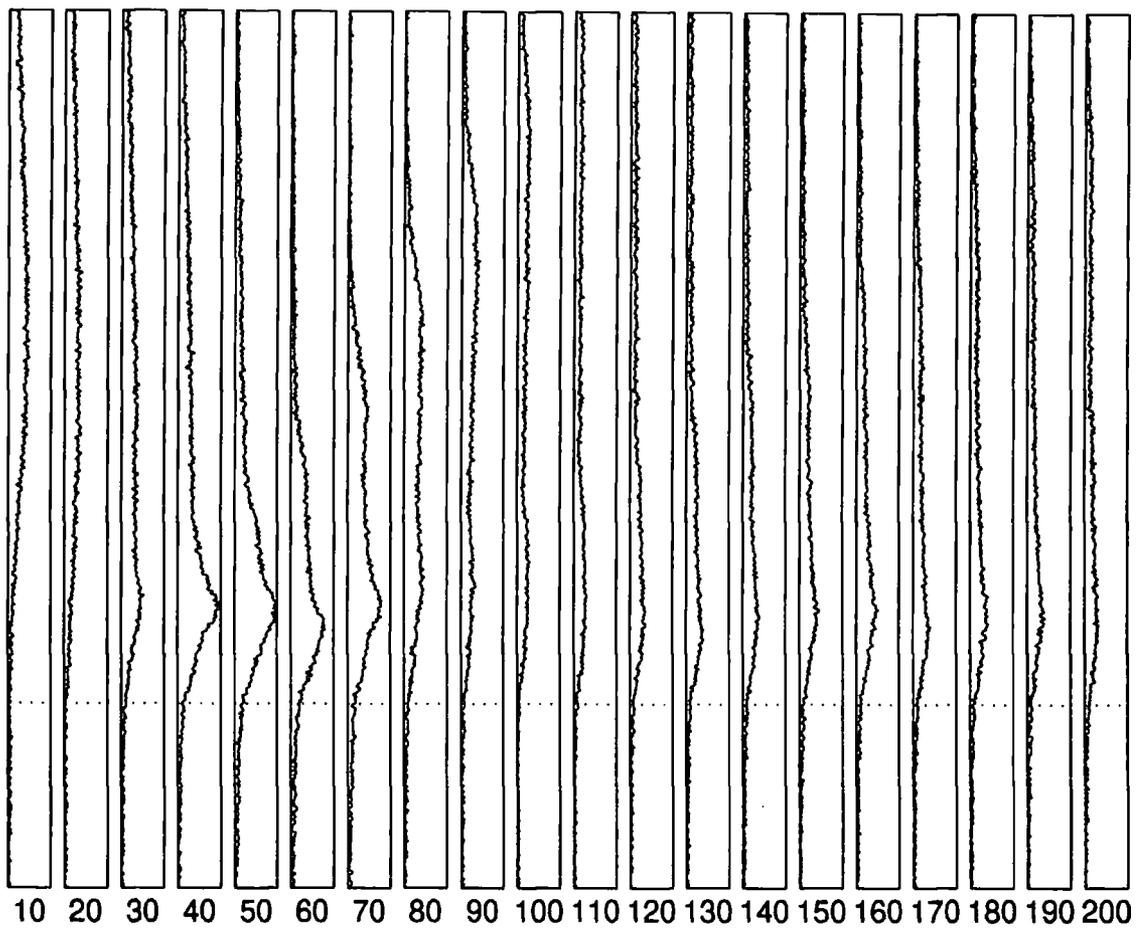
Figure 7.15: Vertical cross-sections through the bouncing atom cloud recorded every 10 ms. The position of the trap door beam is indicated by a dotted line. Each cross-section is 17 mm in length.

to the temperature of the cloud (20 μK, corresponding to 4.4 cms^{-1}). We have positioned the trap door just below the bottom of the cloud. Atoms falling from a height of 1.2 cm above the trap door have a potential energy of 1.2 mK, which is therefore the necessary barrier height if most atoms are to be trapped. Typical parameters were a power of 40 mW and a detuning of 20 GHz from resonance giving a trap depth of 200 mK, i.e., more than sufficient for all the atoms to be trapped.

The large vertical spread of the cloud means that atoms fall onto the trap door from different heights and therefore have very different bouncing periods. This leads to interesting dynamical phenomena. A typical sequence of images of bouncing atoms taken at 10 ms intervals is shown in figure 7.14, together with vertical cross-sections through the centre of the images. Since the imaging technique is destructive each image is obtained from a new load of atoms. The length of the image is 17 mm. The position of the trap door beam is indicated on the figure as a thick white line.

During the first 100 ms after closing the trapdoor, the cloud develops two distinct maxima. This is purely an artifact of the initial position distribution and after a further 100 ms, the motion of the atoms is sufficiently out of phase for this structure to have disappeared. Similar splittings of thermal clouds bouncing on repulsive light sheets has been observed by Bongs et al. [130]. In our case the initial size of the cloud is larger than the mean drop height. In other experiments the parameters are very different with the initial cloud size being much smaller than the drop height. The general shape of the bouncing cloud can be simply explained using classical trajectories. Figure 7.16 plots height versus time for particles initially at rest falling from heights ranging between 0 and 1.2 cm, onto a hard potential. The leading edge of the bouncing cloud occurs where each parabola intersects the one above it and these points fall along a curve that can be approximately fit by a parabola with

$$s \approx \left(\frac{t}{n}\right)^2, \qquad \qquad (7.4)$$

where s is height and t is time and n is the number of the bounce. The parabolas become progressively less steep. Two leading edge parabolas are superimposed on the atomic images shown in figure 7.14 and provide a good fit to the data.
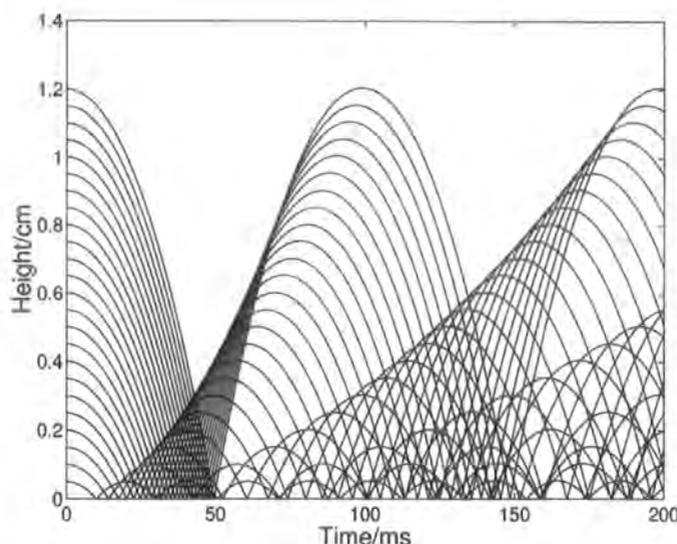
Figure 7.16: Each parabola represents the trajectory of a particle, initially at rest, falling under gravity onto a hard potential and bouncing elastically.

7.4.4 Trap Lifetime

Studies of the trap lifetime provide information on the loss mechanisms from the trap. Figure 7.17 is a typical decay curve showing the number of atoms remaining in the region above the trap door after it has been closed. Since the imaging is destructive each data point was taken for a new load of atoms in the optical dipole trap. Each time point is an average of five measurements. The data can be fitted by a sum of two exponentials:

$$N = N_0 \left[A \exp(-t/\tau_1) + B \exp(-t/\tau_2) \right], \tag{7.5}$$

as shown in the figure. The exponentials have approximately equal amplitudes and the decay constants are $\tau_1 = 147$ ms and $\tau_2 = 1667$ ms.

The variation of the τ_1 with trap depth is plotted in figure 7.18. The data has been fit with a straight line. The trap should be deep enough to confine all the atoms, but this is not the case. From figure 7.14 it can be seen that atoms are in fact falling through the trapdoor but there is no apparent loss through the sides of the trap (i.e. through the dipole guide beam). So, whilst some atoms may be lost through the walls of the trap due to non-specular reflection off the trap door beam, the largest loss is atoms falling through the trap door.
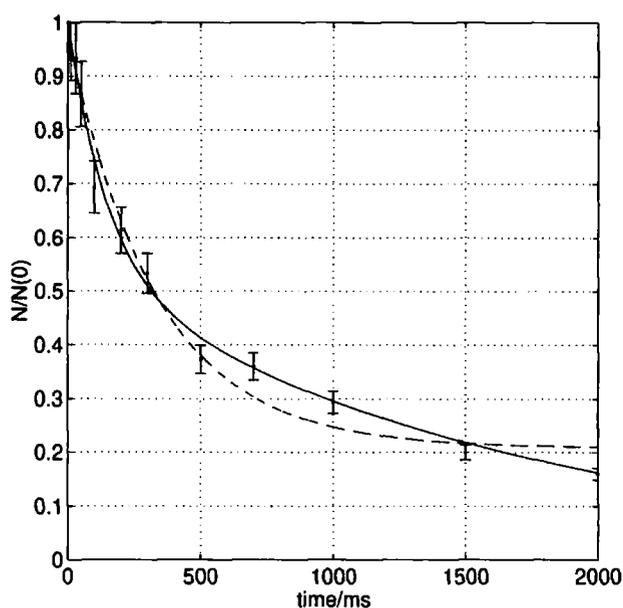
Figure 7.17: The number of atoms above the trap door as a function of time after switching on the trap door. The trap door beam is 20 GHz blue-detuned and has a power of 40 mW. The data has been fit with a curve obeying the equation $N = N_0[A\exp(-t/\tau_1) + B\exp(-t/\tau_2)]$ (solid line), where A is 0.47, τ_1 is 147 ms, B is 0.53 and τ_2 is 1667 ms. Also shown for comparison is a single exponential fit to the data, $N = N_0[A\exp(-t/\tau_1) + B]$ (dashed line), where A is 0.772, B is 0.209 and τ_1 is 335 ms. The error bars are the statistical error obtained from averaging five measurements for each data point.
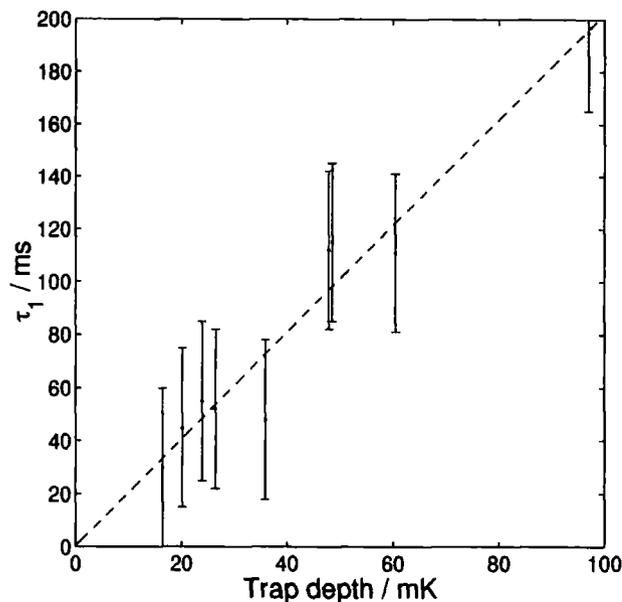
Figure 7.18: τ_1 plotted against barrier height. The data has been fit with a straight line. Each data point was obtained from a fit to a decay curve, such as the one shown in figure 6.17.

Several explanations suggest themselves. The first is that poor alignment of the beam means that the trap depth is significantly less than the calculated value. The alignment was optimised for large detunings and low intensity i.e. shallow trap depths, where the trapping was extremely sensitive to the exact position of the focus. Therefore, this explanation seems unlikely. Interference of the trap door beam at the uncoated walls of the vacuum cell could have degraded the beam quality to the extent that there were holes in the trapping potential. The beam was not spatial filtered in order to avoid power loss and consequently the beam profile was not very clean. Another possibility is that spontaneous scattering plays a role: atoms fall into a dressed state that sees an attractive potential on emitting a photon and are subsequently accelerated through the trap door. The Monte Carlo simulations suggest that this is very unlikely, even allowing for some scattered light in the calculations. The truth is probably a combination of poor beam quality and scattered light.

The double exponential indicates that there is a second loss mechanism, possibly collisions with a background gas or hyperfine state changing collisions. Again, hyperfine state changing collisions should be negligible. This was tested by pumping the atoms into the lower hyperfine state (and absolute ground state) before leaving

the MOT region by switching off all repumping light a few milliseconds before the end of the molasses phase. We observed no change in the lifetime of the trap, indicating that the density in the trap was not high enough for this to be a significant loss mechanism. In fact, the density in the trap is of order 2×10^{10} cm^{-3} and values in the literature give the rate coefficient to be typically around 5×10^{-11} cm^{3}s^{-1} so we would not expect hyperfine state changing collisions to be important.

The most likely second loss mechanism involves collisions with a background gas. The ion gauge, situated close to the ion pump in the upper cell (see figure 4.2) near the upper chamber indicates a pressure of 3×10^{-10} Torr, two orders of magnitude lower than that in the vapour cell. A lifetime of 1667 ms shows the advantage of trapping in a UHV chamber, since the lifetime in the vapour cell was limited to only 370 ms by collisions with the background gas.

The data will only be fit by a sum of two exponentials if two different loss mechanisms affect two different 'populations' of atoms. A fit of this sort has four free parameters and thus should be treated with caution. Here it may be appropriate since the loss mechanisms invoked to explain the decay are loss through the trapdoor (affecting only those atoms in the region of the trapdoor beam) and loss due to collisions with a background gas (affecting all atoms in the entire length of the bouncing cloud). Figure 7.17 also shows a single exponential fit to the data (dashed line) for comparison. If, for example, there are two loss mechanisms which act on the same 'population' of atoms the decay curve will be a product of two exponentials, $N = N_0 \exp(-t/\tau)$, where $1/\tau = 1/\tau_1 + 1/\tau_2$.

7.4.5 Time Sequence for Multiple Loading

In this section the losses which occur during multiple loading are investigated in order to gain insight into the conditions that would be necessary to see any accumulation of atoms.

A typical time sequence is as follows. A first MOT is loaded and atoms are launched within the guide. After allowing 20 ms for the atoms to leave the optical molasses region the MOT is switched back on and reloaded for a variable time t_{MOT}, of a few tens of milliseconds. By operating at high vapour pressures ($\sim 10^{-7}$ Torr) we could load more than 10^7 atoms during this time. Meanwhile the initial cloud reaches the UHV chamber and is trapped above the trap door. The second load of atoms is launched. When they reach the trap door it is opened for t_{open} to allow

most of the second load to enter but minimise trap leakage. A third bunch of atoms arrives ~ 100 ms later and the sequence can be repeated an arbitrary number of times.

7.4.6 Results

After optimising the MOT loading time ($t_{\text{MOT}} \sim 70$ ms) and duration of the opening the trap door ($t_{\text{open}} \sim 15$ ms), 15% of the trapped atoms were lost during each refill. The trap loss between refills was 20%. By using a higher power, further detuned trap door beam, it should be possible to reduce the trap loss to the 1% level. Based on these numbers one could expect to accumulate in steady state around 7 times the number obtained from a single load.

Unfortunately, there is another mechanism intrinsic in our vacuum system design that leads to substantial loss from the trap and could not be eliminated without rebuilding the vacuum chamber. Since the vapour cell and UHV chamber are made completely of quartz, there is no optical shielding of the optical dipole trap from scattering light from the MOT. The problem is compounded by the fact that the quartz is not anti-reflection coated. Absorption of only a few tens of photons of near resonant scattered light is sufficient to knock atoms out of the guiding beam. Consequently, if the MOT is reloaded whilst atoms are trapped above the trap door or travelling in the guide to the UHV chamber, the atoms are lost in a few milliseconds.

7.4.7 Repumper Effects

One way to combat this effect is to pump the atoms into a dark state before they leave the MOT (the lower hyperfine state of the ground state, $F = 2$) such that they do not see the resonant light. This can be achieved by using a mechanical shutter to switch off the repumper several milliseconds before extinguishing the cooling light. The mechanical shutters switch off the light in 400 μs.

Figure 7.20 shows the proportion of atoms remaining in the upper hyperfine state a given time after switching off the repumping beam. The data has been fit with a double exponential:

$$N(0)_{(F=3)} = A \exp(-t/\tau_A) + B \exp(-t/\tau_B) \tag{7.6}$$

where τ_A is 0.41 ms and τ_B is 26 ms and A and B are 0.77 and 0.23 respectively. τ_A is consistent with the optical pumping time but τ_B suggests that there is a mechanism which pumps atoms back to the upper hyperfine state. Our initial thought was that this is caused by scattered repumping light from the optical bench. Considerable effort was made to shield the experiment from scattered light but without successfully changing the decay curve illustrated. Alternatively the repumping could be caused by spectral impurity of the cooling laser.

7.4.8   Rate of Loss due to Scattered photons

Figure 7.20 shows how the number of atoms remaining in the guide is affected by the length of time that the repumper and MOT beams are on during the atoms' flight. Initially, the MOT was loaded until the number of atoms saturated. The atoms were launched within the guide and pumped into the lower hyperfine state by switching off the repumper before the end of the molasses phase. All the light (except the guiding laser) was then extinguished for 20 ms to allow the atoms to leave the region of the MOT beams. After this time the MOT was switched back on for a variable time, T. The measurements were all taken after a constant delay of 120 ms, corresponding to the time when the atoms are at the apex of the fountain. Integrating the CCD camera signal gives the number remaining in the guide, N.

If the MOT is switched back on for 45 ms, 80% of the initial number remain in the guide, but after 80 ms only 20% remain. This indicates that scattered repumper photons pump atoms back into $F = 3$, where they can be heated by near-resonant light. The error in the measurements is largely due to fluctuations in the initial number of atoms collected in the MOT which varied from load to load.

7.4.9   Effect of Intensity of the Repumping Light

We can optimise the intensity of the repumping light in the MOT to minimise the losses caused by scattered light. The number of atoms in the MOT is plotted as a function of the repumper intensity in figure 7.21. For high repumper intensities the number of atoms in the MOT saturates. It falls off when the repumper power is below around 2 mW. To optimise the intensity of the repumper there will be a trade-off between the number of atoms collected in the MOT and the probability that scattered light from the loading of a second MOT will knock atoms out of the guide during their flight.
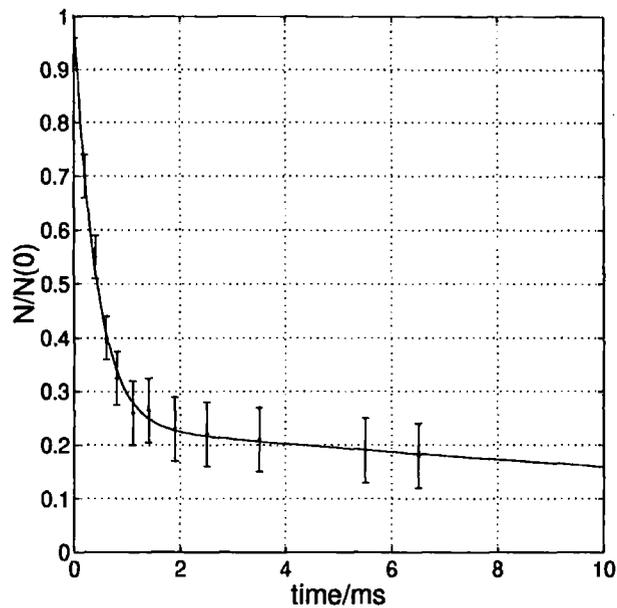
Figure 7.19: Number of atoms detected in the upper hyperfine state versus time that the cooling light remains on after the repumper is switched off.
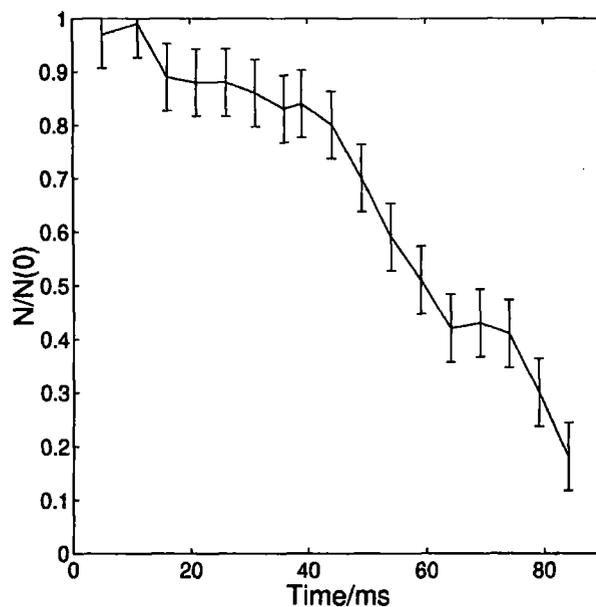
Figure 7.20: Fraction of atoms that remain in the dipole guide as a function of the duration (T) of the MOT which is turned on during the atomic flight.
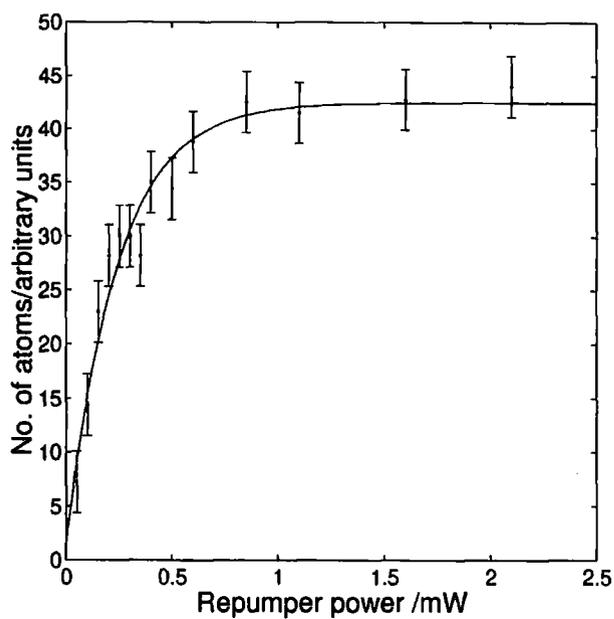
Figure 7.21: Number of atoms in the MOT as a function of the power of the re-pumper. The data has been fit with a curve of the form $N = N_{max}[1 - \exp(-\gamma P)]$.
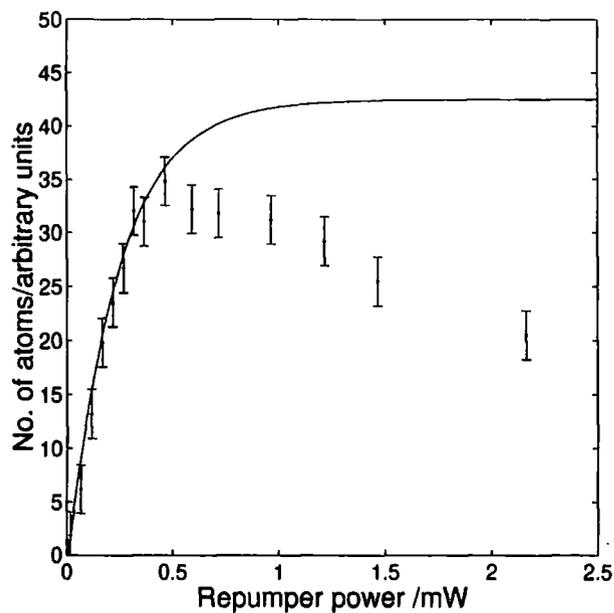
Figure 7.22: Number of atoms remaining in the guide after a second MOT phase of 25 ms as a function of the repumper power in the MOT. Also plotted is the signal from figure 7.21 (solid line).

Figure 7.22 shows the corresponding signal from the atoms remaining in the guide as a function of repumper intensity when the MOT is switched back on during their flight. The signal increases with repumping intensity for low intensities since the number of atoms in the MOT also increases. The maximum occurs for a repumper power of 0.5 mW, after which it falls again due to the increased probability that scattered light from the MOT will knock atoms out of the guide.

7.5 Summary

We have demonstrated a technique for loading a conservative atom trap spatially separated from the MOT without the aid of near-resonant light. The guided fountain is an essential component for delivering the cold atoms efficiently to the trap. The technique is readily adapted for multiple loading and could be used for the accumulation of atoms.

The optical trap door is distinct from other optical dipole traps for a number of reasons. The trap has a large volume and consequently can trap more atoms than traps loaded by overlapping with the MOT, where the trapped number is limited by a volume/trap depth trade-off. A similar geometry was realised by a combination of a vertical dipole trap and an electrostatic floor by Lemonde *et al.* [131]. The optical trap door is separated by a distance of a few centimetres from the MOT and hence it is possible to reload the MOT, whilst atoms remain trapped above the trap door. This allows for multiple loading schemes. Other traps spatially separated from the MOT are all loaded by dropping the atoms from the MOT, in which case they gain kinetic energy as they fall. Some form of cooling, typically a variation of Sisyphus cooling, is necessary to prevent elastic bouncing back to the MOT region. In our fountain geometry, at the apex the atoms are nearly at rest. Therefore no additional cooling was required.

Our existing apparatus requires a number of adaptions. The most important of these would be a new design for the vacuum chamber with the vapour cell optically isolated from the UHV chamber. Ideally the aperture would be placed only 1 cm above the MOT, such that the atoms were unaffected by scattered near-resonant light for most of their flight time. A further improvement to the optical trap door would be to use a higher power beam to reduce losses though the trap door. Anti-reflection coated windows would prevent degradation of the quality of the beam profile. With these improvements it would be possible to significantly improve on

the results presented here.

The scheme of multiple loading with a time-dependent input potential is of general applicability. Although we have concentrated on an entirely optical scheme, a similar scheme using a magnetic trap has been outlined in chapter 3. Lifetimes of 200 s in a magnetic trap are fairly typical, reducing trap loss compared to optical dipole traps. Trap leakage is determined by the volume of the trap.

In addition, we have seen evidence for a density enhancement in the region of a crossed dipole trap at the apex of the fountain, in agreement with the simulations presented in chapter 2 (section 3.2). With the improvements to the vacuum design described above, it would be possible to investigate collisional loading of an atom trap in a continuously operating guided fountain.
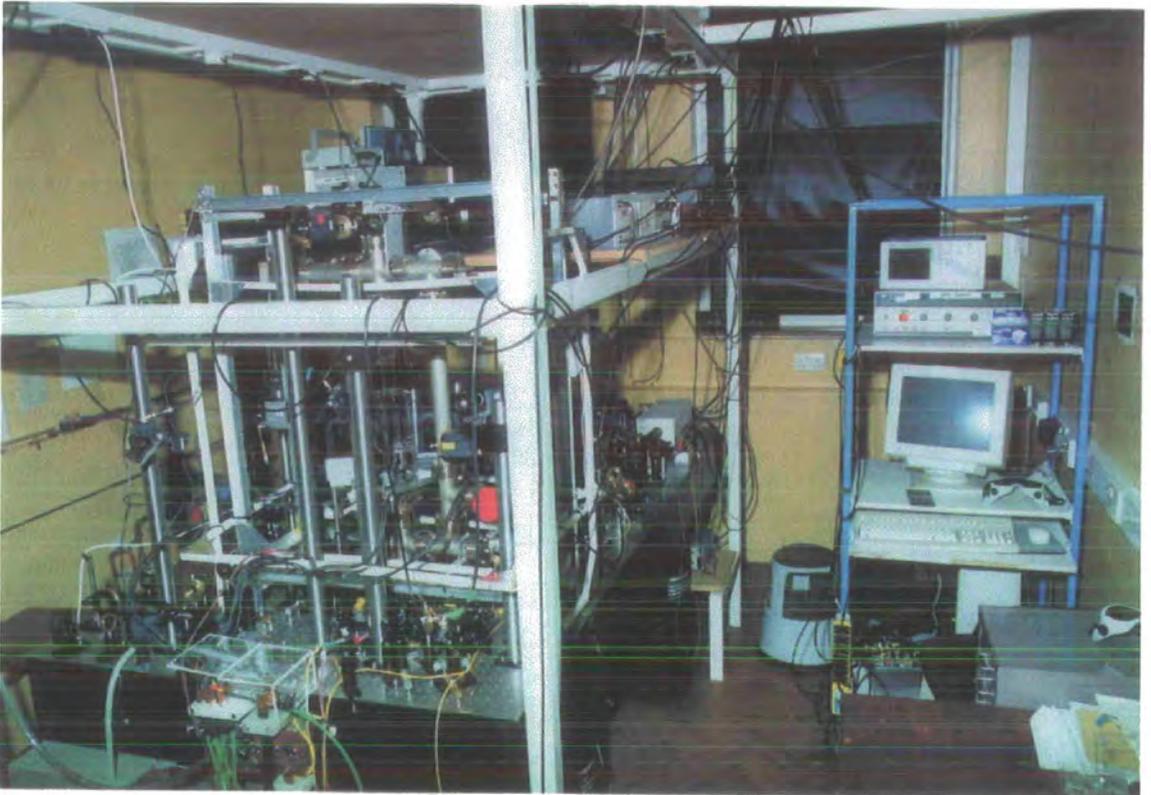
Figure 7.23: Photograph of the lab. in September 1999. Photograph courtesy of Vicki Greener, Physics Audio Visual Department.

Chapter 8

Conclusion

During the course of this work, we have developed a laser cooling experiment from scratch in an initially empty laboratory. We have built a vapour cell magneto-optical trap and demonstrated efficient transfer of atoms from the MOT to an UHV chamber, using a far-off-resonant guide beam. The atoms are transferred over a distance of order 10 cm in a fountain geometry. We compared the flux obtained in pulsed and continuous operation and found that, whilst the atomic flux is greater in the continuous case, the guiding is less efficient. Therefore, fewer atoms are transferred to the UHV chamber. In continuous operation atoms in the fountain are heated by scattered light.

Methods of loading a conservative atom trap at the apex of the guided fountain were investigated. We demonstrated an optical dipole trap loaded using a time-dependent potential. Far-off-resonant optical dipole traps are essentially conservative and therefore do not suffer from the same density and number limits as the MOT. Therefore, in principle, a multiple loading scheme could be used to accumulate a larger number of atoms than has previously been obtained in optical dipole traps. The scheme is generally applicable to any conservative trap.

As this was a first attempt, a number of possible improvements to the design have been highlighted. Most importantly the UHV chamber should be optically isolated from the MOT. With the addition of an opaque partition with a small aperture, just above the MOT or funnel, the atoms would be unaffected by near-resonant light for most of their flight time.

In the future, the work could be extended to look at multiple loading of a magnetic trap. Typical lifetimes for magnetic traps are of order 100 s, implying that many atoms can be collected. The time-dependent potential method of loading with-

out near-resonant light could be adapted for a magnetic trap. Alternatively, optical pumping or collisional loading schemes can be explored. For all these schemes the optical guide is a key component, since it delivers cold atoms with a spatial distribution well matched to that of the atom trap and minimises the phase space density decrease occurring during transfer.

At present some BEC experiments use double MOT schemes to combine efficient collection of atoms from a vapour cell MOT, with the long lifetime of a UHV MOT [76]. The UHV MOT is necessary to regain the phase space density lost during the transfer process. After multiple loading, the UHV MOT is extinguished and atoms loaded into a magnetic trap. An efficient transfer implies that the UHV MOT can be replaced by a conservative trap. Continuous loading of a magnetic trap could provide a route to a steady state Bose-Einstein condensate [79]. Resonant light can destroy a condensate so a collisional loading or time-dependent loading scheme may be a vital tool.

Bibliography

[1] M. Kasevich, E. Riis, S. Chu and R. DeVoe, '*Atomic Velocity Selection Using Stimulated Raman Transitions*', Phys. Rev. Lett. **63**, 612 (1989).

[2] A. Clairon, C. Salomon, S. Guellati and W. D. Phillips, '*Ramsey Resonance in Zacharius Fountain*', Europhys. Lett. **16**, 165 (1991); A. Clairon, P. Laurent, G. Santanelli, S. Ghezali, S. N. Lea and M. Bahoura, IEEE Trans. Instr. Meas. **44**, 128 (1995).

[3] K. Gibble and S. Chu, '*Laser cooled Cs Frequency Standard and a measurement of the frequency shift due to ultracold collisions*', Phys. Rev. Lett. **70**, 1771 (1993).

[4] C. Morgan, G. S. Chen, C. Boothroyd, S. Bailey and C. Humphreys, '*Ultimate Limits of Lithography*', Phys. World **5**, 28 (1992).

[5] J. J. McClelland, R. E. Scholten, E. C. Palm and R. J. Celotta, '*Laser-focused atomic deposition*', Science **262**, 877 (1993).

[6] M. J. Snadden, A. S. Bell, E. Riis and A. I. Ferguson, '*Two-photon spectroscopy of Rb using a mode-locked laser*', Opt. Comm. **125**, 70 (1996).

[7] A. G. Sinclair, B. D. MacDonald, E. Riis and G. Duxbury, '*Double resonance spectroscopy of laser cooled Rb atoms*', Opt. Comm. **106**, 207 (1994).

[8] M. H. Anderson, J. R. Ensher, M. R. Matthews, C. E. Wieman and E. A. Cornell, '*Observation of Bose-Einstein Condensation in a Dilute Atomic Vapour*', Science **269**, pp.198 - 201 (1995).

[9] K. B. Davis, M. -O. Mewes, M. R. Andrews, N. J. van Druten, D. S. Durfee, D. M. Kurn and W. Ketterle, '*Bose-Einstein Condensation in a Gas of Sodium Atoms*', Phys. Rev. Lett. **75**, 22 (1995).

[10] E. W. Hagley, L. Deng, M. Kozuma, J. Wen, K. Helmerson, S. K. Rolston and W. D. Phillips, '*A well-collimated quasi-continuous atom laser*', Science **283**, 5408 (1999).

[11] G. Taubes, '*Physics - First atom laser shoots pulses of coherent matter*', Science **275**, 5300, p.617 (1997).

[12] I. Bloch, T. W. Hänsch and T. Esslinger, '*Atom Laser with a cw Output Coupler*', Phys. Rev. Lett. **82**, 15 (1999).

[13] M. -O. Mewes, M. R. Andrews, D. M. Kurn, D. S. Durfee, C. G. Townsend and W. Ketterle, '*Output coupler for Bose-Einstein condensed atoms*', Phys. Rev. Lett. **78**, 4 (1997).

[14] C. S. Adams and E. Riis, '*Laser Cooling and Trapping of Neutral Atoms*', Prog. in Quant. Elec. **21**, 1 (1997).

[15] R. Srinivasan, '*Laser cooling and trapping of ions and atoms*', Current Science **76**, 2 (1999).

[16] W. D. Phillips, '*Laser Cooling and Trapping of Neutral Atoms*', Rev. of Modern Phys. **70**, 3 (1998).

[17] T. W. Hänsch and A. L. Schawlow, '*Cooling of Gases by Laser Radiation*', Opt. Comm. **13**, 68 (1975).

[18] D. J. Wineland and H. G. Dehmelt, '*Proposed $10^{14}\Delta\nu < \nu$ Laser Fluoresence Spectroscopy on Tl^{+} Mono-Ion Oscillator III*', Bull. Am. Phys. Soc. **20**, 637 (1975).

[19] S. Chu, L. Hollberg, J. E. Bjorkholm, A. Cable and A. Ashkin, '*Experimental Observation of Optically Trapped Atoms*', Phys. Rev. Lett. **55**, 48 (1985).

[20] E. Arimondo, M. Inguscio and P. Vickno, '*Experimental determination of the hyperfine structure in the alkali atoms*', Rev. Mod. Phys. **49**, 31 (1977).

[21] P. D. Lett, R. N. Watts, C. I. Westbrook and W. D. Phillips, '*Observation of Atoms Laser Cooled below the Doppler Limit*', Phys. Rev. Lett. **61**, 169 (1988).

[22] A. Aspect, J. Dalibard, A. Heidmann, C. Salomon and C. Cohen-Tannoudji, '*Cooling Atoms with Stimulated Emission*', Phys. Rev. Lett. **57**, 1688 (1986).

[23] J. Dalibard and C. Cohen-Tannoudji, '*Dressed atom approach to atomic motion in laser light - the dipole force revisited*', J. Opt. Soc. Am. **62**, 1707 (1985).

[24] D. S. Weiss, E. Riis, Y. Shevy, P. J. Ungar and S. Chu, '*Optical molasses and multilevel atoms: experiment*', J. Opt. Soc. Am. **B6**, 2072 (1989).

[25] P. J. Ungar, D. S. Weiss, E. Riis and S. Chu, '*Optical molasses and multilevel atoms: theory*', J. Opt. Soc. Am. **B6**, 2058 (1989).

[26] J .Dalibard and C. Cohen-Tannoudji, '*Laser cooling below the Doppler limit by polarisation gradients: simple theoretical models*', J. Opt. Soc. Am. B, **6**, 2023 (1989).

[27] A. Aspect, E. Arimondo, R. Kasier, N. Vansteenkiste and C. Cohen-Tannoudji, '*Laser cooling below the one-photon recoil limit by velocity selective coherent population trapping*', Phys. Rev. Lett. **61** , 826 (1988).

[28] M. Kasevich and S. Chu, '*Laser cooling below a photon recoil with 3-level atoms*', Phys. Rev. Lett. **69**, 1741 (1992).

[29] E. L. Raab, M. Prentiss, A. Cable, S. Chu and D. E. Pritchard, '*Trapping of Neutral Sodium Atoms with Radiation Pressure*', Phys. Rev. Lett. **59**, 2631 (1987).

[30] C. Monroe, W. Swann, H. Robinson and C. Wieman, '*Very cold atoms in a vapor cell*', Phys. Rev. Lett. **65**, 1571 (1990).

[31] C. J. Cooper, G. Hillenbrand, J. Rink, C. G. Townsend, K. Zetie and C. J. Foot, '*The temperature of atoms in a magneto-optical trap*', Europhys. Lett. **28**, 397 (1994).

[32] D. Sesko, T. Walker, C. Monroe, A. Gallagher and C. Wieman, '*Collisional Losses from a Light-Force Atom Trap*', Phys. Rev. Lett. **63**, 9 (1989).

[33] T. Walker, D. Sesko and C. Wieman, '*Collective Behaviour of Optically Trapped Neutral Atoms*', Phys. Rev. Lett. **64**, 4 (1990).

[34] C. G. Townsend, N. H. Edwards, C. J. Cooper, K. P. Zetie, C. J. Foot, A. M. Steane, P. Szriftgiser, H. Perrin and J. Dalibard, '*Phase-space density in the magneto-optical trap*', Phys. Rev. A. **52**, 1423 (1995).

[35] G. Hillenbrand, C. J. Foot and K. Burnett, '*Effect of scattered radiation on sub-Doppler cooling*', Phys. Rev. A. **50**, 1479 (1994).

[36] W. Ketterle, K. B. Davis, M. A. Joffe, A. Martin and D. E. Pritchard, '*High Densities of Cold Atoms in a Dark Spontaneous-Force Optical Trap*', Phys. Rev. Lett. **70**, 15 (1993).

[37] C. G. Townsend, N. H. Edwards, K. P. Zetie, C. J. Cooper, J. Rink and C. J. Foot, '*High-density trapping of cesium atoms in a dark magneto-optical trap*', Phys. Rev. A. **53**, 1702 (1996).

[38] M. H. Anderson, W. Petrich, J. R. Ensher and E. A. Cornell, '*Reduction of light-assisted collisional loss rate from a low-pressure vapor-cell trap*', Phys. Rev. A **50**, 5, R3597 - R3600.

[39] O. Stern and W. Gerlach, '*Über die Richtungsquantelung im Magnetfeld*', Ann. Physik **74**, 673 (1924).

[40] I. I. Rabi, '*On the process of space quantisation*', Phys. Rev. **49**, 324 (1936).

[41] '*Atomic and Molecular Beam Methods*', edited by G. Scoles, Oxford University Press, Oxford (1988).

[42] A. Ashkin, '*Atomic beam deflection by resonance radiation pressure*', Phys. Rev. Lett. **25**, 1321 (1970).

[43] R. Schieder, H. Walther and L. Woster, Opt. Comm. **5**, 377 (1972).

[44] V. I. Balykin, V. S. Letokhov and V. I. Mushin, '*Observation of the cooling of free sodium atoms in a resonance laser field with a scanning frequency*', JETP Lett. **29**, 560 (1979).

[45] V. I. Balykin, V. S. Letokhov and A. I. Sidorov, '*Intense stationary flow of cold atoms formed by laser deceleration of atomic beams*', Opt. Comm. **49**, 248 (1984).

[46] R. N. Watts and C. E. Wieman, '*Manipulating Atomic Velocities using Diode Lasers*', Opt. Lett. **11**, 291 (1986).

[47] M. Zhu, C. W. Oates and J. L. Hall, '*Continuous high flux monovelocity atomic-beam based on a broadband laser cooling technique*', Phys. Rev. Lett. **67**, 46 (1991).

[48] W. Ketterle, A. Martin, M. A. Joffe and D. E. Pritchard, '*Slowing and Cooling Atoms in Isotropic Laser Light*', Phys. Rev. Lett. **69**, 17 (1992).

[49] E. Riis, D. S. Weiss, K. A. Moler and S.Chu, '*Atom Funnel for the Production of a Slow, High-Density Atomic Beam*', Phys. Rev. Lett. **64**, 1658 (1990).

[50] T. B. Swanson, N. J. Silva, S. K. Mayer, J. J. Maki and D. H. McIntyre, '*Rubidium Atomic Funnel*', J. Opt. Soc. Am. B **13**, 9 (1996).

[51] P. Berthoud, A. Joyet, G. Dudle, N. Sagna and P. Thomann, 'A continuous beam of slow, cold cesium atoms magnetically extracted from a 2D magneto-optical trap', Europhys. Lett. **41**, 2 (1998); S. Weyers, E. Aucouturier, C. Valentin and N. Dimarcq, 'A continuous beam of cold caesium atoms extracted from a two-dimensional magneto-optical trap', Opt. Comm. **143**, 1-3 (1997).

[52] Z. T. Lu, K. L. Corwin, M. J. Renn, M. H. Anderson, E. Cornell and C. E. Wieman, 'Low-Velocity Intense Source of Atoms from a Magneto-Optical Trap', Phys. Rev. Lett. **77**, 3331 (1996).

[53] K. Dieckmann, R. J. C. Spreeuw, M. Weidemüller and J. T. M. Walraven, 'Two-dimensional magneto-optical trap as a source of slow atoms', Phys. Rev. A. **58**, 3891 (1998).

[54] K. I. Lee, J. A. Kim, H. R. Noh and W. Jhe, 'Single-beam atom trap in a pyramidal and conical hollow mirror', Opt. Lett. **21** , pp.1177 - 1179 (1996).

[55] R. S. Williamson III, P. A. Voytas, R. T. Newell and T. Walker, 'A magneto-optical trap loaded from a pyramidal funnel', Optics Express III, **3**, 3 (1998).

[56] J. J. Arlt, O. Marago, S. Webster, S. Hopkins and C. J. Foot, 'A pyramidal magneto-optical trap as a source of slow atoms', Opt. Comm. **157**, 303 (1998).

[57] H. Friedburg, 'Optische Abbildung mit neutralen Atomen', Z. Phys., **130**, 493 (1951); H. Friedburg and W. Paul, 'Optische Abbildung mit neutralen Atomen', Naturwissenschafen **38**, 159 (1951).

[58] W. G. Kaenders, F. Lison, I. Muller, A. Richter, R. Wynands and D. Meschede, 'Refractive components for magnetic atom optics', Phys. Rev. A. **54**, 5067 (1996).

[59] C. J. Myatt, E. A. Burt, R. W. Ghrist, E. A. Cornell and C. E. Wieman, 'Production of two overlapping Bose-Einstein condensates by sympathetic cooling', Phys. Rev. Lett. **78**, 4 (1997).

[60] J. Schmiedmayer 'Guiding and trapping a neutral atom on a wire', Phys. Rev. A. **52**, 1 (1995); J. Denschlag, D. Cassettari and J. Schmiedmayer, 'Guiding neutral atoms with a wire', Phys. Rev. Lett. **82**, 10 (1999).

[61] E. A. Hinds, M. G. Boshier and I. G. Hughes, 'Magnetic waveguide for trapping cold atom gases in two dimensions', Phys. Rev. Lett. **80**, 645 (1998).

[62] K. Berg-Sorensen, M. M. Burns, J. A. Golovchenko and L. V. Hau, 'Waveguide for cold atoms : Spin-1 magnetic particles and a filamentary current', Phys. Rev. A. **53**, 1653 (1996).

[63] V. I. Balykin, 'Atom Waveguides', Adv. At. Mol. Opt. Phys. **41**, pp.181-260 (1999).

[64] E. A. Hinds and I. G. Hughes, 'Magnetic atom optics: mirrors, guides, traps and chips for atoms', J. Phys. D: Appl. Phys. **32**, R119 (1999).

[65] C. Cohen-Tannoudji, J. Dupont-Roc and G. Grynberg, 'Processus d'interaction entre photons et atomes', InterEditions, Editions du CNRS (1988), english translation: 'Atom-photon interactions: basic processes and applications', Wiley, New York (1992).

[66] J. E. Bjorkholm, R. R. Freeman, A. Ashkin and D. B. Pearson 'Observation of Focusing of Neutral Atoms by the Dipole Forces of Resonance-Radiation Pressure', Phys. Rev. Lett. **41**, 1361 (1978).

[67] M. J. Renn, D. Montgomery, O. Vdovin, D. Z. Anderson, C. E. Wieman and E. A. Cornell, 'Laser guided atoms in hollow core optical fibres', Phys. Rev. Lett. **75**, 3235 (1995)

[68] H. Ito, T. Nakata, K. Sakaki, M. Ohtsu, K. L. Lee and W. Jhe, 'Laser spectroscopy of atoms guided by evanescent waves in micron-sized hollow optical fibres', Phys. Rev. Lett. **76**, 4500 (1996).

[69] H. Ito, K. Sakati, W. Jhe and M. Ohtsu, 'Evanescent-light induced atom-guidance using a hollow optical fibre with light coupled sideways', Optics Comm. **141**, 1 (1997).

[70] G. Workurka, K. Keupp, K. Sengstock and W. Ertmer, in Int. Quantum Electronics conf., vol. 7, 1998 OSA Technical Digest Series, 235 (OSA, New York, 1998).

[71] J. P. Yin, Y. M. Lin, K. I. Lee, H. Nha, H. R. Noh, Y. Z. Wang, K. H. Oh, U. C. Paek and W. H. Jhe, 'Guiding of atoms in a dark hollow laser beam', J. Korean Phys. Soc. **33**, 3 (1998).

[72] M. J. Renn, E. A. Donley, E. A. Cornell, C. E. Wieman and D. Z. Anderson, 'Evanescent wave guiding of atoms in hollow fibres', Phys. Rev. A. **53**, R648 (1996).

[73] I. Manek, B. Yu, Ovchinnikov and R. Grimm, '*Generation of a hollow laser beam for atom trapping using an axicon*', Opt. Comm. **147**, 67 (1998).

[74] J. Yin, Y. Zhu, W. Jhe and Z. Wang, '*Guiding of atoms in a dark hollow laser beam*', Phys. Rev. A **58**, 1 (1998).

[75] M. Schiffer, M. Rauner, S. Kuppens, N. Zinner, K. Sengstock and W. Ertmer, '*Guiding, focusing and cooling of atoms in a strong dipole potential*', Appl. Phys. B - Lasers and Optics **67**, 6, pp.705 - 708 (1998).

[76] C. J. Myatt, E. A. Burt, R. W. Ghrist, S. Loutzenheiser and C. E. Wieman, '*Multiply Loaded Magneto-optical Trap* ', Opt. Lett. **21**, 290 (1996)

[77] E. A. Cornell, C. Monroe and C. E. Wieman, '*Multiply Loaded, ac Magnetic Trap for Neutral Atoms*', Phys. Rev. Lett. **67**, 18 pp.2439 - 2442 (1991).

[78] J. R. Waldram, '*The theory of thermodynamics*', Cambridge University Press (1985).

[79] J. Williams, R. Walser, C. Wieman, J. Cooper, M. Holland, '*Achieving Steady State Bose-Einstein Condensation*', Phys. Rev. A **57**, 3, pp.2030 (1998).

[80] K. M. O'Hara, S. R. Granada, M. E. Gehn, T. A. Savard, S. Bali, C. Freed and J. E. Thomas, '*Ultrastable CO_2 Laser Trapping of Lithium Fermions*', Phys. Rev. Lett. **82**, 4024 (1999).

[81] J. M. Doyle, B. Friedrich, J. H. Kim and D. Patterson, '*Buffer-gas loading of atoms and molecules into a magnetic trap*', Phys. Rev. A **52**, 4 (1995).

[82] J. H. Kim, B. Friedrich, D. P. Katz, C. Patterson, J. D. Weinstein, R. DeCarvalho and J. M. Doyle, '*Buffer gas loading and magnetic trapping of atomic europium*', Phys. Rev. Lett. **78**, 3665 (1997).

[83] J. D. Weinstein, R. deCarvalho, T. Guillet, B. Friedrich and J. M. Doyle, '*Magnetic trapping of calcium monohydride molecules at milliKelvin temperatures*', Nature **395**, 148 (1998).

[84] J. D. Weinstein, R. deCarvalho, J. Kim, D. Patterson, B. Friedrich and J. M. Doyle, '*Magnetic trapping of atomic chromium*', Phys. Rev. A, **57**, R3173 (1998).

[85] W. Ketterle and N. J. Van Druten, '*Evaporative Cooling of Trapped Atoms*', Adv. At. Mol. and Opt. Phys. **37**, 181 (1996).

[86] H. J. Davies, K. Szymaniec and C. S. Adams, in *Int. Quantum Electronics Conf.*, vol 7 (1998) OSA Technical Digest Series, p.118 (OSA, New York, 1998).

[87] H. Wu and C. J. Foot, *'Direct Simulation of Evaporative Cooling'*, J. Phys. B: At. Mol. Opt. Phys. **29**, L321 (1996).

[88] W. H. Press, S. A. Teukolsky, W. T. Vetterling and B. P. Flannery, *'Numerical Recipes in Fortran: The Art of Scientific Computing'*, (Cambridge University Press, 1992).

[89] L. Santos and M. Lewenstein, *'Dynamical cooling of trapped gases: One-atom problem'*, Phys. Rev. A. **59**, 613 (1999).

[90] D. G. Fried, T. C. Killian, L. Willmann, D. Landhuis, S. C. Moss, D. Kleppner and T. J. Greytak, *'Bose-Einstein Condensation of atomic hydrogen'*, Phys. Rev. Lett. **81**, 3811 (1998).

[91] A. N. Nesmeyanov, *'Vapor pressure of the chemical elements'* (Elsevier, Amsterdam, 1963).

[92] Song-Quan Shang and H. J. Metcalf, *'Narrow-band, high power light from diode lasers'*, App. Opt. **28**, 1618 (1989).

[93] C. E. Wieman and L. Hollberg, *'Using Diode lasers for atomic physics'*, Rev. Sci. Instrum. **62**, 1 (1991).

[94] G. D. Rovera, G. Santarelli and A. Clairon, *'A laser diode system stabilised on the caesium D_2 line'*, Rev. Sci. Instrum. **65**, 5 (1994).

[95] L. Ricci, M. Weidemüller, T. Esslinger, A. Hemmerich, C. Zimmmermann, V. Vuletic, W. Konig and T. W. Hänsch, *'A compact grating stabilised diode laser system for atomic physics'*, Opt. Comm. **117**, 541 (1995).

[96] K. B. MacAdam, A. Steinbach and C. Wieman, *'A narrow-band tunable diode laser system with grating feedback, and a saturated absorption spectrometer for Cs and Rb'*, Am. J. Phys. **60**, 1098 (1992).

[97] L. Nilse, H. J. Davies and C. S. Adams, *'Synchronous tuning of extended cavity diode lasers : the case for an optimum pivot point'*, Appl. Opt. **38**, 548 (1999).

[98] Michael Snadden, thesis, Strathclyde University, 1997.

[99] C. Zimmermann, V. Vuletic , A. Hemmerich and T.W.Hänsch, '*All solid state laser source for tunable blue and ultraviolet radiation* ', Appl. Phys. Lett. **66**, 2318 (1995); Lew Goldburg and W. K. Burns, '*Deep UV to mid-IR generation with laser diodes and non-linear frequency conversion*', Proc. LEOS '95, edited by T. Fan, 459 (IEEE, Piscatoway, NJ, 1995).

[100] A. M. Steane, M. Chowdhury and C. J. Foot, '*Radiation force in the magneto-optical trap*', J. Opt. Soc. Am. B, **9**, 2142 (1992).

[101] K. E. Gibble, S. Kasapi, S. Chu, '*Improved Magneto-Optical Trapping in a Vapor Cell*', Optics Lett. **17**, 526 (1992).

[102] C. D. Wallace, T. P. Dinneen, K. Y. N. Tan, A. Kumarakrishnan, P. L. Gould and J. Javanainen, '*Measurements of temperature and spring constant in a magneto-optical trap*', J. Opt. Soc. Am. b **11**, 703 (1994).

[103] C. Fertig and K. Gibble, '*Laser-Cooled* ^{87}Rb *Clock*', IEEE Transactions on Instrumentation and Measurement, **48**, 2 (1999).

[104] J. R. Zacharius, '*Precision measurements with molecular beams*', Phys. Rev. **94**, 751 (1954).

[105] N. F. Ramsey, '*Molecular Beams*', (Oxford University Press , Oxford 1956).

[106] M. Kasevich, D. S. Weiss, E. Riis, K. Moler, S. Kasapi and S. Chu, '*Atomic Velocity Selection Using Stimulated Raman Transitions*', Phys. Rev. Lett. **66**, 2297 (1991).

[107] K. Szymaniec, H. J. Davies and C. S. Adams, '*An atomic fountain guided by a far-off resonance laser beam*', Europhys. Lett. **45**, 450 (1999).

[108] A. M. Steane and C. J. Foot, '*Laser cooling below the Doppler limit in a magneto-optical trap*', Europhys. Lett. **14**, 231 (1991).

[109] E. Riis and S. M. Barnett, '*A dynamic electric trap for ground state atoms*', Europhys. Lett. **21**, 533 (1993).

[110] R. A. Cline, J. D. Miller and D. J. Heinzen, '*Study of Rb₂ long-range states by high-resolution photoassociation spectroscopy*', Phys. Rev. Lett. **73**, 632 (1994).

[111] J. R. Gardner, R. A. Cline, J. D. Miller, D. J. Heinzen, H. M. J. M. Boesten and B. J. Verhaar, '*Collisions of doubly spin-polarised ultracold Rb-85 atoms*', Phys. Rev. Lett. **74**, 3764 (1995).

[112] C. C. Tsai, R. S. Freeland, J. M. Vogels, H. M. J. M. Boesten, B. J. Verhaar and D. J. Heinzen, '*Two-color photoassociation spectroscopy of ground state Rb-2*', Phys. Rev. Lett. **79**, 1245 (1997).

[113] R. Grimm, M. Weidemuller and Y. B. Ovchinnikov, '*Optical Dipole Traps for Neutral Atoms*', Adv. At. Mol. and Opt. Phys. **42**, 95 (2000).

[114] D. Sesko, T. Walker, C. Monroe, A. Gallagher and C. Wieman, '*Collisional Losses from a Light-Force Atom Trap*', Phys. Rev. Lett. **63**, 961 (1989).

[115] C. D. Wallace, T. P. Dinneen, K. -Y. N. Tan, T. T. Grove and P. L. Gould, '*Isotopic Difference in Trap Loss Collisions of Laser Cooled Rubidium Atoms*', Phys. Rev. Lett. **69**, 897 (1992).

[116] D. M. Stamper-Kurn, M. R. Andrews, A. P. Chikkatur, S. Inouye, H. -J. Meisner, J. Stenger and W. Ketterle, '*Optical confinement of a Bose-Einstein condensate* ', Phys. Rev. Lett. **80**, 2027 (1998).

[117] S. L. Winoto, M. T. DePue, N. E. Bramall and D. S. Weiss, '*Laser cooling at high density in deep far-detuned optical lattices*', Phys. Rev. A. **59**, 1 (1999).

[118] Y. B. Ovchinnikov, I. Manek, A. I. Sidorov, G. Wasik, R. Grimm, '*Gravito-optical atom trap based on a conical hollow beam*', Europhys. Lett. **43**, 5 (1998).

[119] C. G. Aminoff, A. Steane, P. Bouyer, P. Desboilles, J. Dalibard and C. Cohen-Tannoudji, '*Caesium atoms in a stable gravitational cavity*', Phys. Rev. Lett. **71**, 3083 (1993).

[120] Y. B. Ovchhinnikov, I. Manek and R. Grimm, '*Surface trap for Cs atoms based on evanscent wave cooling*', Phys. Rev. Lett. **79**, 2225 (1997).

[121] J. Dalibard, Y. Castin and K. Mølmer, '*Wave-Function Approach to Dissipative Processes in Quantum Optics*', Phys. Rev. Lett. **68**, 580 (1992).

[122] F. Bardou, J. P. Bouchard, O. Emile, A. Aspect and C. Cohen-Tannoudji, '*Subrecoil Cooling and Levy Flights*', Phys. Rev. Lett. **72**, 203 (1994).

[123] J. Lawall, S. Kulin, B. Saubamea, N. Bigelow, M. Leduc and C. Cohen-Tannoudji, '*Three-Dimensional Laser Cooling of Helium Beyond the single-Photon Recoil Limit*', Phys. Rev. Lett. **75**, 4194 (1995).

[124] W. Seifert, C. S. Adams, V. I. Balykin, C. Heine, Y. Ovchinnikov and J. Mlynek, '*Reflection of metastable argon atoms from an evanescent wave*', Phys. Rev. A. **49**, 3814 (1994).

[125] K. Szymaniec, S. Ghezali, L. Cognet and A. Clairon, '*Injection locking of diode lasers to frequency modulated source*', Opt. Commun. **144**, 50 (1997).

[126] M. J. Snadden, R. B. M. Clarke and E. Riis, '*Injection-locking technique for heterodyne optical phase locking of a diode laser*', Opt. Lett. **22**, 892 (1997).

[127] J. P. Bouyer and C. Breant, '*Injection-locking mechanisms in semi-conductor lasers*', J. de Physique III, **2**, 1623 (1992).

[128] C. G. Aminoff, A. M. Steane, P. Bouyer, P. Desboilles, J. Dalibard and C. Cohen-Tannoudji, Phys. Rev. Lett. **71**, 3083 (1993).

[129] C. V. Saba, P. A. Barton, M. G. Boshier, I. G. Hughes, P. Rosenbusch, B. E. Sauer and E. A. Hinds, '*Reconstruction of a cold atom cloud by magnetic focusing*', Phys. Rev. Lett. **82**, 468 (1999).

[130] K. Bongs, S. Burger, G. Birkl, K. Sengstock. W. Ertmer, K. Rzazewski, A. Sanpera and M. Lewenstein, '*Coherent Evolution of Bouncing Bose-Einstein Condensates*', Phys. Rev. Lett. **83**, 3577 (1999).

[131] P. Lemonde, O. Morice, E. Peik, J. Reichel, H. Perrin, W. Hansel and C. Salomon, '*An opto-electric trap for cold atoms*', Europhys. Lett. **32**, 555 (1995).

Appendix

Timing and Data Acquisition

This appendix describes the timing and data acquisition system used for the experiment. A brief overview of the structure is as follows:

The graphical interface is provided by Matlab. Pushbuttons toggle between the various modes (pulsed, continuous, temperature measurement etc.). Various parameters can be changed interactively. For each mode there is a matlab .m file which writes appropriate values for the intensity, detuning etc. to a *waveform buffer*.

Matlab communicates with NIDAQ (National Instruments Data Acquisition) cards via MEX-files which are c files for Matlab. A timing card, PC-TIO-10, generates pulses for the various timescales involved. An analogue output card, the AT-AO-10 is triggered by the PC-TIO-10 and updates voltages sent to the component parts of the experiment. The relevant voltages for each analogue output are read from the waveform buffer.

Data acquisition is performed by a Matrox Meteor frame grabber which records data from a CCD camera (CV-M50 from Alrad Instruments Ltd.) and transfers it to a Matlab array. Both the CCD camera and the frame grabber are triggered by the PC-TIO-10.

More details are given below.

A.1 Timing

The card for controlling the timing of the experiment was a PC-TIO-10. Figure A.1 illustrates the pulse sequences generated by the card.
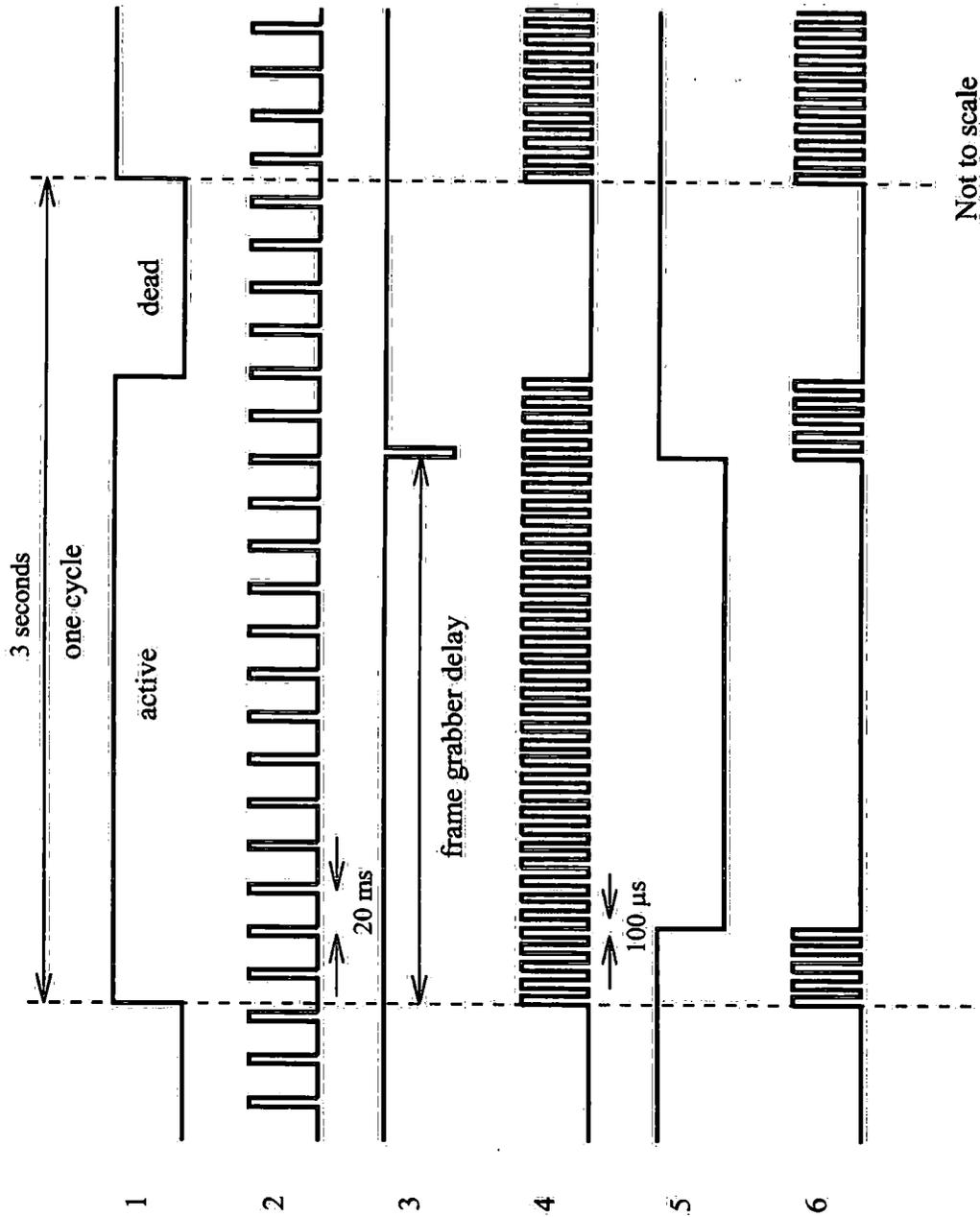
141

Figure A.1: Pulse sequences generated by card PC-TIO-10 for timing the experiment.

1. The main clock: defines the length of a single whole cycle, i.e., the MOT time, molasses time, delay before acquistion, acquisition time and time for data transfer from the CCD camera to Matlab. Typically the 'active' time would be one second and the 'dead' time would be around two seconds. The 'dead' time must be long enough to allow data acquisition from the CCD camera. If this is not the case, the sequence cannot trigger correctly and the detection and data acquisition are no longer synchronised.

2. CCD camera trigger: square pulse with a timebase of 20 ms and a variable duty cycle which is set such that the detection pulse coincides with the opening of the camera shutter. The CCD camera takes a picture every 20 ms.

3. The frame grabber trigger: triggers the Matrox Meteor frame grabber to record data from the CCD camera.

4. Update timebase: Sets the frequency for updating the analogue output channels which control parameters such as the intensity and detuning. The timebase is a square wave with a duty cycle of 50 μs by 50 μs.

5. AND gate control: this signal and the update timebase are sent to an AND gate and the resulting signal is illustrated by 6. For signal 6 a large number of the 100 μs period pulses are replaced by a single pulse.

6. External Update: The result of 4. $\wedge$ 5. This signal is send to the AT-AO-10 card to trigger the analogue output channels to read a new value from the waveform buffer when the signal goes from low to high. Thus the channels are only updated when the values of intensity and detuning are changing rapidly, preventing the waveform buffer from becoming unmanageably long.

All the outputs must be synchronised and this is achieved using gates. The main clock is gated by the CCD camera trigger. The frame grabber trigger, the update timebase and the signal for the AND gate are all gated by the output from the main clock as illustrated by figure A.2.

A.1.1 Repeated pulse sequences

The minimum time of a single cycle (i.e. the active time + the dead time in figure A.1) is limited by the time for the data transfer from the CCD camera to matlab (about 2 seconds). In some cases, for example the multiple loading of an atom trap described in chapter 5, it might be necessary to repeat the same pulse sequence several times with only a single detection pulse and data transfer at the end, after
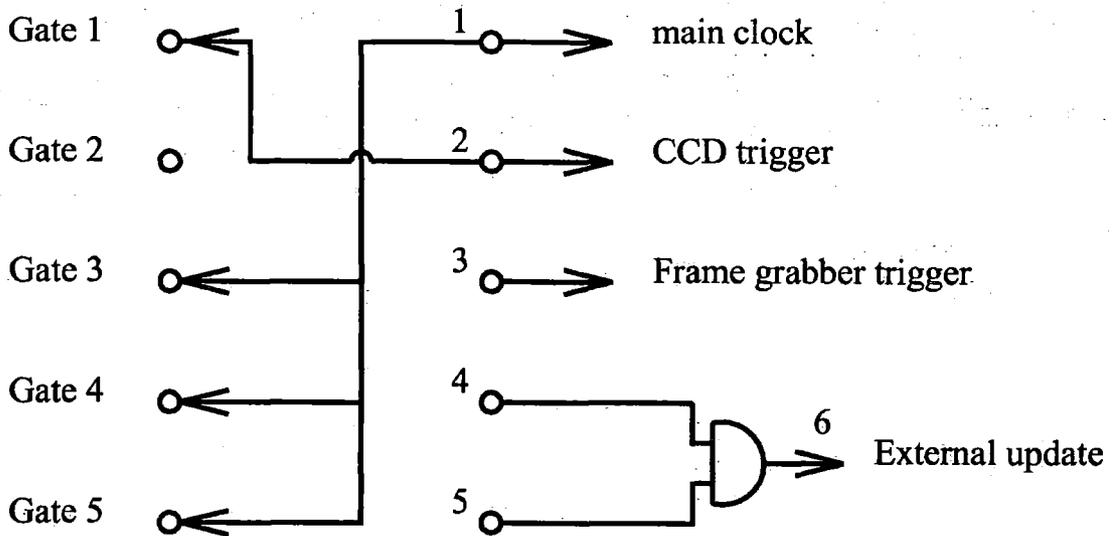
Figure A.2: Schematic of the outputs and gating for the timing control.

many identical sequences. For this case, to prevent the waveform buffer from becoming unmanageably long the repeated sequence is stored in a minibuffer. Output 5 which is sent to the AND gate is modified as shown in figure A.3. An additional output (out 6) is the inverse of output 5 and is sent to the external trigger of the data acquisition card, LabPC1200. The trigger is used to indicate the start of each minibuffer. The result is output 7 on the figure which is the external update sent to AT-AO-10. Hence the minibuffer can be repeated an arbitrary number of times.

A.1.2 Triggering the CCD camera

The frame grabber for the CCD camera is Matrox Meteor, which can grab images using an external hardware-controlled trigger. The frame grabber is triggered by the rising edge of a signal changing from 0.8V to 2V and will then record the next frame from the CCD camera.

A CCD camera frame consists of an even field and an odd field, each field lasting 20 ms. The frame grabber starts collecting data at the beginning of the first even field after the trigger. This adds a complication to the data collection since the time from the frame grabber trigger can vary between zero and the time for one full frame. The situation is illustrated in figure A.4. The CCD camera shutter is triggered every 20 ms and in each frame two sets of data will be collected. In case (1), the grame grabber will record a set of data 2 ms and 22 ms after the trigger. In case (2), it will record data 22 ms and 42 ms after the trigger. Both sets of data are
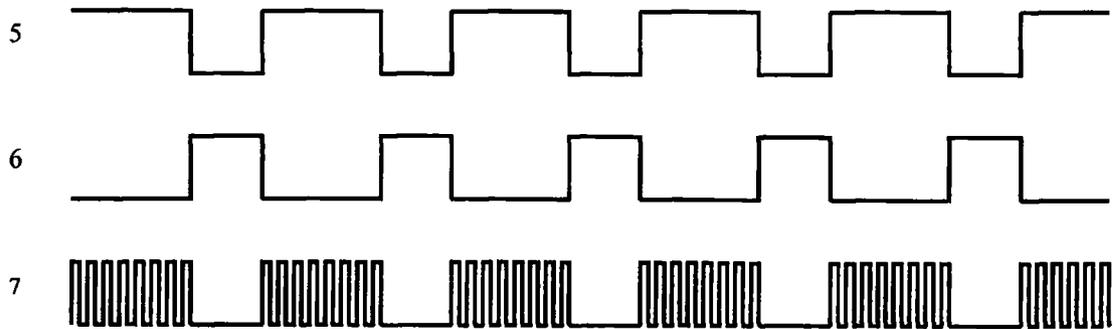
Not to scale

Figure A.3: Modified pulse sequences generated by card PC-TIO-10 for the case of a repeated minicycle. Output 5 is the signal sent to the AND gate, output 6 is a trigger for the start of each minibuffer and output 7 is the external update signal sent to card AT-AO-10.

transferred to Matlab arrays. In general the appropriate data set can be selected by comparing the size of the two arrays and selecting the larger.

A.2 Input and Output Signals

The external update (signal 6 in figure A.1) is used as the control timer for the AT-AO-10 which is a high performance analogue output and digital I/O board for PCs. A new value from the buffer is written to the analogue outputs each time the external update signal goes from high to low. The analogue output channels are used to control:

0. Magnetic Field Switch: 0 or 5 V for MOSFET gate switching the current in the magnetic field coils.

1. Intensity Control: 0 - 1 V to the intensity control of the acousto-optic modulators on the cooling beams.

2. Detuning Control: 0 - 10 V to the frequency control of the acousto-optic modulators on the cooling beams.

3. Launch Trigger: 0 or 5 V for the RF switch to switch between cooling and launching frequencies.

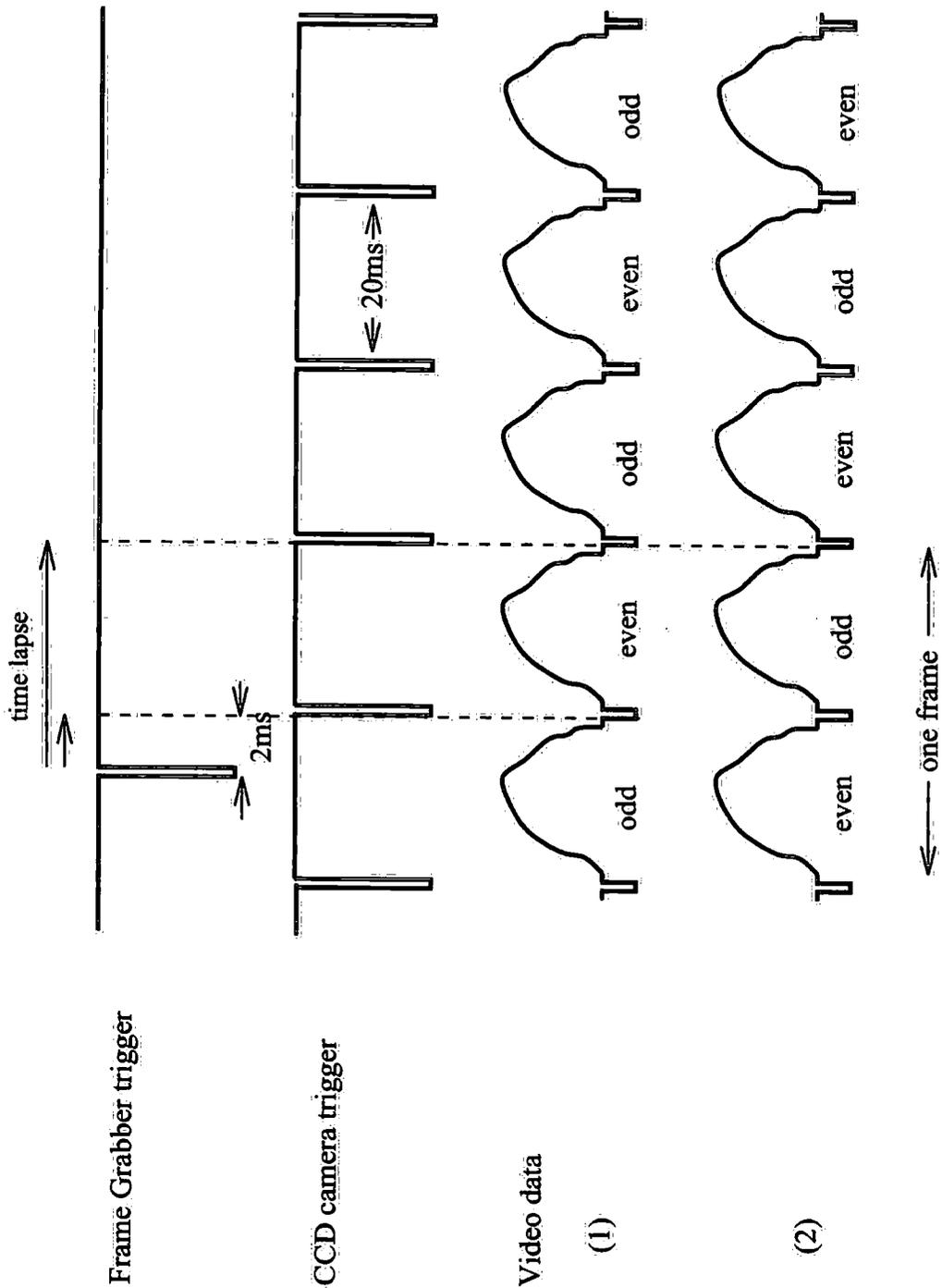4. 5. Mechanical shutters: 0 or 5 V for mechanical shutters.

Figure A.4: Timing of data acquisition from the CCD camera. The vertical dotted lines indicate the position of the beginning of the first frame after the frame grabber trigger for case (1) and case(2).

6. Trap door: 0 or 5 V to switch AOM for trap door beam.

7. Detection beam: 0 or 5 V to switch AOM for detection beam.

A third board, the Lab-PC-1200 consists of a number of analogue and digital inputs and outputs. A single analogue input is used on this board for the signal from the photodiode monitoring fluorescence from the MOT. Loading rate curves can be recorded by triggering this input using the main clock from the PC-TIO-10.

A.3   Graphical Interface

The graphical interface, Matlab, can communicate with the data acquisition cards via MEX files, which are c files for matlab. The .c files are compiled using the command line:

mex filename.c nidaq32.lib, nidex32.lib

nidaq32.lib and **nidex32.lib** are libraries for the data acquistion software. If the .c file also involves calls to the Matrox Meteor frame grabber the additional libraries named **Mil.lib** and **Milmet.lib** must be added. The result is a file called **filename.dll** which can be read by matlab.

Figure A.5 is a schematic of the graphical interface. Various parameters can be set interactively. An image from the CCD camera and a cross-section through the image are displayed for each cycle (i.e. about every 3 seconds). A number of different operation modes are available. For example, 'Pulsed' mode operates the MOT in a pulsed fashion with a loading phase, a molasses phase, free ballistic expansion of the atomic cloud, detection and data transfer. Clicking on 'Pulsed' runs the matlab file **motpulse.m**.

motpulse.m calls:

setinfopulse.m sets the colours, positions of the figures etc for the display.

startpulse.m defines the waveform controlling the intensity, detuning etc. for the pulsed mode.

ks_WFM_LowLevel.c assigns a waveform buffer to the analogue output channels and selects the rate and the number of times the data in the buffer is to be generated. (This is a MEX-file for matlab).

ks_trigim.c function that grabs an image from a CCD camera using Matrox Meteor frame grabber and transfers the image buffer to a Matlab array. (This is a MEX-file for matlab.)

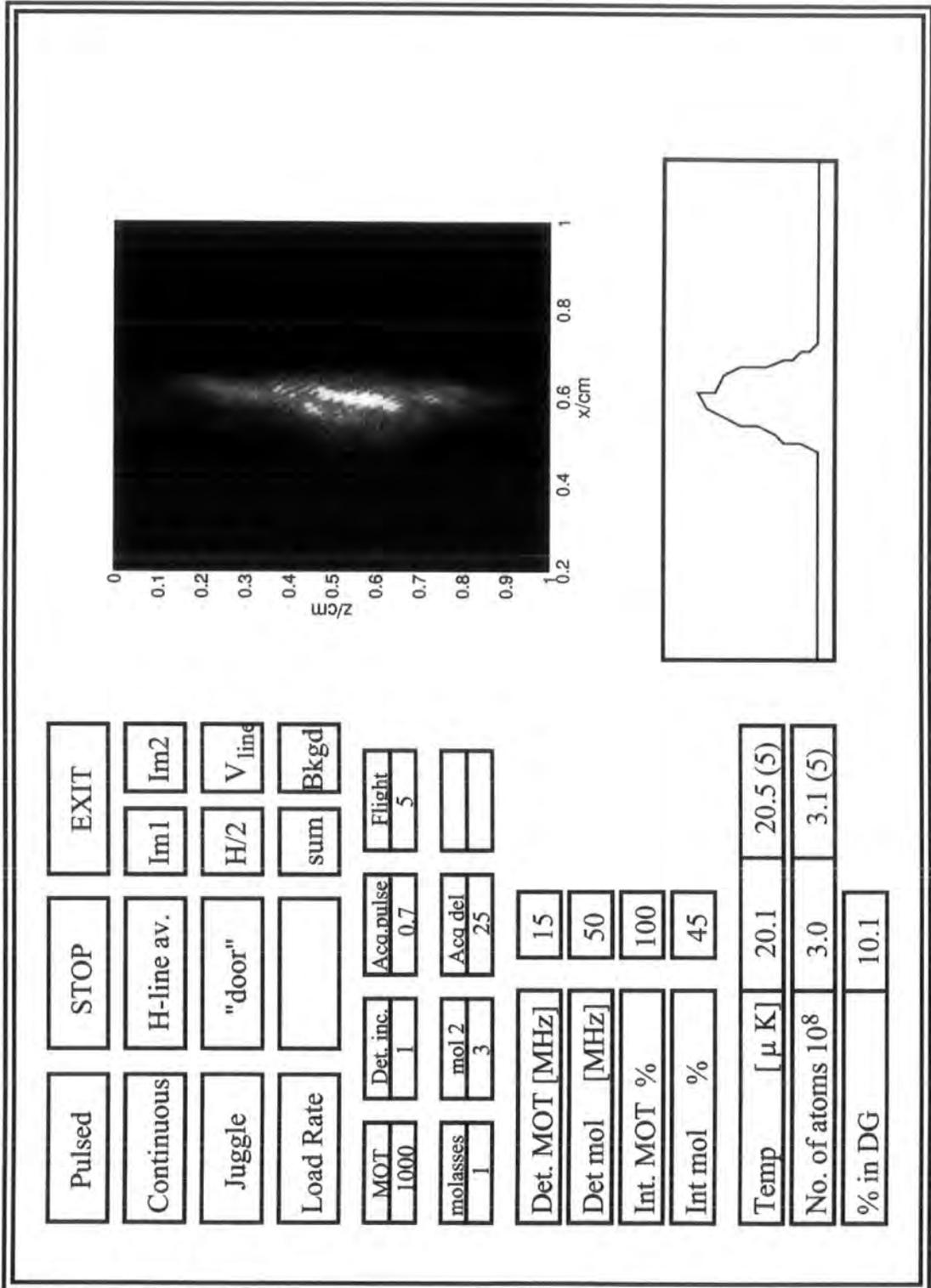The file **motpulse.m** then displays the image and performs any calculations required. A similar program structure exists for each mode.

Figure A.5: The graphical interface